Bachelor's Degree in Telecommunication Technologies Engineering

Bachelor's Thesis

Separation of Electromyographic Signals According to Their Muscle of Origin

Author
Anton Cobian Iregui

Supervised by
Romano Giannetti

Madrid
June 2026

Declaración de originalidad

Declaro bajo mi responsabilidad que el Proyecto presentado con el título **"Separación de señales electromiográficas según el músculo de procedencia"** en la ETS de Ingeniería – ICAI de la Universidad Pontificia Comillas en el curso académico 2025-2026 es de mi autoría y no ha sido presentado con anterioridad a otros efectos. El Proyecto no es plagio de otro, ni total ni parcialmente, y la información que ha sido tomada de otros documentos está debidamente referenciada.

Firmado (alumno):

Antón Cobian Iregui

Fecha: June 1, 2026

Uso de Inteligencia Artificial[1]

Declaro bajo mi responsabilidad que (*indicar la opción correcta*):

☐ No he utilizado Inteligencia Artificial en la elaboración del presente documento.

☒ He utilizado Inteligencia Artificial en la elaboración del presente documento y/o del Anexo B siempre en las condiciones permitidas por la Universidad Pontificia Comillas, es decir, aplicando el Nivel 2 de la Escala de Evaluación de Perkins et al. (2024): *«La IA puede utilizarse para actividades previas a la tarea, como la lluvia de ideas, la descripción y la investigación inicial. Este nivel se centra en el uso de la IA para la planificación, las síntesis y la generación de ideas, pero las evaluaciones deben hacer hincapié en la capacidad de desarrollar y refinar estas ideas de forma independiente».*

En concreto, la Inteligencia Artificial ha sido empleada para:

> *Lluvia de ideas, investigación inicial y síntesis orientativa de artículos científicos. A nivel lingüístico, también se ha empleado la IA para traducciones puntuales de términos o expresiones y para la revisión de ortografía en inglés.*

Firmado (alumno):

Antón Cobian Iregui

Fecha: June 1, 2026

[1]Esta declaración se refiere al uso de la Inteligencia Artificial generativa para realizar los documentos del Proyecto (Anexo B y Memoria). No aplica a Proyectos donde, por su naturaleza, deban emplear inteligencia artificial como parte de los mismos (aplicación de técnicas de aprendizaje automático, redes neuronales, análisis de datos...).

Autorización para la entrega del Proyecto

El Director del Proyecto	**El Co-Director del Proyecto** (*si aplica*)
Firmado por GIANNETTI ROMANO - ****3425* el día 02/06/2026 con un certificado emitido por AC FNMT Usuarios Fdo: _____ Fecha: _____	Fdo: _____ Fecha: _____

Bachelor's Degree in Telecommunication Technologies Engineering

Bachelor's Thesis

Separation of Electromyographic Signals According to Their Muscle of Origin

Author
Anton Cobian Iregui

Supervised by
Romano Giannetti

Madrid
June 2026

Resumen

Separación de señales electromiográficas según el músculo de procedencia

Autor: Anton Cobian Iregui
Director: Romano Giannetti
Entidad Colaboradora: Universidad Pontificia Comillas, ICAI

Este Trabajo Fin de Grado estudia la separación de señales EMG débiles mezcladas con interferencias musculares más intensas en escenarios de músculos reinervados. Se comparan ICA, SOBI, ICA restringido y regresión bajo condiciones controladas, mostrando que la recuperación depende de la mezcla, el retardo y la información previa.

Palabras clave: Procesamiento de señal, EMG, Separación de fuentes, Prótesis

Introducción

Este Trabajo Fin de Grado está motivado por un proyecto de investigación desarrollado en el Instituto de Investigación Tecnológica de la Universidad Pontificia Comillas, comúnmente conocido como IIT. El proyecto se centra en sistemas EMG implantables para ortesis mioeléctricas y reconstrucción biónica tras lesiones graves de nervios periféricos. En este contexto, las señales EMG se utilizan para estimar la intención de movimiento del usuario y traducirla en comandos de control para prótesis.

Sin embargo, en escenarios de músculos reinervados, la señal EMG medida puede verse afectada por atenuación, retardos temporales, patrones de activación atípicos y contaminación procedente de músculos donantes. Esto es especialmente relevante cuando la componente objetivo es más débil que la actividad muscular que interfiere, ya que la información deseada puede ser enmascarada por fuentes de mayor amplitud.

Por tanto, este trabajo estudia si las técnicas de separación de fuentes pueden ayudar a recuperar componentes EMG débiles a partir de las mezclas observadas. En lugar de reconstruir exactamente la forma de la señal original, el objetivo principal es preservar el patrón de activación de la fuente deseada, puesto que contiene la información más relevante para el control basado en EMG.

Definición del problema

El problema específico que se aborda en este trabajo está inspirado en la interferencia que puede aparecer en sistemas VDMT (*Vascularized Denervated Muscle Target*). En estos casos, el músculo reinervado puede generar una señal EMG débil, mientras que el músculo auxiliar puede introducir una contribución de mayor amplitud en el canal.

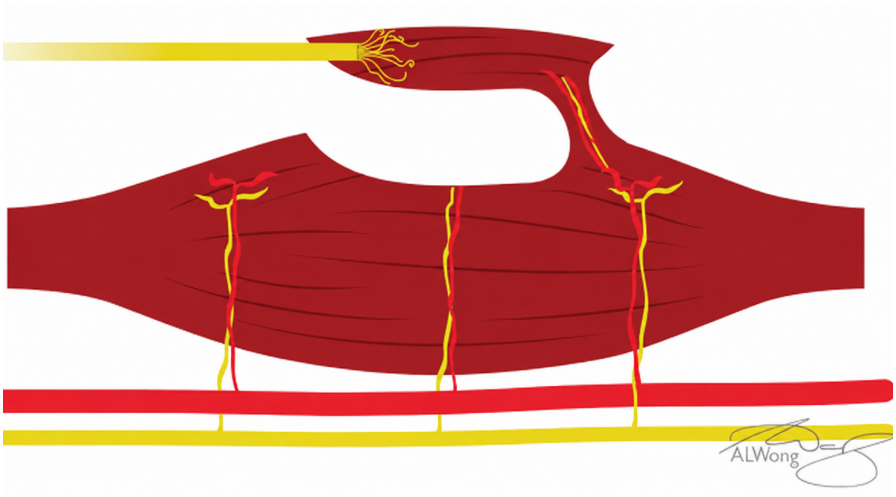

Figura 1: Ilustración esquemática de un VDMT, adaptada de [1].

Por ello, el problema de separación se modela como un sistema de dos fuentes y dos canales. La fuente objetivo se expresa como s_1, mientras que la fuente de interferencia de mayor amplitud se denomina s_2. Aunque a lo largo del trabajo se consideran varios modelos para analizar el efecto de la interferencia, el ruido y el retardo, el caso del estudio del IIT se modela como un escenario asimétrico con una fuente débil, como se describe en la Ecuación 1.

$$\begin{cases} c_1(t) = s_1(t) + \beta s_2(t-\tau) + n_1(t) \\ c_2(t) = 0.01 s_1(t-\tau) + s_2(t) + n_2(t) \end{cases} \tag{1}$$

donde β representa el factor de interferencia en la fuente débil, τ el retardo temporal entre canales y $n_1(t), n_2(t)$ ruido aditivo con varianza σ^2.

El modelo describe una mezcla asimétrica en la que la señal objetivo débil está fuertemente contaminada por el músculo auxiliar, mientras que el canal del donante contiene una contribución mínima de dicha señal. Por este motivo, el objetivo es estimar la fuente débil s_1 a partir de las mezclas observadas y obtener una estimación $\hat{s}_1$ que mantenga sus patrones de activación.

Metodología

La metodología experimental se estructura en varias etapas. Dado que todavía no se dispone de datos experimentales específicos de sistemas VDMT, las pruebas

se realizan con señales EMG procedentes de una base de datos de pacientes con TMR (otra técnica de reinervación muscular). Estas señales se emplean como base experimental, junto con señales artificiales diseñadas para simular diferentes frecuencias de activación. A continuación, las señales seleccionadas se adaptan y se mezclan mediante los modelos propuestos con el fin de simular distintos niveles de interferencia, ruido y retardo.

Antes de aplicar los algoritmos de separación, las señales se preprocesan mediante filtrado, escalado de canales y blanqueamiento. El filtrado reduce componentes espectrales no deseadas, el escalado mejora la comparabilidad entre canales y el blanqueamiento prepara los datos para la etapa de separación.

Posteriormente, se implementan y comparan varios métodos. FastICA se utiliza como el principal algoritmo de separación ciega basado en la no gaussianidad. SOBI se estudia como un método alternativo basado en la correlación temporal. ICA restringido se propone para evaluar si la información previa puede guiar la separación hacia la fuente deseada. Finalmente, la regresión lineal se considera cuando uno de los canales puede aproximarse a la fuente de interferencia.

Los resultados se evalúan mediante la correlación con la envolvente RMS, la correlación temporal y la SNR. Entre estas métricas, se prioriza la correlación con la envolvente RMS, ya que el control de prótesis mediante EMG depende principalmente de la detección del patrón de activación. En este contexto, la reconstrucción exacta de la onda original tiene una importancia secundaria. El flujo experimental se resume en la Figura 2.

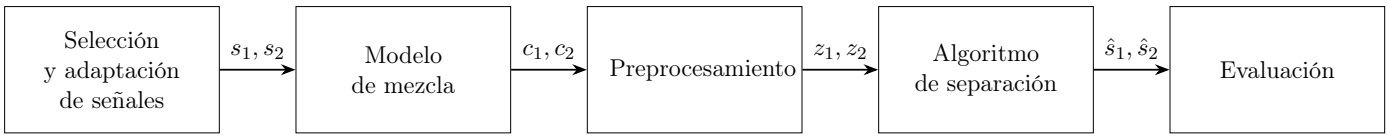

Figura 2: Diagrama de bloques del proceso seguido en los experimentos de este trabajo.

Resultados

Los resultados muestran que ICA funciona adecuadamente en mezclas instantáneas ideales o casi ideales, recuperando las fuentes con las indeterminaciones de orden, signo y escala. Con ruido aditivo, la correlación temporal de la fuente débil disminuye, pero su envolvente RMS se preserva en algunos casos.

Sin embargo, el rendimiento de ICA empeora cuando se introducen retardos temporales. Esto se debe a que una matriz de separación instantánea no puede cancelar completamente las contribuciones retardadas de la fuente dominante. Esto afecta principalmente a la recuperación de la componente débil, especialmente cuando la fuente de interferencia presenta una varianza mucho mayor.

SOBI no proporciona una mejora consistente frente a ICA para las señales EMG reales consideradas, ya que sus patrones de autocorrelación suelen ser demasiado similares. ICA restringido ofrece un marco flexible usando información previa,

pero las referencias binarias evaluadas en este trabajo no muestran una mejora significativa. La regresión con retardo muestra los mejores resultados únicamente si c_2 es una referencia fiable de s_2 y el retardo puede estimarse con precisión. Esto sugiere que las técnicas convolutivas podrían hacer frente a la contribución retardada de s_2, una de las principales limitaciones de los métodos instantáneos estudiados en este trabajo.

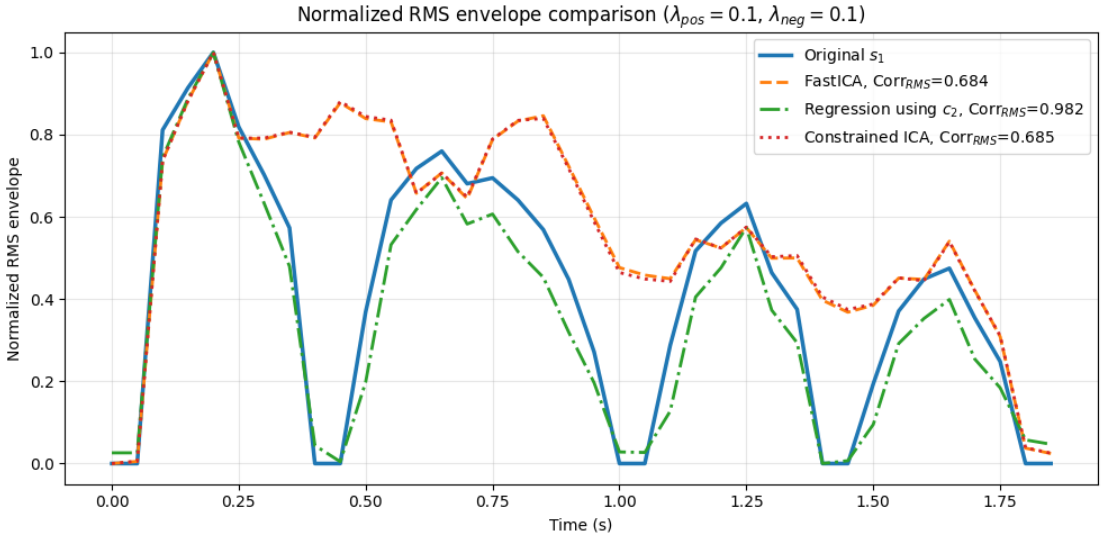

Figura 3: Comparación de las envolventes RMS recuperadas por los algoritmos. Los parámetros se fijaron a $\sigma = 0.1$, $\beta = 0.3$ y $\tau = 5\,\text{ms}$. La regresión con retardo logra una reconstrucción casi perfecta ya que elimina la interferencia retardada procedente de s_2.

Conclusiones

Este trabajo muestra que los métodos de separación de fuentes pueden ser útiles para recuperar componentes EMG débiles, pero su rendimiento depende fuertemente de las condiciones de mezcla. En particular, los retardos temporales, el ruido aditivo y la dominancia de una fuente dificultan significativamente la recuperación de la señal deseada.

La principal conclusión es que la recuperación de una fuente débil no siempre puede resolverse mediante separación ciega e instantánea. Cuando la mezcla se aproxima al caso ideal, los métodos estándar de BSS pueden proporcionar buenos resultados, pero el escenario del IIT introduce información adicional que debería aprovecharse. En concreto, la presencia de un canal de referencia y la estimación del retardo temporal son factores clave en la recuperación del patrón de activación.

En conjunto, los resultados sugieren que recuperar actividad EMG débil en escenarios de músculos reinervados puede requerir más que separación ciega estándar. El trabajo futuro debería centrarse en una mejor estimación del retardo con modelos convolutivos, restricciones fisiológicas significativas, señales EMG multicanal y validación con datos experimentales procedentes del proyecto del IIT.

Abstract

Separation of Electromyographic Signals According to Their Muscle of Origin

Author: Anton Cobian Iregui
Supervisor: Romano Giannetti
Collaborating Entity: Universidad Pontificia Comillas, ICAI

This Bachelor's Thesis studies the separation of weak EMG signals mixed with stronger muscular interference in reinnervated muscle scenarios. ICA, SOBI, constrained ICA and regression are compared under controlled conditions, showing that recovery depends on mixing, delay and prior information.

Keywords: Signal Processing, EMG, Source Separation, Prosthetics

Introduction

This Bachelor's Thesis is motivated by a research project developed at the Institute for Research in Technology of Comillas Pontifical University, commonly known as IIT. The project focuses on implantable EMG systems for myoelectric orthoses and bionic reconstruction after severe peripheral nerve injuries. In this context, EMG signals are used to estimate the user's movement intention and translate it into control commands for prosthetic devices.

However, in reinnervated muscle scenarios, the recorded EMG signal may be affected by attenuation, temporal delays, atypical activation patterns and contamination from donor muscles. This is especially relevant when the target component is weaker than the interfering muscular activity, since the desired information may be masked by stronger sources.

Therefore, this thesis studies whether source separation techniques can help recover weak EMG components from mixed recordings. Rather than reconstruct the exact original waveform, the main goal is to preserve the activation pattern of the target source, which is the most relevant information for EMG control.

Problem definition

The specific problem addressed in this work is inspired by the interference that may appear in Vascularized Denervated Muscle Target (VDMT) configurations. In these cases, the target reinnervated muscle can generate a weak EMG signal, while the auxiliary muscle may introduce a stronger contribution into the recorded channel.

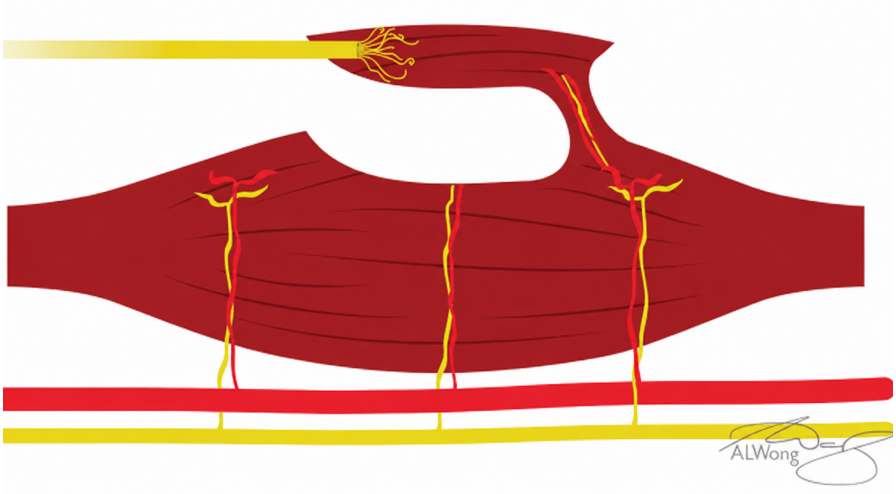

Figure 4: Schematic illustration of a VDMT adapted from [1].

The separation problem is modeled as a two-source, two-channel system. The target source is expressed as s_1, while the stronger interfering source is denoted as s_2. Even though several mixture models are considered throughout the thesis to analyze the effect of interference, noise and delay on the general separation process, the IIT case study is modeled using the asymmetric weak-source scenario described in Equation 2.

$$\begin{cases} c_1(t) = s_1(t) + \beta s_2(t-\tau) + n_1(t) \\ c_2(t) = 0.01 s_1(t-\tau) + s_2(t) + n_2(t) \end{cases} \tag{2}$$

where β represents the interference factor in the weak source, τ the temporal delay between channels and $n_1(t), n_2(t)$ additive noise with variance σ^2.

The model represents an asymmetric weak source regime where the target signal is heavily contaminated by the auxiliary muscle while the donor channel contains a minimal contribution from the target source. For this reason, the objective is to estimate the weak source s_1 from the observed mixtures and achieve a recovered signal $\hat{s}_1$ that maintains its activation patterns.

Methodology

The experimental methodology is structured in several stages. Since specific experimental data from VDMT systems are not yet available, the tests are performed using EMG signals from a dataset of patients with TMR (another muscle reinnervation technique). These signals are used as an experimental basis, along with artificial signals designed to simulate different activation frequencies. The selected signals are then adapted and mixed using the proposed models in order to simulate different levels of interference, noise and delay.

Before applying the separation algorithms, the signals are preprocessed through filtering, channel scaling and whitening. Filtering reduces undesired frequency

components, channel scaling improves numerical comparability between channels and whitening prepares the data for the source separation stage.

Several methods are implemented and compared. FastICA is used as the main blind separation algorithm based on non-Gaussianity. SOBI is studied as an alternative method based on temporal correlation. Constrained ICA is introduced to evaluate whether prior information can potentially guide the separation towards the target source. Finally, linear regression is considered as a practical baseline when one channel can be interpreted as an approximate reference of the interfering source.

The outputs are assessed using RMS envelope correlation, temporal correlation and SNR. Among these metrics, RMS envelope correlation is prioritized because EMG-based prosthetic control mainly depends on detecting the activation pattern of the muscle, rather than reconstructing the exact waveform sample by sample. The complete experimental workflow is summarized in Figure 5.

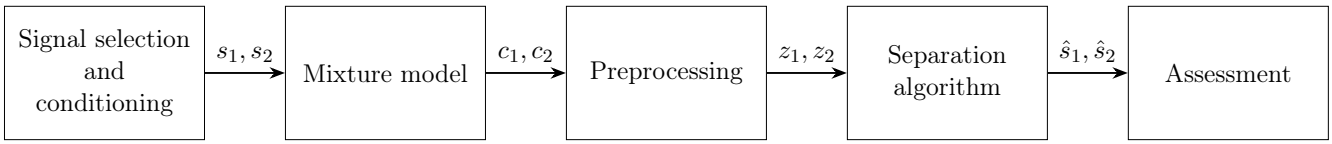

Figure 5: Block diagram of pipeline followed for the experiments in this thesis.

Results

The results show that ICA performs well in ideal or semi-ideal instantaneous mixtures, recovering the sources up to the usual order, sign and scale ambiguities. With additive noise, the temporal correlation of the weak source decreases, although its RMS envelope can still be preserved in some cases.

However, ICA performance worsens when temporal delays are introduced, since an instantaneous separation matrix cannot fully cancel delayed contributions from the dominant source. This mainly affects the recovery of the weak target component, especially when the interfering source has much larger variance.

SOBI does not provide a consistent improvement over ICA for the real EMG signals considered, since their autocorrelation patterns are often too similar. Constrained ICA promises a flexible framework by using prior information, but the binary references tested in this thesis do not show a significant improvement. Delayed regression shows best results only if c_2 is a reliable reference of s_2 and the delay can be accurately estimated. This suggests that delay-aware or convolutive approaches may directly address the delayed contribution of s_2, one of the main limitations of the instantaneous methods studied in this thesis.

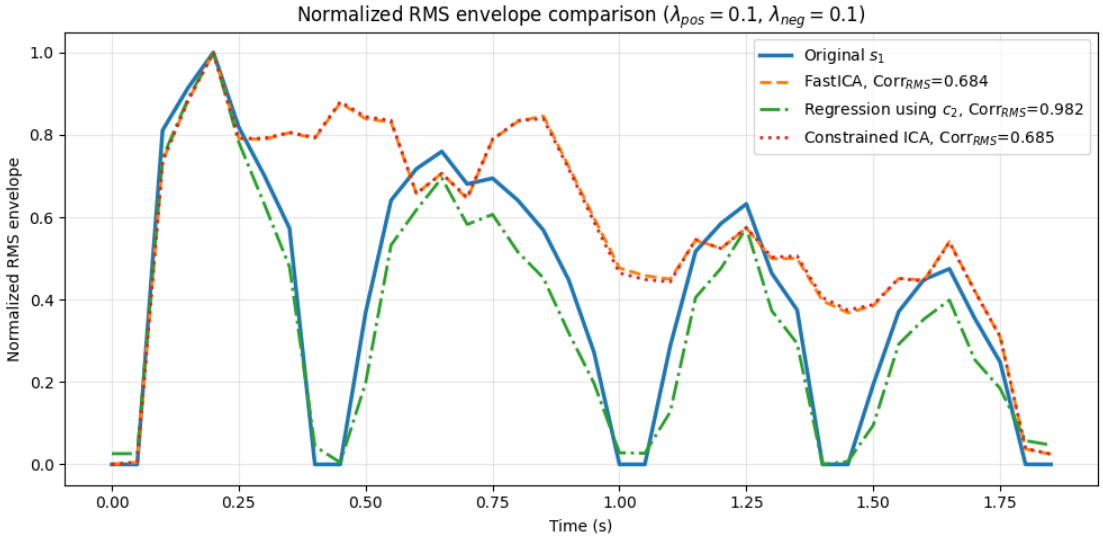

Figure 6: Comparison of the RMS envelopes recovered by the algorithms. Parameters were set to $\sigma = 0.1$, $\beta = 0.3$ and $\tau = 5\,\text{ms}$. The delayed regression achieves an almost perfect reconstruction as it removes the delayed interference from s_2.

Conclusions

This thesis shows that source separation methods can be useful for recovering weak EMG components, but their performance depends strongly on the mixing conditions. Specifically, temporal delays, additive noise and source dominance make the recovery of the target signal significantly more difficult.

The main conclusion is that the weak-source problem cannot always be solved reliably with a purely blind and instantaneous approach. When the mixture is close to ideal, standard BSS methods can provide good results, but the IIT scenario introduces additional information that should be exploited whenever possible. In particular, the presence of a reference channel and the estimation of temporal delay become key factors for improving the recovery of the target activation pattern.

Overall, the results suggest that recovering weak EMG activity in some reinnervated muscle scenarios may require more than standard blind separation. Future work should focus on improved delay estimation with convolutive models, meaningful physiological constraints, multichannel EMG signals and validation with real experimental data from the target IIT application.

Acknowledgments

I would like to thank my thesis supervisor, Romano Giannetti, for his guidance, availability and support throughout the development of this Bachelor's Thesis. His advice has been essential in shaping the direction of this work.

I would also like to thank the professors, classmates and colleagues who have contributed to my academic development throughout my undergraduate studies.

Finally, I am especially grateful to my family and friends for their constant support, patience and encouragement. This work is also the result of everything I have learned from the people who have accompanied me throughout this journey.

Madrid, June 2026
Anton Cobian Iregui

Contents

Chapter 1
Introduction

Telecommunications engineering plays a key role in the development of technologies based on electronics, instrumentation and advanced signal processing. One of the emerging fields where these disciplines converge is biomedical engineering, specifically in the analysis and processing of physiological signals for rehabilitation and prosthetic control applications.

Specifically, the study of signals such as electromyography (EMG) makes it possible to obtain detailed information about muscular activity, which is essential for understanding the neuromuscular system and designing assistive devices. The correct interpretation of these signals depends not only on accurate data acquisition, but also on the use of advanced processing techniques, including feature extraction and source separation algorithms.

Additionally, signal separation is a commonly applied tool in the field of telecommunications, especially given the relevance of wireless communications and radio systems. In these technologies, multiple transmitters may broadcast signals at nearby frequencies, causing them to overlap with one another and with other sources of interference. As a result, it is necessary to separate these signals in order to recover the desired information and monitor the spectrum effectively.

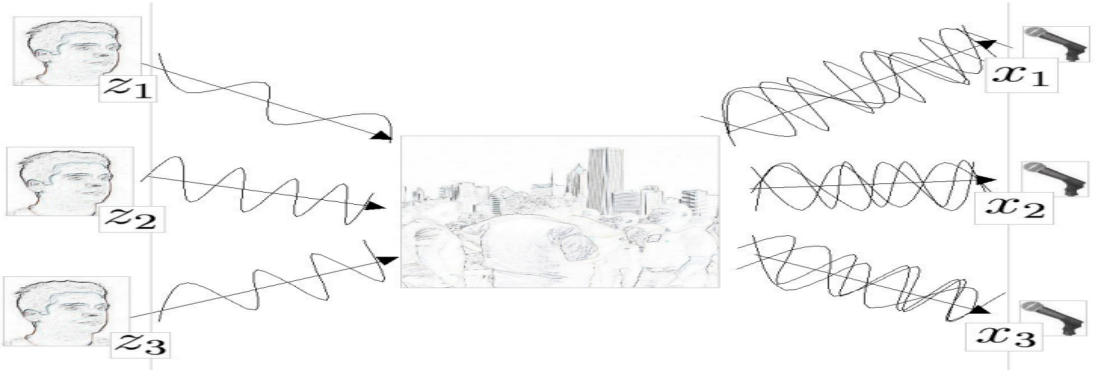

Figure 1.1: Typical example of the cocktail party. Independent speakers are superimposed and recorded by three independent microphones. Figure was extracted from `Biomedical Signal and Image Processing` [2].

Although these applications mainly belong to the field of telecommunications, they contain valuable concepts that can also be applied to biomedical signals such as EMG. This Bachelor's Thesis focuses on the development of separation algorithms for EMG signals, with the aim of improving the quality of the processed signals and facilitating their use in clinical and research environments.

1.1 Background and context

This thesis is closely related to a research project developed at the Institute for Research in Technology of Comillas Pontifical University, commonly known by its Spanish acronym IIT (*Instituto de Investigación Tecnológica*). In particular, it is inspired by the project on implantable EMG systems for myoelectric orthoses and bionic reconstruction after severe peripheral nerve injuries [3].

The project focuses on implantable and wireless myoelectric signal acquisition systems intended for the control of exoskeleton orthoses. These systems belong to the field of human-machine interfaces, where physiological signals such as EMG are used to estimate the user's motor intention and translate it into control commands for devices.

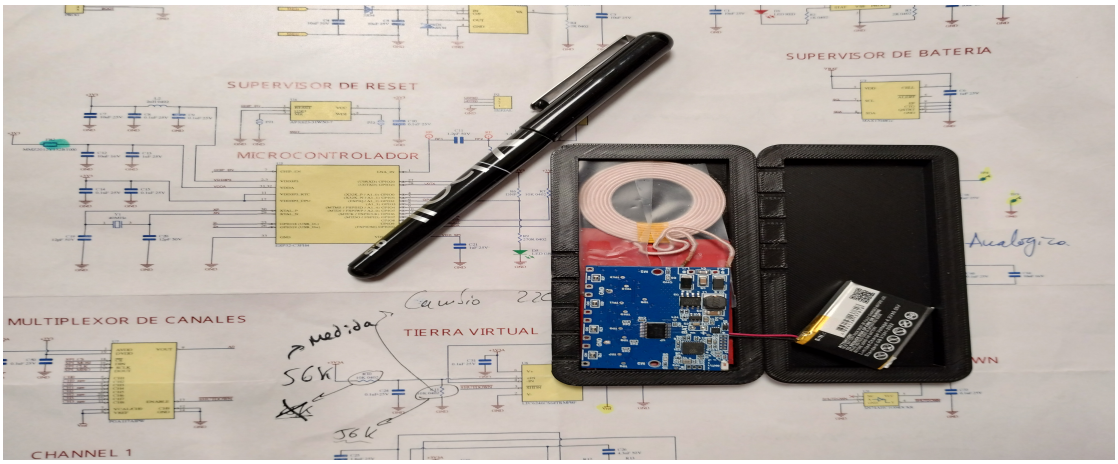

Figure 1.2: Prototype (v2) of a wireless, Bluetooth Low Energy EMG sensor, designed to be long term implanted by the authors of [3].

In this context, EMG signals provide a direct measurement of muscular activation and are therefore widely used in prosthetic and orthotic control. However, their practical use depends strongly on the quality and stability of the recorded signals, especially when these signals are obtained from reinnervated muscles.

1.2 Motivation

Peripheral nerve injuries and limb loss can drastically affect motor function, sensitivity and the ability to perform daily activities. Although reconstructive surgery has advanced significantly over the past few years, functional recovery is not always sufficient to restore natural control of the affected limb. For this reason, myoelectric prostheses have become an important technological alternative, as they use EMG signals to infer the user's motor intention and translate it into control commands.

When a limb is amputated, the motor nerves at the end of the residual limb are sectioned. If they are not reconnected to a functional biological structure, they may form disorganized and painful nerve endings. To improve neuromuscular

integration and provide more reliable control signals, several surgical strategies have been proposed. One of the most established techniques is Targeted Muscle Reinnervation (TMR), where motor nerves are redirected to reinnervate residual muscles that no longer serve their original function. These muscles then act as biological amplifiers of the neural commands, generating EMG activity that can be detected and used for prosthetic control.

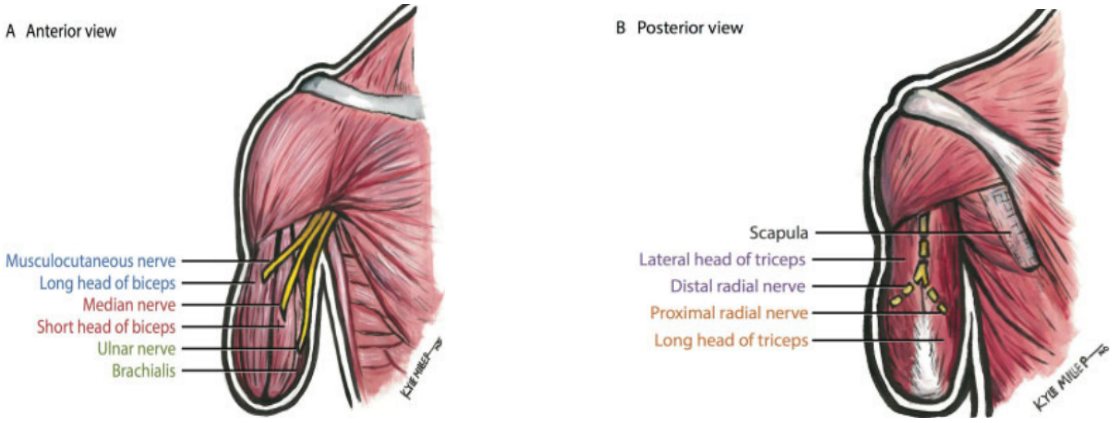

(a) Anterior view (b) Posterior view

Figure 1.3: Schematic representation of the surgical plan for TMR in transhumeral amputation [4]. Labels of the same color represent the muscles and their innervation origin.

Additionally, Regenerative Peripheral Nerve Interfaces (RPNIs) consist of implanting a free denervated muscle graft directly onto the affected nerve, creating a localized biological amplifier that can generate high-quality EMG signals with reduced contamination from nearby muscles [5]. More recently, Vascularized Denervated Muscle Targets (VDMTs) have also been explored as an alternative interface, combining the idea of a denervated muscle target with vascularized tissue to improve long-term viability and signal quality [6], [7].

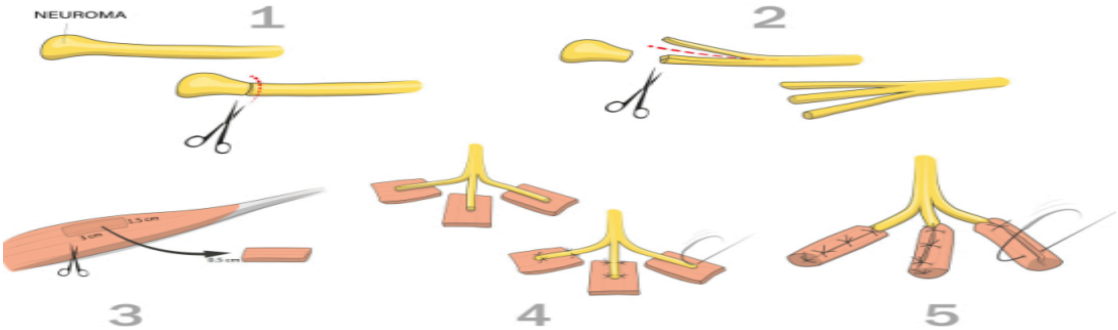

Figure 1.4: Illustration of the Regenerative Peripheral Nerve Interface (RPNI) procedure [5].

However, although these techniques improve the quality and acquisition of control signals, they also introduce new signal processing challenges. When auxiliary

muscles are used as biological amplifiers, the redirected nerve interacts with a new muscular environment. This can modify the morphology, amplitude and temporal structure of the recorded EMG signal. Changes in the geometry and density of motor unit sources affect how the motor unit action potentials propagate through tissue, leading to signals that may differ significantly from those recorded in healthy muscles.

As a result, EMG recordings in these contexts may present amplitude attenuation, temporal delays, atypical activation patterns and contamination from adjacent muscular sources. These effects can make the desired information difficult to identify, especially when the target component is weak compared to other dominant sources. This is particularly relevant for prosthetic control, where inaccurate detection of muscular activation can reduce quality of responses and reliability.

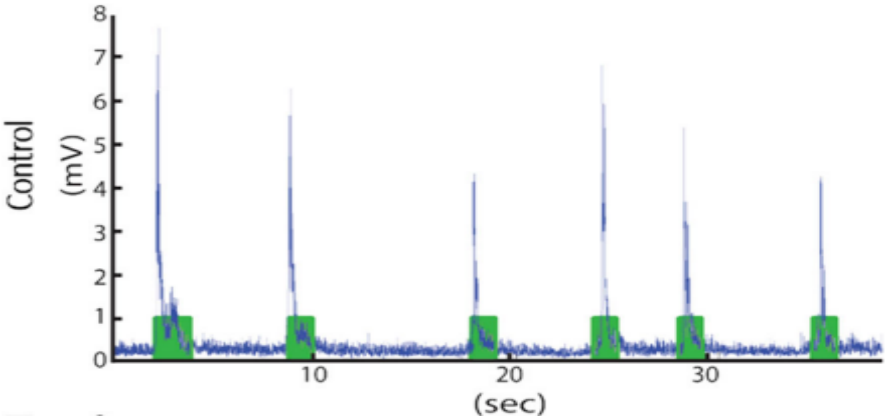

Figure 1.5: Native muscle EMG activity during a 40 second recording [8]. Activation patterns identified by algorithms.

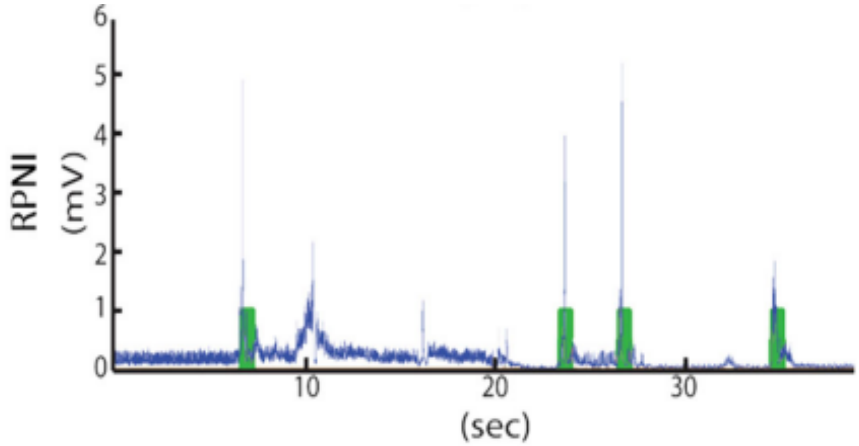

Figure 1.6: EMG activity recorded from the RPNI during a 40 second trial [8]. Activation patterns are irregular and delayed, which makes it harder for EMG prosthetic control.

Therefore, the motivation of this Bachelor's Thesis is to study whether signal separation techniques can help recover weak EMG components from mixed recordings. By identifying and separating the target activity from stronger interfering components, the objective is to improve the quality of the processed EMG signals, ultimately contributing to more reliable EMG control strategies for prosthetic applications.

1.3 Problem statement

VDMTs help prevent the reinnervated muscle from atrophying by maintaining a vascularized muscular environment. However, this configuration can also introduce significant interference from the donor muscle when measuring the EMG activity associated with the reinnervated target. As a result, the recorded signal may contain a weak component of interest superimposed with a stronger contribution from the surrounding donor muscle.

Although this thesis studies EMG signal separation under several possible conditions, its main motivation is the interference problem introduced by the IIT project. For this reason, the work focuses on separating a weak reinnervated-muscle signal from stronger donor muscle interference under controlled mixing conditions.

To achieve this, several obstacles must be considered, including source dominance, additive noise and possible temporal delays between channels. These factors are especially relevant because they determine whether each separation method can recover the target activity reliably or whether the weak component remains masked by the interfering source.

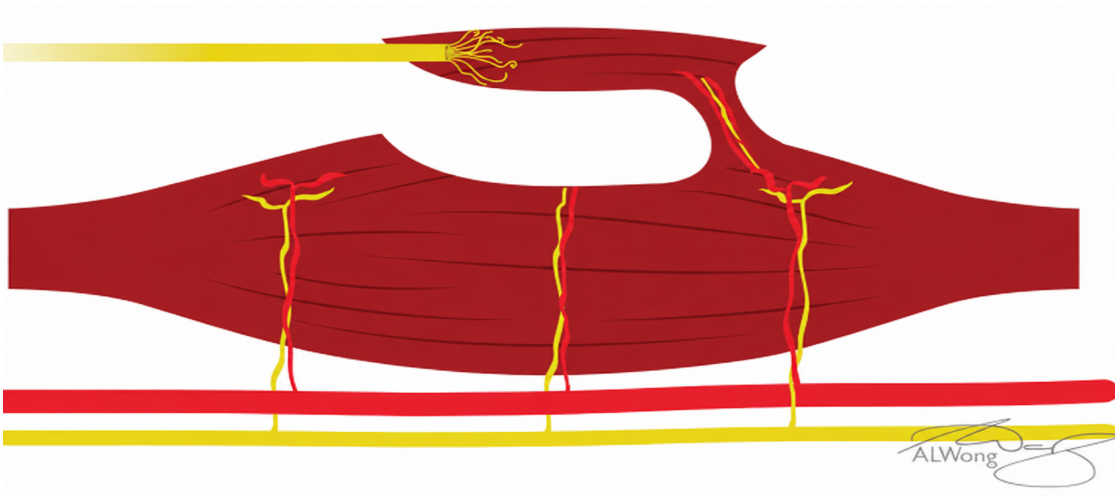

Figure 1.7: Adapted schematic illustration of a VDMT [1]. The connection between the reinnervated muscle and the vascularized donor tissue motivates the interference problem addressed in this thesis.

1.4 Objectives

The main objective of this thesis is to evaluate source separation strategies for recovering weak EMG components in reinnervated muscle scenarios affected by donor-muscle interference.

To achieve this goal, the following specific objectives are proposed:

- Analyze EMG signals generated by reinnervated muscles.
- Design a preprocessing pipeline to prepare EMG signals for the separation process.
- Discuss different source separation algorithms and study their performance under realistic scenarios.
- Assess whether instantaneous separation models can efficiently separate sources in the presence of small delays and additive noise.
- Evaluate whether including physiological information can improve the separation process.
- Assess whether the proposed algorithms can be implemented in real time.

Chapter 2

State of the art

This chapter presents a review of current signal separation techniques and their application to biomedical signals. The aim is to provide the necessary background on blind and semi-blind source separation methods, with particular attention to their use in EMG and other physiological recordings. In addition, the chapter discusses the main assumptions, advantages and limitations of these approaches, establishing the context for the separation problem addressed in this thesis. Finally, this chapter concludes by identifying the current research gap in the mentioned field.

2.1 Blind Source Separation in biomedical signals

Blind Source Separation (BSS) refers to a family of signal processing methods whose objective is to recover a set of unknown source signals from a set of observed mixtures. In these cases, both the original sources and the mixing process are generally unknown, which makes the problem especially relevant in scenarios where several physiological activities are recorded simultaneously by the same sensor system.

Biomedical signals are a clear example of this situation. Recordings such as electroencephalography (EEG), electromyography (EMG) or electrocardiography (ECG) are often affected by the superposition of different biological sources, motion artifacts, environmental noise and instrumentation interference. As a result, the measured signal does not usually represent a single isolated physiological event, but a mixture of multiple contributions.

Among the different BSS approaches, ICA has become one of the most widely used techniques in biomedical signal processing. This method assumes that the observed signals can be expressed as linear combinations of statistically independent sources. Under this assumption, the method seeks a transformation that maximizes the independence of the recovered components. This has made ICA particularly useful in EEG analysis, where it is commonly applied to separate neural activity from artifacts such as eye movements, muscle activity or power-line interference [9], [10].

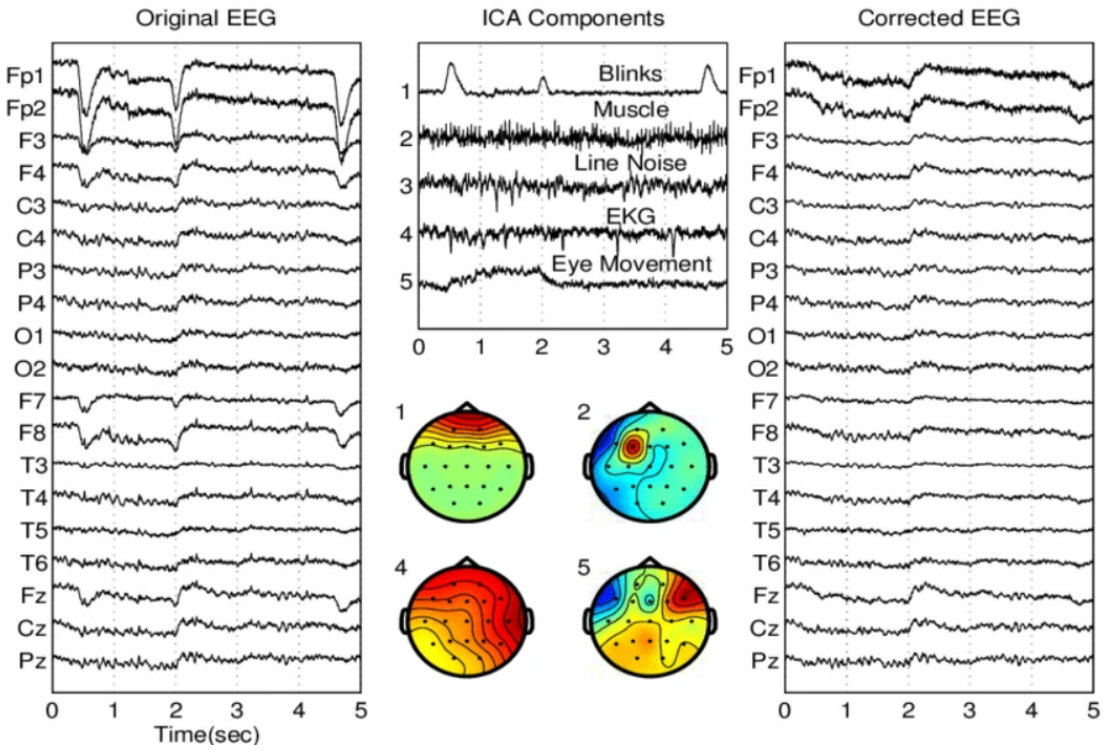

Figure 2.1: Application of ICA in EEG preprocessing. ICA can separate physiological artifacts from the original EEG signal. [11].

The success of ICA in EEG and other biomedical applications has motivated its use in EMG processing. However, these signals present specific challenges due to their amplitude variability and dependence on electrode position, muscle anatomy and activation patterns. For this reason, although BSS algorithms provide a useful approach for EMG source separation, its assumptions and limitations must be carefully considered before applying it to reinnervated muscle recordings.

2.2 BSS Applied to EMG Decomposition

In the context of EMG, the most relevant applications of blind source separation methods are found in high-density surface EMG decomposition. This is mainly because HD-sEMG recordings contain a large number of channels, which include spatial information about the original muscular activity. As a result, these recordings can be interpreted as mixtures of several physiological sources, making ICA and other separation algorithms suitable candidates for their decomposition.

ICA methods have been used to separate EMG recordings into components associated with different muscles or motor unit activity. By exploiting the statistical independence between sources, ICA can help isolate hidden components that are not directly observable from the raw electrode recordings. This is particularly useful when several muscles are active at the same time or when the activity recorded by one electrode is contaminated by nearby sources [12]–[14].

However, applying separation algorithms to EMG is not straightforward. EMG

sources are not always perfectly isolated and the recorded signals may be affected by noise, amplitude differences and temporal delays. These limitations become especially important in reinnervated muscle scenarios, where the target source may be weaker than the interfering donor-muscle activity. Therefore, although ICA provides a strong starting point for EMG decomposition, its assumptions and limitations must be carefully considered in the context of this thesis.

Even though separation algorithms have shown promising results in the applications mentioned above, their use in asymmetric mixtures dominated by a stronger interfering source has been less extensively studied. This is particularly relevant for this thesis, where the objective is to recover a weak EMG target component from that type of mixture.

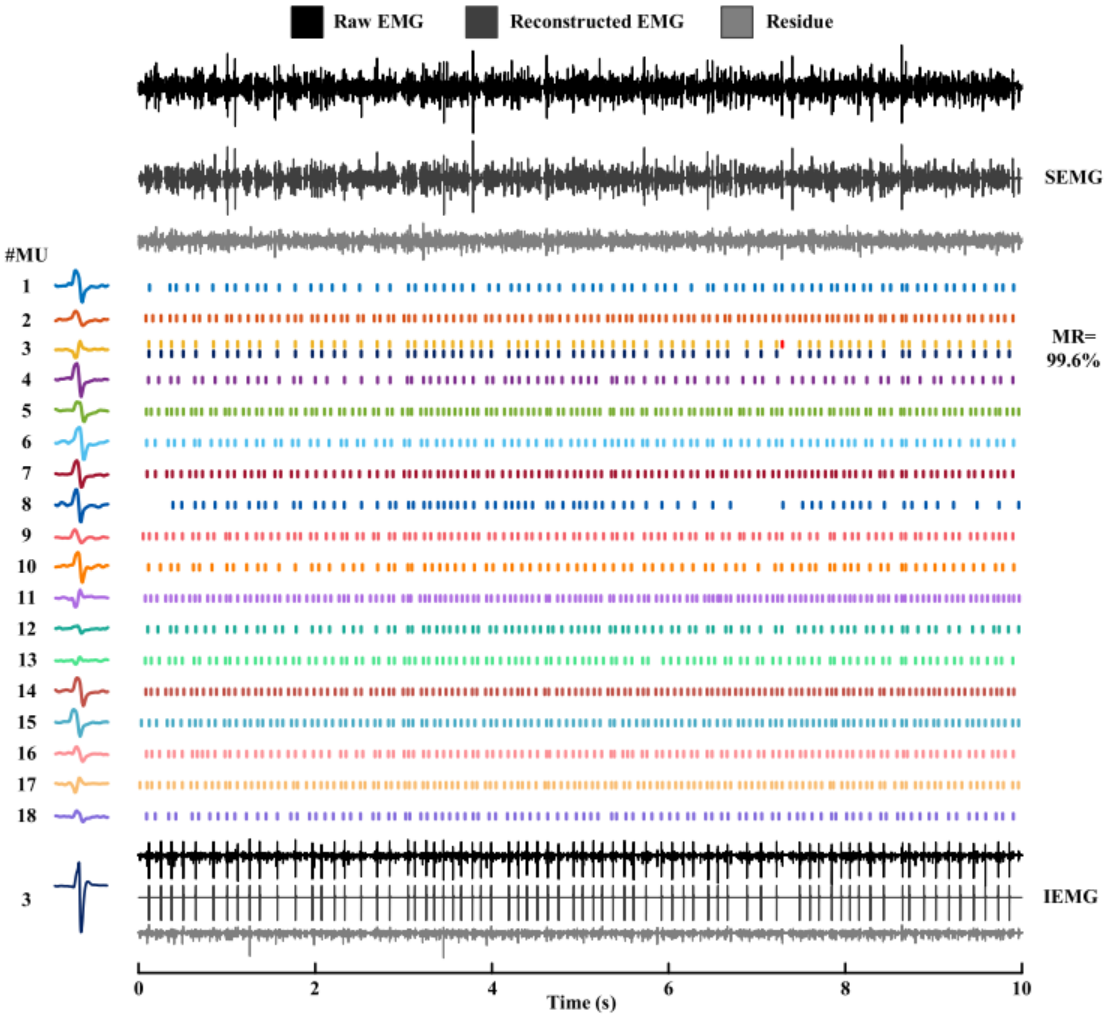

Figure 2.2: High density surface EMG decomposition into motor unit activity using 2CFastICA [15].

2.3 Current Advances in Reinnervated EMG

Recent research on reinnervated EMG has focused on improving the quality and stability of the signals generated by nerve interfaces. Techniques such as TMR, RPNIs and VDMTs have already been introduced in Section 1.2. Therefore, this section focuses on how these interfaces are currently evaluated from a signal processing perspective.

A common trend in the EMG literature is the use of recordings to assess functional recovery after reinnervation. These recordings are used to evaluate whether the reinnervated muscle produces detectable activation patterns, sufficient signal amplitude and reliable interpretation of the activity. In this sense, EMG is used as a control signal as well as a tool to evaluate the success of the biological interface.

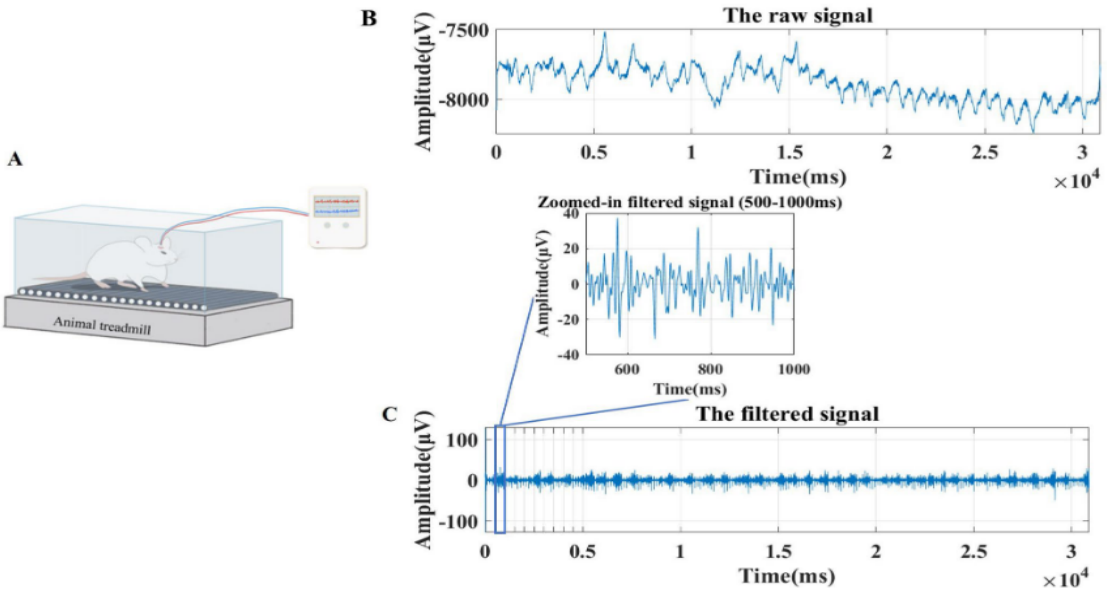

Figure 2.3: Example study of reinnervated EMG assessment in animals. Current advances in reinnervated EMG are often first evaluated in experimental animal models [16].

Figure 2.3 illustrates this type of experimental evaluation, where EMG measurements are used to assess nerve and muscle function after reinnervation. Several current studies still rely on animal models before implementation in human prosthetic applications, which allows controlled analysis of nerve regeneration, muscle response and signal evolution over time.

From a signal processing perspective, these studies show that reinnervated EMG is a promising but complex source of information. Current work mainly focuses on demonstrating functional recovery, signal detection and prosthetic control. However, fewer studies directly address how to separate a weak target EMG component when it is mixed with stronger donor muscle activity. This limitation connects the current advances in reinnervated EMG with the research gap identified in the last section.

2.4 Summary of source separation techniques in the literature

The previous sections show that source separation methods have been applied in different biomedical contexts, although with objectives that may differ from the specific problem addressed in this thesis.

Classical ICA methods, including FastICA, Infomax and JADE, are mainly based on statistical independence and have been widely used in EEG preprocessing, where they allow the separation of neural activity from artifacts. Their success in multichannel EEG has motivated their application to EMG, especially in high-density recordings where the distribution of the electrodes provides additional information about the muscular activity.

Other methods exploit different assumptions. SOBI uses delayed covariance matrices and is more appropriate when the sources present different temporal structures. Constrained ICA methods introduce prior information, reference signals or correlation constraints to guide the separation towards components with specific characteristics. Finally, regression approaches are practical when a reliable interference reference is available.

Table 2.1 summarizes the main techniques found in the literature, their typical application field and their relevance to the recovery of weak EMG components.

Technique	**Application field**	**Main observation**
ICA / FastICA	EEG preprocessing and EMG decomposition	Commonly used for artifact removal and source decomposition when the mixture is approximately linear and instantaneous [11], [14].
Infomax / JADE	Biomedical BSS, especially EEG	Alternative ICA implementations with similar assumptions [10].
SOBI	Signals with temporal structure	Useful when sources have different temporal patterns, but less robust when EMG activations are temporally similar [17].
Constrained ICA / 2CFastICA	HD-sEMG decomposition	Improves decomposition when useful prior information or references can guide the separation [15].
Regression-based methods	Interference reduction in biomedical signals	Practical when a reliable reference of the interference is available, but sensitive to delay, noise and reference contamination [18], [19].

Table 2.1: Summary of source separation techniques reported in the literature.

Overall, these methods have shown good results in EEG artifact removal and HD-sEMG decomposition. However, few studies focus specifically on the recovery of a weak EMG target source from an asymmetric mixture dominated by stronger muscle interference. This limitation motivates the research gap addressed in the following section.

2.5 Research gap

Previous studies have shown that BSS and semi-blind methods can be useful for biomedical signals, especially in EEG artifact removal and HD-sEMG decomposition [11], [15]. However, most of these works focus on artifact removal or motor unit decomposition, rather than on the recovery of a weak EMG source masked by a stronger interfering muscle component.

This limitation is especially relevant in reinnervated EMG, where donor muscles may contaminate the target signal [1], [16], [20]. In addition, standard separation methods assume instantaneous mixtures and comparable source contributions, assumptions that may be weakened by noise, source dominance and small temporal delays.

Therefore, this thesis addresses the gap between general EMG decomposition methods and the recovery of weak target components in reinnervated muscle recordings. In particular, it focuses on cases affected by stronger interference, additive noise and possible temporal delays.

Chapter 3
Methodology

In order to achieve the objectives presented in Section 1.4, this chapter establishes the methodological framework followed throughout this thesis. The purpose of this chapter is to define how the separation problem is approached, which data are used and how the different experiments are designed and evaluated.

To ensure that the study is carried out in a realistic and reproducible way, the chapter first describes the general approach adopted for the problem, including the separation algorithms considered and their motivation. Then, the two main datasets used in the project are discussed. Finally, the chapter describes the experimental procedure followed in each test, including the signal selection process, signal conditioning, mixing and evaluation metrics. For reference, Figure 3.1 shows a block diagram of procedure followed throughout the thesis for the experiments.

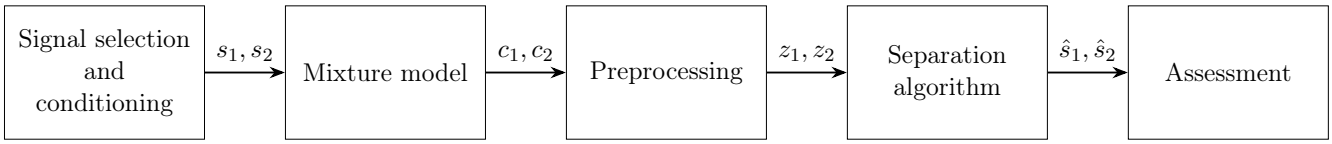

Figure 3.1: Block diagram of pipeline followed for the experiments in this thesis.

3.1 Problem modeling

This section introduces the signal model used throughout the thesis. Rather than attempting to describe the full physiological complexity of reinnervated EMG, the aim is to define a simplified mathematical framework that captures the main aspects relevant to source separation. The modeling approach is developed progressively. First, a general linear mixture model with multiple sources and observations is presented. After that, it is reduced to the two-source, two-channel case. Finally, it is specialized to the scenario of interest for the study, in which the target source is weaker and the donor-muscle contribution dominates one of the observed channels. For clarity, in the 2D cases, $\mathbf{s_1}$ denotes the **target flap-related source** and $\mathbf{s_2}$ the **donor-muscle source**.

3.1.1 General model

The recorded EMG channels are modeled as mixtures of latent source signals. In a general setting, let $s_1(t), s_2(t), ..., s_n(t)$ denote the underlying physiological sources and let $x_1(t), x_2(t), ..., x_n(t)$ denote the observed channels. Each observation is expected to contain a weighted contribution of all sources, together with an additive noise term. This model can be expressed as a system of linear equations as shown in equation 3.1. Under the simplest instantaneous linear model, the observation vector can also be written as a linear transformation of the source vector plus noise, as shown in equation 3.2.

$$\begin{cases} x_1(t) = a_{11}s_1(t) + a_{12}s_2(t) + \cdots + a_{1n}s_n(t) + n_1(t) \\ x_2(t) = a_{21}s_1(t) + a_{22}s_2(t) + \cdots + a_{2n}s_n(t) + n_2(t) \\ \qquad \vdots \\ x_n(t) = a_{n1}s_1(t) + a_{n2}s_2(t) + \cdots + a_{nn}s_n(t) + n_n(t) \end{cases} \tag{3.1}$$

$$x(t) = As(t) + n(t) \tag{3.2}$$

where a_{ij} represents the contribution of source j to observation i and A denotes the mixing matrix formed by the a_{ij} coefficients.

This representation alone is not intended to fully describe the physical propagation of EMG through human tissue. Since the electrical activity generated by nearby muscles does not reach all electrodes under exactly the same conditions, each observation may contain contributions that are not only attenuated, but also slightly delayed with respect to one another. These delays may arise from differences in propagation path, electrode position, tissue properties and the spatial distribution of the underlying sources [21]. As a result, the contribution of a given source to one channel does not necessarily appear at the same instant in another channel.

To account for this effect, the instantaneous mixture model can be extended by introducing delayed source terms. This leads to a convolutive mixture model, in which each observation depends on present and past values of the sources. However, for the purposes of this thesis, it is enough to only consider a single delay per channel and observation. This delay is implemented in equations 3.3 and 3.4, which represent the extended convolutive version of 3.1 and 3.2.

$$\begin{cases} x_1(t) = a_{11}s_1(t) + a_{12}s_2(t - \tau_{12}) + \cdots + a_{1n}s_n(t - \tau_{1n}) + n_1(t) \\ x_2(t) = a_{21}s_1(t - \tau_{21}) + a_{22}s_2(t) + \cdots + a_{2n}s_n(t - \tau_{2n}) + n_2(t) \\ \qquad \vdots \\ x_n(t) = a_{n1}s_1(t - \tau_{n1}) + a_{n2}s_2(t - \tau_{n2}) + \cdots + a_{nn}s_n(t) + n_n(t) \end{cases} \tag{3.3}$$

$$x(t) = A_\tau s(t) + n(t) \tag{3.4}$$

where τ_{ij} denotes the delay associated with the contribution of source j to travel to observation i. The notation A_τ is used as a compact representation of the delayed mixing model.

While the previous equations describe the general n-source case, the remainder of this chapter focuses on a two-source, two-observation model. This reduced formulation is the simplest one in which source separation remains meaningful and it already captures the main features of the problem studied in this thesis. Equation 3.5 shows the general delayed model in the two-dimensional case.

$$\begin{cases} x_1(t) = a_{11}s_1(t) + a_{12}s_2(t-\tau_{12}) + n_1(t) \\ x_2(t) = a_{21}s_1(t-\tau_{21}) + a_{22}s_2(t) + n_2(t) \end{cases} \tag{3.5}$$

3.1.2 Symmetric attenuation

The model introduced in the previous section can be considered as a standard *Blind Source Separation (BSS)* setting, since no prior information is assumed about the values of the mixing coefficients a_{ij} or about the properties of the original sources. However, given that this thesis aims to study specific scenarios related to the problem of interest, the current model proposed can be further improved by including additional information.

In invasive EMG (or in surface EMG of relatively isolated muscles), each recorded channel can be approximated as the sum of the intended target source and an interfering contribution from the other source. Although invasive recordings are usually more selective than surface EMG, they do not guarantee perfect source isolation, since the adjunct muscular activity can still interfere with the measured channel [22], [23]. Each channel is assumed to be dominated by its corresponding source, so the direct coefficients are simplified to $a_{ii} = 1$. If both muscles are equally dominant and their interference is balanced, the off-diagonal terms can be expressed by a parameter β, where $a_{ij} = \beta$ for $\forall i \neq j$. Equation 3.6 expresses the new model after taking into account these two considerations.

$$\begin{cases} x_1(t) = s_1(t) + \beta s_2(t-\tau_{12}) + n_1(t) \\ x_2(t) = \beta s_1(t-\tau_{21}) + s_2(t) + n_2(t) \end{cases} \tag{3.6}$$

3.1.3 Weak-source regime

Unfortunately, in reinnervated muscle configurations, the interaction between the two muscular contributions is not necessarily balanced. In some cases, one source may display a stronger influence on the observed mixtures than the other, so the coupling between channels cannot always be assumed to be symmetric. In fact, in procedures like VDMT, the contribution of the auxiliary muscle over the target flap-related source (a_{12}) is generally greater than the reverse interaction (a_{21}), which can barely be noticed in the auxiliary muscle observation. Mathematically, this can be expressed as $\mathbf{a_{21}} = \alpha$ with $\alpha << \mathbf{1}$ (for most experiments $\alpha \approx \mathbf{0.01}$). Equation 3.7 reflects the mentioned piece of information.

$$\begin{cases} x_1(t) = s_1(t) + \beta s_2(t-\tau) + n_1(t) \\ x_2(t) = \alpha s_1(t-\tau) + s_2(t) + n_2(t) \end{cases} \tag{3.7}$$

With these assumptions, this last model may also be viewed as a regression problem, where one channel consists of a dominant source and scaled interfering contribution that can be measured as a reference. However, the central perspective of this thesis remains that of a signal separation problem, since the objective is to discuss general scenarios, even those where there is no reliable reference. A regression formulation will be revisited later in the thesis for comparison, together with its main advantages and limitations.

One final note about this model is that since the tissue propagation is generally assumed to attenuate rather than amplify cross-talk contributions, the β parameter is restricted to the interval $[0, 1]$. However, it can be expected that the variance of the auxiliary signal $\text{Var}(s_2)$ is greater than the variance of the target flap-related source $\text{Var}(s_1)$, which will favor the recovery of the auxiliary muscle source.

3.2 Approach

Each proposed algorithm is addressed in a dedicated chapter, where its mathematical foundations, main assumptions, implementation details and other considerations are presented. This structure allows each method to be first introduced from a theoretical perspective, explaining the principles on which it is based and the conditions under which it is expected to perform successfully.

Additionally, each algorithm chapter contains a section dedicated to experimental evaluation of the specific method. In these sections, the algorithm is applied to the specific models and test scenarios to assess the performance with the metrics defined in this methodology chapter.
The main algorithms and their key principle are enumerated for reference.

- **Independent Component Analysis (ICA)**

  ICA exploits non-Gaussianity to find the rotation that best separates the original sources. This algorithm and its results are discussed in **Chapter 5**.

- **Second Order Blind-Identification (SOBI)**

  SOBI separates signals in mixtures by exploiting the temporal correlation of the sources. This algorithm and its results are discussed in **Chapter 6**.

- **Constrained ICA**

  Constrained Independent Component Analysis builds on the traditional ICA separation method by adding problem specific constraints to guide the separation towards the correct solution in case of ambiguity. This algorithm and its results are discussed in **Chapter 7**. Additionally, **linear regression** is also addressed in this chapter.

For the planning of the thesis, Figure 3.2 shows the chronogram included in the bachelor's thesis proposal, detailing the estimated time allocated to each task. It

should be noted that this schedule was an initial approximation made before the development of the project. In fact, a considerable portion of the time allocated to ICA was redistributed to constrained ICA. Nevertheless, the overall planning has been followed throughout the work.

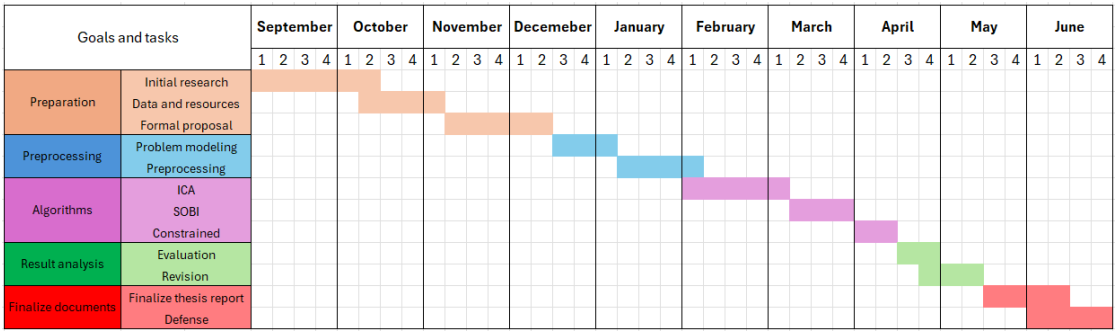

Figure 3.2: Estimated work chronogram presented in the bachelor's thesis proposal.

3.3 Datasets

The experiments performed in this thesis mainly use two distinct datasets: a real TMR EMG dataset and a synthetic dataset. The real dataset provides physiological EMG recordings, while the synthetic dataset enables controlled experiments that would be difficult to perform using publicly available data. Together, they allow the algorithms to be evaluated under realistic and simulated conditions.

3.3.1 TMR patients dataset

This dataset was collected as part of a study on myoelectric prosthesis hand grasp control in individuals with unilateral transradial amputation [24]. This data is particularly relevant to this thesis since it provides physiological EMG data of patients **before and after reinnervation procedures** (TMR). This may be useful to both understand the characteristics of these signals as well as test the quality of separation algorithms on these signals. For clarity, the main characteristics of the dataset are summarized below.

- Six individuals with unilateral transradial amputation.
- EMG recorded before and after TMR surgery.
- 32 bipolar EMG channels placed along the residual forearm.
- Multiple hand, finger, wrist and rest movements.
- Each contraction was held for 2 seconds and repeated 8 times.
- Sampling frequency: 1000 Hz.

To provide context for the possible relationships between EMG channels, Figure 3.3 illustrates the 32 channel electrode placement for patient TR2. For further reference, the electrode configurations of the remaining five patients are included in the original dataset description [24].

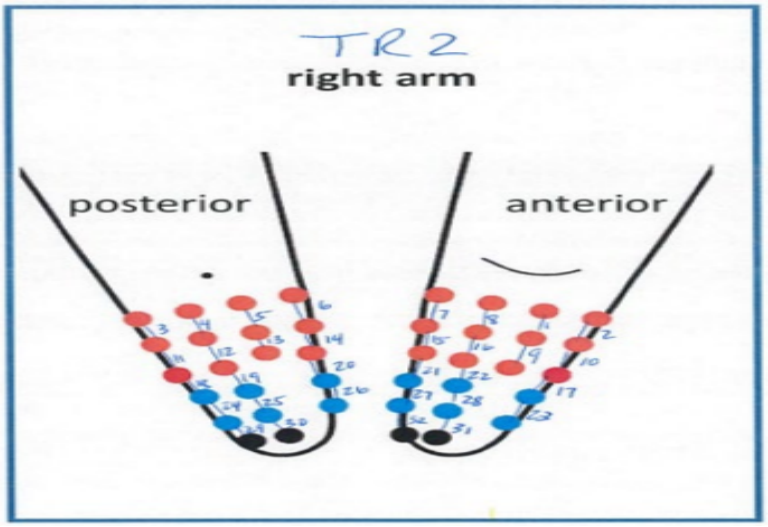

Figure 3.3: Electrode placement for patient 2 of the TMR database. Both anterior and posterior views are shown for reference [24].

3.3.2 Synthetic Dataset

This dataset is designed to test source separation under controlled conditions, especially when the muscle sources present clearly different activation patterns and signal amplitudes. Since EMG data with these specific characteristics are not easily available in public datasets, synthetic signals were generated following realistic EMG properties [25]. This dataset is mainly used for the experiments presented in Chapter 6.

Figure 3.4 presents an example of the synthetic signals generated for the experimental tests. Further details on the signal generation process are provided in **Appendix II.1.1**.

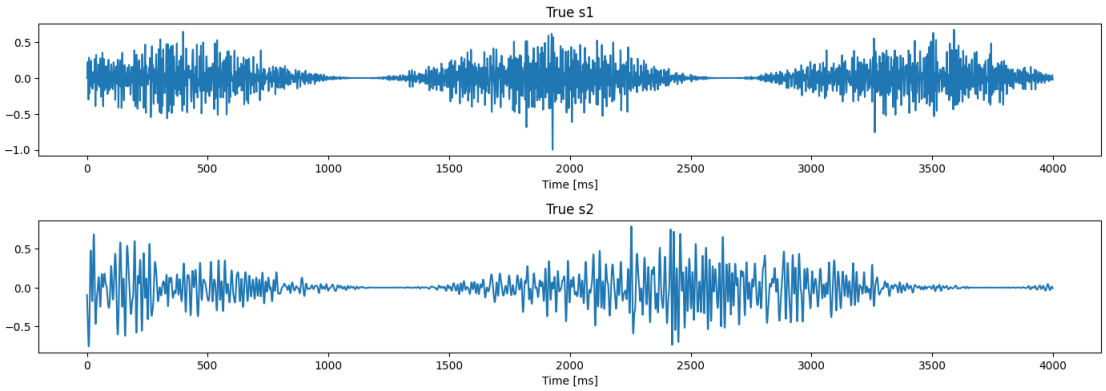

Figure 3.4: Example of synthetic signals generated for the artificial dataset.

3.4 Experimental procedure

This final subsection aims to establish and clarify the procedure followed when performing the experiments. An important clarification is that the experiments are performed with preprocessed signals, but the original sources are represented before the whitening step (see Chapter 4 for reference). It is also important to note that, since the synthetic dataset was designed for this thesis, it already includes the considerations mentioned in Subsection 3.4.1 and 3.4.2.

3.4.1 Signal selection

For simplification, the experiments performed throughout this thesis assume that the target flap related source is statistically independent from the donor muscle source. Therefore, when utilizing the TMR dataset, it is vital to perform the experiments with two independent EMG channels. Figure 3.5 illustrates the simplified correlation matrix for patient TR2 (post TMR surgery), which is the main subject selected for the experiments.

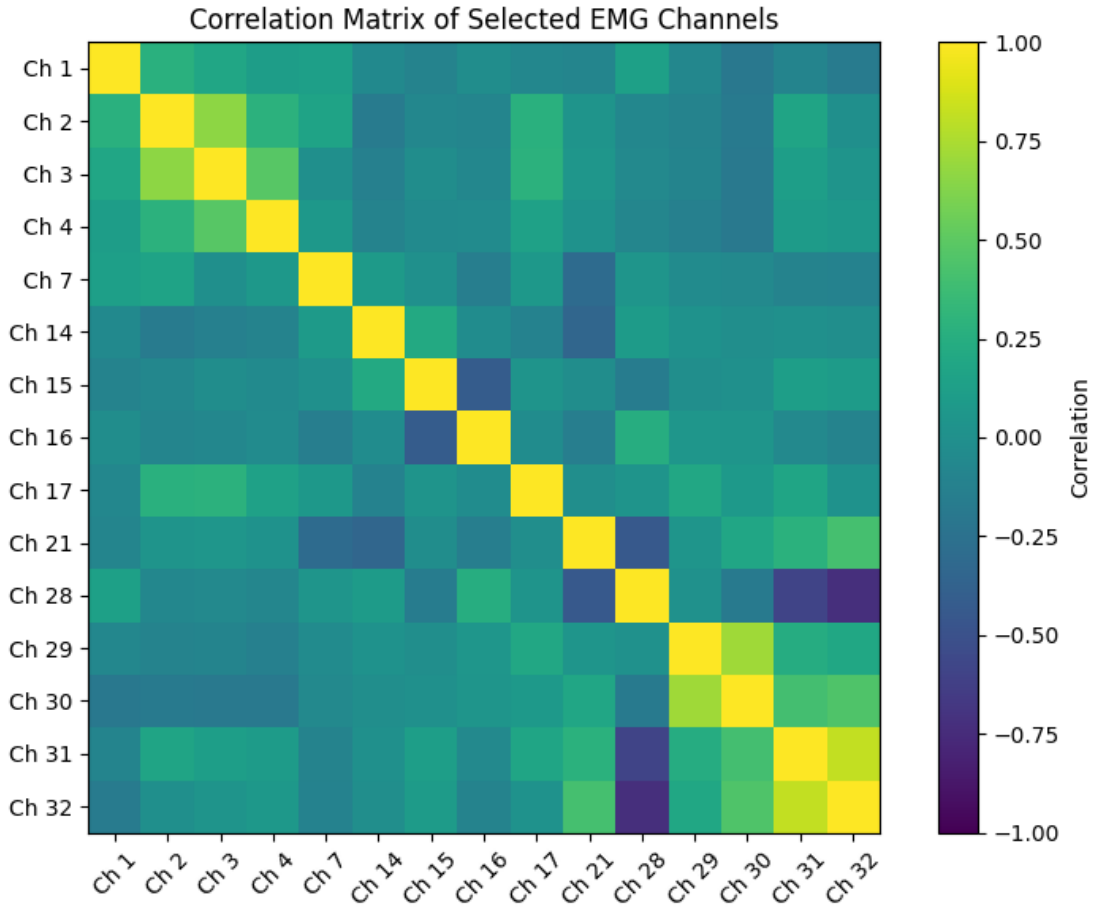

Figure 3.5: Correlation matrix of EMG channels in the TMR dataset. This figure is a reduced version of the original 32x32 correlation matrix.

Some adjacent channels show strong correlation, suggesting that they likely capture EMG activity from the same motor unit or nearby muscle regions. However, adjacency in channel number does not always lead to strong correlation, since the electrode configuration is not purely sequential as shown in Figure 3.3. For example, channels 31 and 32 present one of the strongest correlations because they are physically close to each other. By contrast, the correlation between channels 16 and 17 is considerably less significant, despite being consecutive channel numbers.

For this reason, to satisfy the statistical independence condition, channels with negligible correlations are selected for the experimentation. **Channels 4 and 21** are chosen for the main experiments shown in the algorithm chapters, while **channels 7 and 28** are used for the weak source and noise discussions.

3.4.2 Signal conditioning

Since in the IIT study these EMG signals can be either activated simultaneously or at different times, it can be of interest to adapt the selected sources to reflect this key aspect. For this reason, arbitrary binary masks were applied to the TMR dataset signals to simulate this effect. **See Appendix II.1.2 for reference.** Figure 3.6 shows a visual representation of how these EMG signals are adapted to satisfy this key aspect.

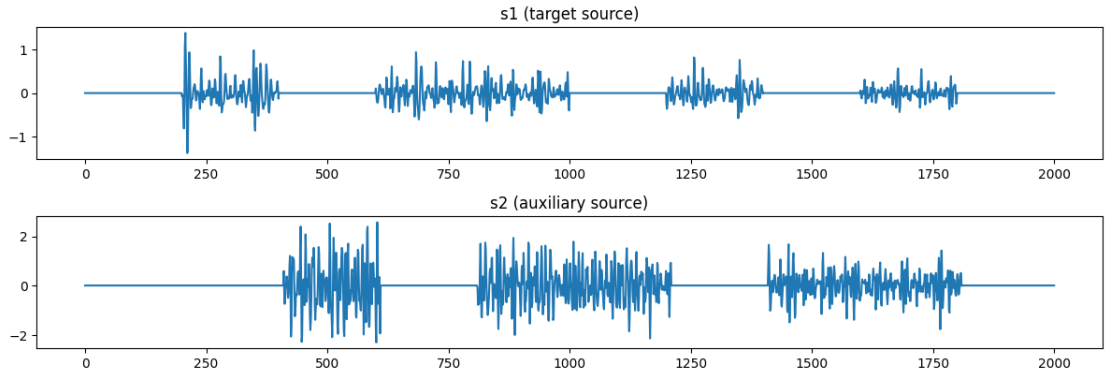

Figure 3.6: Example of the signal conditioning used to adapt the EMG signals from the TMR database to the considerations of this study. Signals are not always simultaneously activated. Instead their activations can be simultaneous or at different periods.

3.4.3 Mixing models

To simulate the effect of muscles interference and reinnervation, different mixing models are considered in order to evaluate the separation performance under different scenarios. Though chapter 3.1 provides a more detailed discussion of the mixing models considered for this work, Figure 3.7 shows an example of how the signals selected in Figure 3.6 are combined following the model described in Section 3.1.3, which is the model of main interest of this thesis. Equation 3.8 shows this model again for reference.

$$\begin{cases} x_1(t) = s_1(t) + \beta s_2(t-\tau) + n_1(t) \\ x_2(t) = 0.01 s_1(t-\tau) + s_2(t) + n_2(t) \end{cases} \tag{3.8}$$

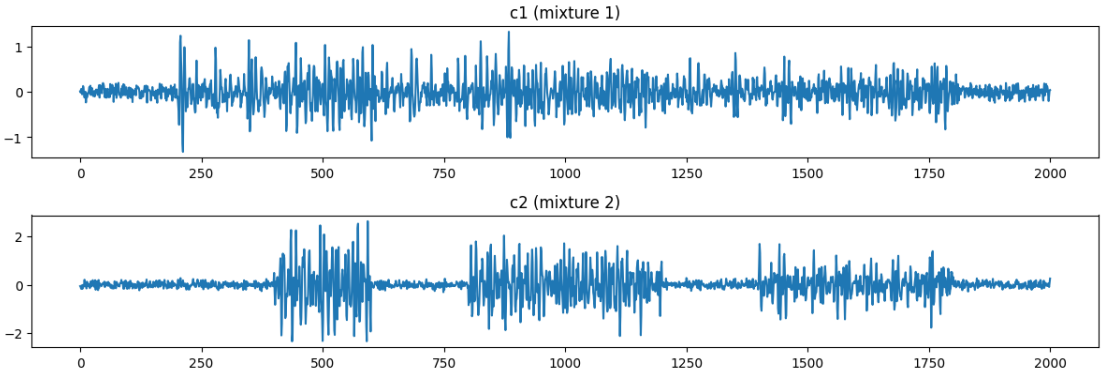

Figure 3.7: Example of source mixing following the model detailed in Section 3.1.3. Parameters were set to $\beta = 0.3$, $\sigma = 0.1$ and $\tau = 10\,\text{ms}$.

3.4.4 Metrics

Given the nature of this study, it is crucial to define a series of metrics to be able to quantify the performance of the mentioned algorithms in the different models and scenarios tested. Therefore, this subsection provides an enumeration of the metrics evaluated in this thesis, ranked by their importance when assessing the algorithms for the study. For clarification, the estimated source is $\hat{s}_1$ and the original source is s_1. The operator $\rho(\cdot,\cdot)$ denotes the Pearson correlation coefficient and RMS$(\cdot)$ refers to the RMS envelope of a specific signal. Equation 3.9 shows their mathematical expressions.

$$\rho(x,y) = \frac{\text{cov}(x,y)}{\sigma_x \sigma_y}, \qquad \text{RMS}(x)[k] = \sqrt{\frac{1}{N_w}\sum_{n=1}^{N_w} x_k^2[n]} \tag{3.9}$$

1. **RMS envelope correlation**

$$\text{Corr}_{\text{RMS}}(s_1, \hat{s}_1) = \rho\left(\text{RMS}(s_1), \text{RMS}(\hat{s}_1)\right)$$

This metric measures how well the estimated source preserves the activation pattern of the original signal through its RMS envelope rather than directly comparing the waveform sample by sample. Its scale varies from -1 to 1, where negative values indicate inverse relationship.

2. **Temporal correlation**

$$\text{Corr}(s_1, \hat{s}_1) = \rho(s_1, \hat{s}_1)$$

This metric measures the similarity between the original and estimated raw waveforms. It evaluates how accurately the algorithm identifies the temporal structure of s_1 sample by sample. Its scale is the same as RMS envelope correlation.

3. **Signal-to-noise ratio**

$$\text{SNR}_1 = \frac{\text{Var}(s_1)}{\text{Var}(error)}$$

This metric measures the ratio of the power (or indirectly of variance) of the original target source and the power of the reconstruction error. Higher values indicate that the estimated source is closer to s_1 and contains less residual interference.

Out of the three presented metrics, the RMS envelope correlation is considered the most relevant metric because EMG-based prosthetic control mainly depends on the preservation of the activation pattern rather than on the exact reconstruction of each individual sample. However, if in some cases temporal correlation is optimized, this implies that activation patterns from the original sources are also recovered.

Chapter 4

Preprocessing

Before testing and assessing source separation algorithms, the raw EMG recordings must be transformed to facilitate the signal analysis. This preprocessing stage is especially important in this work because the objective is not only to visualize or classify EMG activity, but to separate weak target components from stronger interfering muscular sources. Therefore, small differences in amplitude, noise level or signal spectral structure can strongly affect the behavior of ICA, SOBI and the constrained separation methods considered later in this work.

As mentioned in section 3.3.1, the dataset used in this study is 32 channel surface EMG. This chapter will mention the preprocessing for the TMR dataset, but it may also be applied to 2 channel invasive measurements, like in the IIT study.

The preprocessing pipeline developed in this work includes three main stages. First, the observed signals are filtered to eliminate any artifacts or interferences that contaminate the EMG signal during the recording. After this, each channel is scaled to fairly compare different muscle signals. Finally, the observations are whitened to decorrelate the signals and facilitate the separation process. Figure 4.1 shows a conceptual diagram to better understand this pipeline.

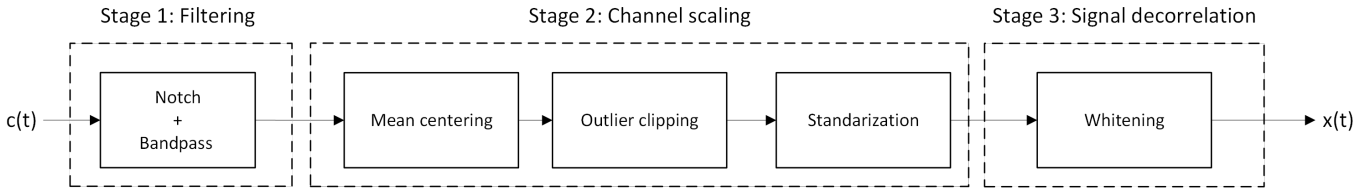

Figure 4.1: Preprocessing pipeline applied to the observed EMG mixtures $c(t)$ to transform data into valid inputs $x(t)$ for the separation algorithms. The pipeline is divided into three stages: filtering, channel scaling and signal decorrelation.

4.1 Filtering

Raw EMG recordings may often contain undesired components introduced by noise, movement artifacts, baseline drift and other possible sources of interferences. For this reason, the first step in the preprocessing pipeline must reduce these unwanted components. Separation algorithms rely on series of assumptions, such as covariance and autocorrelation of the signals, that would not hold without reducing these components.

Additionally, since we are also contemplating a possible live implementation, the selected approach prioritizes a low-complexity **causal filter with reduced**

delay while also still providing sufficient attenuation outside the selected EMG band.

4.1.1 Filter design

In order to design the filter, a desired EMG band must be identified first. Generally, the relevant EMG content is considered to lie approximately within the 20 Hz to 450 Hz range [26]. Additionally, in many real-life situations, there is a power line interference at 50 Hz or 60 Hz, which pollutes the EMG passband. Given the causality and low delay requirements, the best approach is to mainly consider low order IIR filters. Even though higher order filters would provide steeper transitions, they increase the phase distortion and group delay, which directly affect the real-time analysis of the EMG signals. For simplification, this study mainly considers **Butterworth** filter design, since its smooth and flat passband response helps preserve the relevant EMG components without passband ripple. Alternatively, a Bessel filter would better preserve the waveform, but this is less critical for the present analysis and Butterworth provides a sharper transition band.

Consequently, this first preprocessing stage must design two filters to address these two specific aspects: a power-line removal filter and an EMG frequency range filter.

Power-line removal filter

This filter intends to specifically remove the artifact associated with the power line interference. Since the dataset was collected in the United States, this interference is expected to be located around 60 Hz. For notch specific characteristics, it is necessary to determine a reasonable stopband to ensure that the power-line interference is minimized. A common notch bandwidth estimation is the one shown in Equation 4.1, where Q is the quality factor and f_{remove} is the notch center frequency. Once the bandwidth is obtained, the lower and upper cutoff frequencies can be defined by assuming symmetric rejection band around f_{remove}[27].

$$BW = \frac{f_{remove}}{Q}, \quad f_1 = f_{remove} - \frac{BW}{2}, \quad f_2 = f_{remove} + \frac{BW}{2} \tag{4.1}$$

In this work, $f_{remove} = 60\,\text{Hz}$ and $Q = 30$ were selected, resulting in a bandwidth of $BW = 2\,\text{Hz}$. Consequently, the cutoff frequencies used for the notch filter are $f_1 = 59\,\text{Hz}$ and $f_2 = 61\,\text{Hz}$. Given all these considerations, the final notch filter characteristics are listed below:

- **Response type**: Bandstop
- **Design method**: Butterworth (approx $-3\,\text{dB}$ at cutoff frequencies)
- **Order**: 2
- **Cut-off frequencies**:
  - $f_1 = 59\,\text{Hz} \implies \omega_1 = 2\pi\frac{59}{1000} = 0.118\pi\,\text{rad/sample}$.

– $f_2 = 61\,\text{Hz} \implies \omega_2 = 2\pi\frac{61}{1000} = 0.122\pi\,\text{rad/sample}.$

Figure 4.2 shows the magnitude response of the designed filter, which effectively attenuates the 60 Hz component while preserving the neighboring frequencies. This is especially important since these frequencies may contain useful information about the EMG signal.

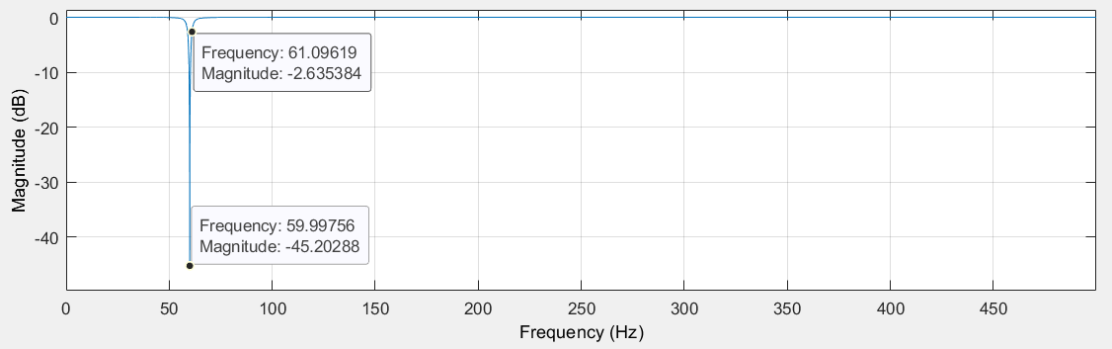

Figure 4.2: Magnitude response of the designed notch filter. The frequency component at 60 Hz is attenuated while having minimal effect on the EMG band.

However, the main drawback of this design is the considerable variation in group delay around the power-line frequency. As shown in Figure 4.3, the delay near cutoff frequencies reaches approximately 73-74 samples and remains high over the closer frequencies before decreasing.

This may impact the temporal structure of the signal components close to 60 Hz. Even considering this effect, the IIR notch filter remains a realistic option for live implementation. In real world scenarios, the preferred solution would be to reduce the power-line interference at the signal acquisition stage instead of relying on digital signal processing. For this study, the anti-causal tool ***filtfilt*** is used in order to prevent this major effect.

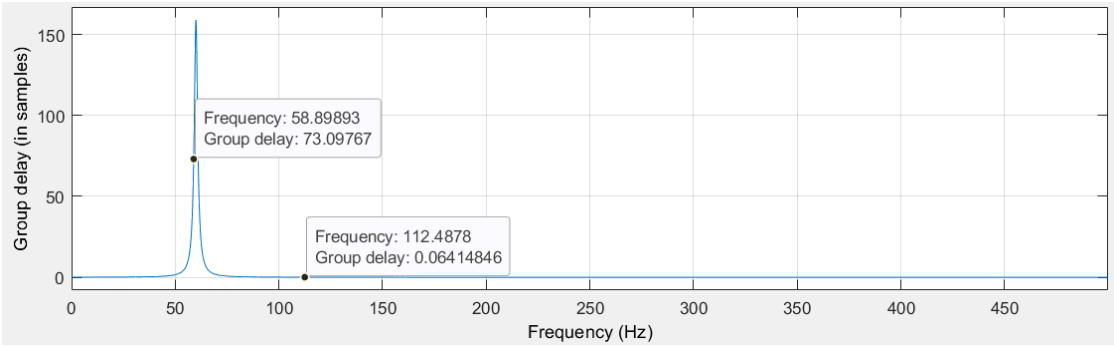

Figure 4.3: Group delay of the designed notch filter. The cut-off frequencies experience a delay around 73 samples which has to be considered when processing the signal. The best option in real world cases is to minimize power-line interference beforehand.

EMG Frequency Range Filter

Once the main power-line artifact has been attenuated, the next step is to retain only the frequency range that contains relevant EMG information, while suppressing components outside this range. For this reason, a filter with the following characteristics is needed:

- **Response type**: Bandpass
- **Design method**: Butterworth
- **Order**: 2
- **Cut-off frequencies**:
  - $f_{HP} = 20\,\text{Hz} \implies \omega_{HP} = 2\pi\frac{20}{1000} = 0.04\pi\,\text{rad/sample}.$
  - $f_{LP} = 450\,\text{Hz} \implies \omega_{LP} = 2\pi\frac{450}{1000} = 0.9\pi\,\text{rad/sample}.$

The magnitude and phase responses of the designed IIR Butterworth filter are shown in Figure 4.4. The magnitude response confirms that the filter preserves the mentioned EMG passband while attenuating the frequency components outside the range, showing a $-3\,\text{dB}$ attenuation at the cutoff frequencies. Additionally, phase response shows a non-linear phase behavior which leads to different frequency components experiencing different phase shifts.

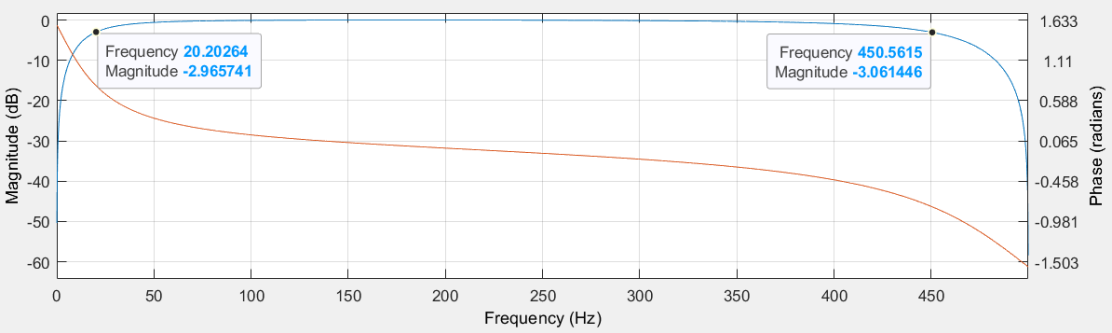

Figure 4.4: Magnitude and phase response of the designed bandpass filter.

To better understand this effect, Figure 4.5 shows that the delay experienced at f_H is around 4 samples, which at f_s =1 kHz is about 4 ms. This delay decays over the 20-100 Hz band to approximately 0.21 ms and then increases across the 400 Hz to 450 Hz band, reaching around 1.68 ms. Although group delay often introduces frequency dependent temporal distortion, the magnitude of these delay variations is small compared to the duration of the signal and EMG activation. For this reason, the effect can be considered negligible for the posterior processing of the signal.

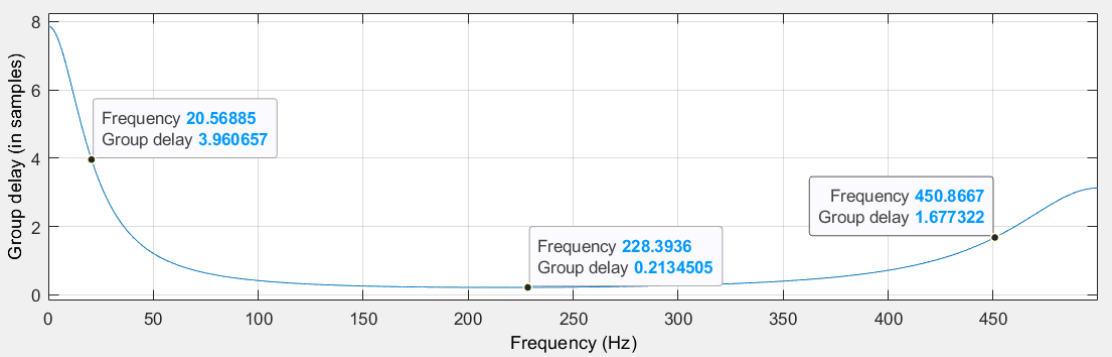

Figure 4.5: Group delay of the designed bandpass filter. Although a Bessel filter would provide a more constant delay, the Butterworth filter has a lower and nearly constant group delay within the EMG bandwidth.

4.1.2 Filtering results

This section aims to evaluate the effect of the discussed filtering stage on the recorded EMG signals. To illustrate the filtering results, channel 1 is used as a representative example. The signal is analyzed both in the time domain and in the frequency domain before and after filtering. Although only one channel is shown, the same filtering procedure was applied to all channels.

Time-Domain Analysis

Given that EMG mainly conveys information about motor unit activation, this analysis should mainly focus on the RMS envelope of the signal in the time-domain. Figure 4.6 compares the RMS envelope of Channel 1 before and after filtering. The filtered signal presents a lower RMS amplitude due to the attenuation of undesired frequency components. However, the main EMG activation peaks still occur at approximately the same moments and the overall envelope shape is preserved. This suggests that the filtering stage reduces the artifacts without significantly altering the temporal activation pattern of the signal.

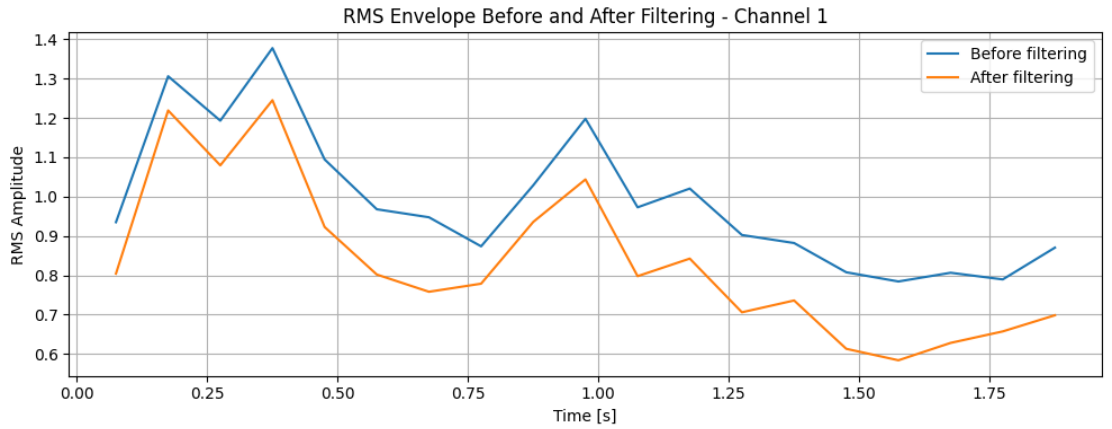

Figure 4.6: Envelope comparison of filtered and unfiltered EMG channel 1 signal.

Frequency-Domain Analysis

The main goal of this analysis is to assess whether the designed filtering stage manages to remove undesired frequency components while preserving the original EMG frequency range. For this reason, the FFT magnitude spectrum and the power spectral density (PSD) of channel 1 were compared before and after filtering. Figure 4.7 shows the frequency-domain comparison, which shows that the filtering stage attenuates the frequencies associated with the power-line interference as well as components outside the mentioned EMG band. The PSD of both unfiltered and filtered EMG signals, which confirms that the filtering stage manages to retain only the useful EMG frequencies.

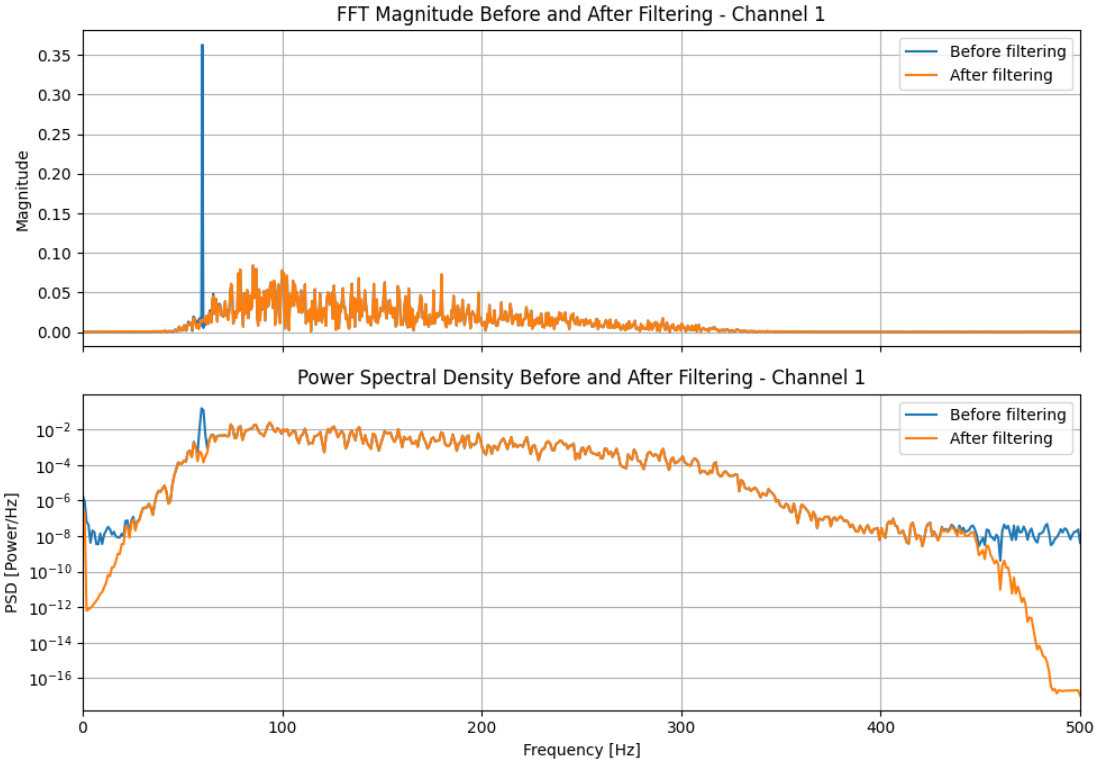

Figure 4.7: Comparison of the FFT and PSD of Channel 1 before and after filtering. In regions where both signals have similar values, the filtered curve appears superimposed on the unfiltered curve. It is also worth mentioning that the FFT magnitude plot is in natural scale while PSD is in logarithmic scale.

4.2 Channel scaling

The goal of this section is to transform the recorded channels to a comparable numerical scale. This is especially important for multichannel EMG, since impedance, amplification or distance can make some channels dominate the covariance matrix even if they are not the most informative channels physiologically. Therefore, in this study, channel scaling is established as the combination of mean centering, outlier clipping and standardization as shown in Figure 4.1. However, it is impor-

tant to note that scaling is mainly used to improve the numerical behavior of the separation algorithms rather than to interpret the final source amplitudes directly.

4.2.1 Mean centering

Mean centering mainly intends to remove the DC component of each channel. Even though the EMG signal should ideally be zero mean after the filtering stage due to the bandpass filter, small offsets or motion artifacts may remain. This step is also required before covariance estimation and whitening. Considering the 32 channel EMG dataset, Equation 4.2 shows the mathematical procedure used for mean centering.

$$\mu_j = \frac{1}{N}\sum_{n=1}^{N} x_j[n], \qquad x_{c,j}[n] = x_j[n] - \mu_j \quad \forall j = 1, 2, \ldots, N \tag{4.2}$$

4.2.2 Outlier clipping

The next step in the preprocessing is to apply outlier clipping to each observed EMG channel. The objective of this stage is to limit isolated high-amplitude artifacts that could affect the RMS normalization and the covariance estimation used in later stages. This is especially relevant in the weak-source model considered in this work (section 3.1.3) where the target source may be masked by a dominant component. To perform this operation, a robust median and median absolute deviation (MAD) criterion is used, since it is less sensitive to extreme values than mean and standard deviation thresholds[28]. This choice is also motivated by the presence of transient artifacts and noise contamination in EMG recordings [29].

For each observed channel $c_j[n]$, the median and median absolute deviation are computed as shown in Equation 4.3. Afterwards, the signal is then clipped to a channel-dependent interval. Equation 4.4 depicts the mathematical expression for the clipping, where k is a parameter that controls the clipping threshold in terms of MAD units.

$$m_j = \text{median}\left(x_j[n]\right), \quad \text{MAD}_j = \text{median}\left(|x_j[n] - m_j|\right) \quad \forall j = 1, 2, \ldots, N \tag{4.3}$$

$$x_{\text{clip},j}[n] = \min\left(\max\left(x_j[n],\, m_j - k\,\text{MAD}_j\right),\, m_j + k\,\text{MAD}_j\right) \quad \forall j = 1, 2, \ldots, N \tag{4.4}$$

In this study, $k = 8$ was selected as a conservative threshold. Since clipping is a nonlinear operation, the value of k should be large enough to avoid attenuating actual EMG bursts, especially those related to the weak target component.

4.2.3 RMS normalization

After outlier clipping, each observed EMG channel is normalized by its RMS value. This step places all channels on a comparable energy scale before whitening and

source separation.

$$z_j[n] = \frac{x_{\text{clip},j}[n]}{\text{RMS}_j + \varepsilon} \quad \forall j = 1, 2, \ldots, N \tag{4.5}$$

where ε is a small constant added to avoid indetermination problems when the RMS value is close to zero. Unlike the traditional z-score standardization, this operation does not subtract the mean during the scaling stage, as the mean centering has already been applied previously in 4.2.1.

4.3 Whitening

Whitening is the last stage of the preprocessing pipeline. Its objective is to transform the scaled observations into a new representation whose components are uncorrelated and have unit variance. This step is especially useful before applying source separation algorithms as it removes second-order dependencies between channels and simplifies the conditioning of the problem.

Instead of describing the complete whitening derivation, this section only introduces its practical effect on the preprocessed EMG signals. Let $\mathbf{X}_{\mathbf{scaled}}$ denote the centered channel-scaled observation matrix and $\mathbf{Z}$ the whitened data. The whitening transformation is expressed as a linear transformation applied to the centered observations:

$$\mathbf{X}_w = \mathbf{P}\,\mathbf{X}_{\mathbf{scaled}} \tag{4.6}$$

where $\mathbf{P}$ represents the whitening transformation. The main idea of this operation is to obtain transformed observations whose covariance matrix is approximately equal to the identity matrix.

$$\text{Cov}(\mathbf{X}_w) \approx \mathbf{I} \tag{4.7}$$

This means that the resulting components are decorrelated and normalized to unit variance. Figure 4.8 shows this effect in a two-dimensional example. After whitening, the data are projected into a representation with approximately circular covariance, which simplifies the subsequent source separation stage.

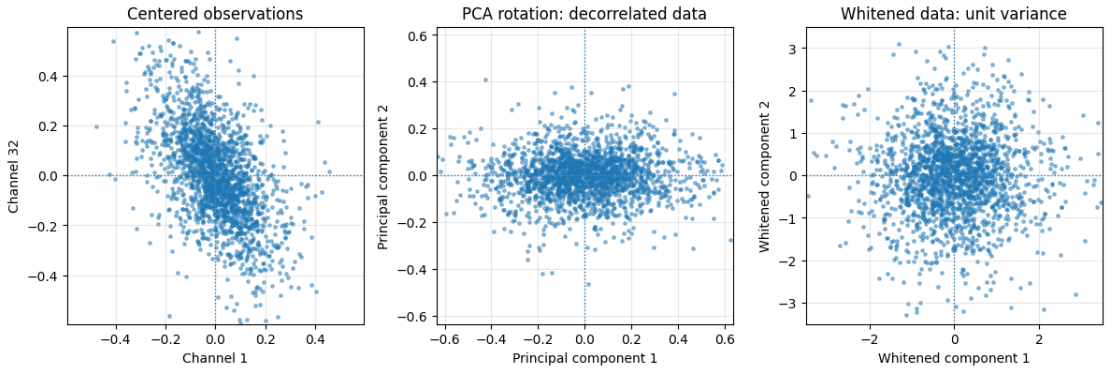

Figure 4.8: Visual whitening process for channels 1 and 32

It is important to note that whitening does not perform source separation by itself. It only removes linear correlation and normalizes the variance of the observed components. Therefore, the resulting signals are decorrelated but not necessarily statistically independent. The remaining separation must be carried out by the subsequent algorithms, such as ICA, SOBI or constrained ICA. A more detailed geometric interpretation of whitening in the context of ICA is presented later in Section 5.3.

4.4 Considerations for real-time preprocessing

Though the first filtering stage is designed to be implemented live, the channel scaling and signal decorrelation stages are inherently offline. Since the experiments of this thesis are mainly carried out with a prerecorded dataset, this may not result in a problem, but for real prosthetic implementation one of the following approaches should be considered:

- **Fixed calibration strategy**

Preprocessing parameters are estimated once during an initial calibration stage:

$$\mu_j, \quad \mathrm{MAD}_j, \quad \mathrm{RMS}_j, \quad \mathbf{P}$$

where $\mathbf{P}$ denotes the whitening matrix. These values are then kept fixed during online operation:

$$\text{calibration data} \rightarrow \text{parameter estimation} \rightarrow \text{fixed online preprocessing}$$

This approach is simple and stable, but assumes that the recording conditions do not change significantly after calibration.

- **Sliding window adaptive strategy**

Preprocessing parameters are continuously updated using the most recent L samples:

$$\mu_j[n], \quad \mathrm{MAD}_j[n], \quad \mathrm{RMS}_j[n], \quad \mathbf{P}[n]$$

This allows the system to adapt over time:

$$\text{recent window} \rightarrow \text{updated parameters} \rightarrow \text{adaptive online preprocessing}$$

However, the main trade-off of this approach is:

$$L \uparrow \Rightarrow \text{more accurate estimates, higher delay}$$

$$L \downarrow \Rightarrow \text{lower delay, noisier estimates}$$

Given all these considerations, calibration-based preprocessing may be more stable and easier to implement if there is reliable calibration data. Otherwise, a sliding window approach is more adaptive but may introduce significant latency when preprocessing the EMG signals.

Chapter 5

Independent Component Analysis

Independent Component Analysis (ICA) is a fundamental processing technique within Blind Source Separation aimed at recovering latent source signals from observed mixtures without any prior knowledge of the sources or mixing process [30]. As mentioned in previous sections, EMG signals may benefit from this powerful tool as it allows to decompose multichannel recordings into meaningful physiological components, potentially corresponding to muscle and neural sources.

This section introduces the mathematical formulation and derivation of ICA as well as its basic assumptions and principles. Additionally, a widely used implementation (FastICA) is described, followed by a discussion of ICA's challenges and limitations.

5.1 Problem formulation

ICA is originally formulated for linear and instantaneous mixing models. Let $s(t) = [s_1(t), ..., s_n(t)]$ be an array of source signals and $x(t) = [x_1(t), ..., x_n(t)]$ the recorded mixtures. The relationship between both is then given by:

$$x(t) = As(t) + n(t) \tag{5.1}$$

where $\mathbf{A}$ is an unknown mixing matrix and $\mathbf{n}(t)$ represents additive noise.

Considering the given case, the objective of ICA is to estimate a separating matrix $\mathbf{W}$ such that:

$$\hat{\mathbf{s}}(t) = \mathbf{W}\mathbf{x}(t) \tag{5.2}$$

recovers the original sources with no prior information.

However, the recovery of the sources is subject to inherent ambiguities. In particular, ICA cannot determine the original scaling or ordering of the sources. This is due to the fact that any scaling or permutation applied to the sources can be compensated by the mixing matrix without affecting the observed signals. As a result, the estimated sources can be expressed as:

$$\hat{\mathbf{s}}(t) = \mathbf{P}\mathbf{D}\mathbf{s}(t) \tag{5.3}$$

where $\mathbf{P}$ is a permutation matrix and $\mathbf{D}$ is a diagonal scaling matrix. These ambiguities are inherent to the ICA algorithm and, for that reason, the original order and amplitude of the sources cannot be uniquely determined by the observed mixtures.

5.2 Assumptions of ICA

The ICA framework relies on a set of assumptions that ensure the identifiability of the source signals from the observed mixtures. These assumptions are fundamental to the correct operation of the algorithm and must be considered when applying ICA to real-world signals such as EMG.

- **Statistical independence** $\rightarrow p(s_1, s_2, ..., s_n) = p(s_1)p(s_2)...p(s_n)$

  The source signals $s_i(t)$ are assumed to be mutually independent. This is the key assumption of ICA, as the separation is achieved by maximizing statistical independence between the estimated components.

- **Non-Gaussianity**

  At most one source is allowed to follow a Gaussian distribution. ICA exploits higher-order statistics (such as kurtosis or negentropy) to separate signals and therefore relies on the non-Gaussian nature of the sources.

- **Linear instantaneous mixing**

  The observed signals are assumed to be linear combinations of the sources without temporal delays. If this were not true, there could not be any static matrix $\mathbf{A}$ that represents the mixing.

- **Full-rank mixing matrix**

  The mixing matrix $\mathbf{A}$ must be invertible. This ensures that the sources can potentially be recovered from the mixtures.

- **Number of observations** $\rightarrow n_{mixtures} \geq n_{sources}$

  The number of observed mixtures must be greater than or equal to the number of sources, allowing the separation problem to be well-posed.

In practice, these assumptions are only approximately satisfied, particularly in biomedical applications such as EMG signal processing. For example, sources may show partial statistical dependence, the mixing process may include delays and measurements are typically affected by noise. These non-idealities from real world applications can significantly impact the performance of ICA-based methods.

5.3 ICA derivation (2D)

To gain further understanding of the ICA process, a geometric and mathematical derivation is presented in the two-dimensional case, which corresponds to the specific model analyzed in this work.

Let $\begin{pmatrix} x_1(t) \\ x_2(t) \end{pmatrix} = \overbrace{\begin{pmatrix} a_{11} & a_{12} \\ a_{21} & a_{22} \end{pmatrix}}^{\mathbf{A}} \begin{pmatrix} s_1(t) \\ s_2(t) \end{pmatrix}$, where $x_1(t)$ and $x_2(t)$ are coordinates of $X(t)$ in $\mathbb{R}^2$. Since we do not know the values of $a_{i,j}$ the problem cannot be solved by simply calculating $W = A^{-1}$. Instead, the proposed objective is to find a series of transformations that recover a new coordinate system in which components are statistically independent. For this reason, the mixing matrix $\mathbf{A}$ can be interpreted through its singular value decomposition (SVD)[1]:

$$\mathbf{A} = \mathbf{U}\mathbf{\Sigma}\mathbf{V}^T \tag{5.4}$$

where $\mathbf{V}^T$ represents a rotation of the source signals, $\mathbf{\Sigma}$ applies a scaling along the principal directions and $\mathbf{U}$ corresponds to a final rotation in the observation space.

This decomposition is useful for interpreting the geometry behind the mixing process. However, since the mixing matrix is still unknown, ICA does not estimate these factors directly. Instead, it uses the statistical properties of the observations to recover an equivalent geometric transformation.

The first step towards recovering the sources consists of compensating for the transformations associated with $\mathbf{U}$ and $\mathbf{\Sigma}$. The effect associated with $\mathbf{U}$ can be interpreted as a rotation in the 2D space, which can be parameterized by an angle ϕ. Therefore, assuming data has been centered [2], the variance of the observations projected onto that direction can be expressed as shown in equation (5.5) and the principal axis is obtained by selecting the angle that maximizes it (5.6).

$$\mathrm{Var}(\phi) = \frac{1}{N}\sum_{j=1}^{N}\left(\begin{bmatrix} x_1(j) & x_2(j) \end{bmatrix}\begin{bmatrix} \cos\phi \\ \sin\phi \end{bmatrix}\right)^2 \tag{5.5}$$

$$\phi^\star = \arg\max_{\phi} \mathrm{Var}(\phi) \tag{5.6}$$

Once the data has been rotated onto its principal axes, each component still has its own variance. These variances correspond to the eigenvalues of the covariance matrix and represent the scaling introduced by $\mathbf{\Sigma}$. To remove this effect, each component is normalized by its standard deviation, that is,

$$z_i(j) = \frac{y_i(j)}{\sqrt{\lambda_i}}, \qquad \forall i = 1, 2 \tag{5.7}$$

where y_i expresses the $i-th$ component after projection onto the axis and λ_i is the corresponding eigenvalue. In matrix form, the combination of the rotation onto the principal directions and the posterior variance normalization can be written as

$$z = \Lambda^{-1/2}E^T x = \Sigma^{-1}U^T x \tag{5.8}$$

The transformation in equation (5.8) is known as whitening, since it produces a new representation whose components are uncorrelated and have unit variance.

[1] SVD factorizes a matrix as $\mathbf{A} = \mathbf{U}\mathbf{\Sigma}\mathbf{V}^T$, separating rotation and scaling components.

[2] $Var(y) = \mathbb{E}[y^2] - E[y]^2$, but since data is zero mean, $Var(y) = \mathbb{E}[y^2]$

After whitening, the observed vector is reduced to a rotated version of the original sources. For this reason, the only remaining transformation is an orthogonal rotation. In the 2D case, this transformation can be represented by a single angle θ, such that

$$\mathbf{y} = \mathbf{R}(\theta)\mathbf{z} \tag{5.9}$$

where $\mathbf{R}(\theta)$ is the rotation matrix

$$\mathbf{R}(\theta) = \begin{bmatrix} \cos\theta & -\sin\theta \\ \sin\theta & \cos\theta \end{bmatrix}. \tag{5.10}$$

Since the whitening step already guarantees that the components in the 2D space are uncorrelated and have unit variance, second-order statistics no longer provide information to determine the correct orientation. Therefore, ICA relies on higher-order statistics. The most typical criterion is kurtosis, which is defined as

$$\text{kurt}(y) = \mathbb{E}[y^4] - 3\left(\mathbb{E}[y^2]\right)^2 \tag{5.11}$$

For unit-variance data, kurtosis is simplified to $kurt(y) = \mathbb{E}[y^4] - 3$. Therefore the final ICA solution can be interpreted as the rotation angle θ that maximizes kurtosis of the projected signal:

$$\theta^\star = \arg\max_\theta |\text{kurt}(y_\theta)| \tag{5.12}$$

Overall, the whole ICA process can be interpreted as the estimation of a series of geometric transformations by using the statistical properties of the observed mixtures. In the 2D case specifically, the transformations can be explained graphically as shown in figure 5.1.

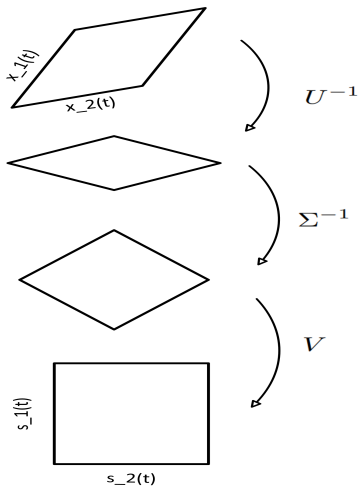

Figure 5.1: Geometric interpretation of ICA in the 2D case. The observed mixtures are decorrelated with PCA (first step) and normalized (second step). Once the data is whitened the final step corresponds to the rotation that best recovers the statistically independent sources.

5.4 Implementations: FastICA

Although the ICA framework provides a clear approach for separating mixed sources, obtaining the final separation matrix is not trivial. The algorithm relies on finding the projection directions that maximize the non-Gaussianity of the estimated sources, which can be computationally expensive if performed directly through kurtosis maximization. Therefore, this section focuses on **FastICA** [31], one of the most practical implementations of ICA. Even though this algorithm is already available in libraries, reviewing its steps is useful to later introduce the modified algorithm for constrained ICA (chapter 7) .

FastICA relies on **fixed-point iteration**, which updates an initial guess repeatedly until the result stops significantly changing. This initial guess is a randomized separation direction, which is constantly corrected by the algorithm until it stabilizes. Equation 5.13 shows the general form of this fixed-point update, where each new estimate $w^{(k+1)}$ is obtained by applying the update function $F(\cdot)$ to the previous estimate $w^{(k)}$ until $w^{(k+1)}$ and $w^{(k)}$ become similar.

$$\mathbf{w}^{(k+1)} = F(\mathbf{w}^{(k)}) \tag{5.13}$$

Additionally, FastICA mainly uses **negentropy** as the measure of non-Gaussianity, since it is more robust than directly maximizing kurtosis. Negentropy essentially measures how far a random variable is from a Gaussian distribution, being zero for a Gaussian variable and positive for non-Gaussian variables. In practice, it is not calculated directly, but approximated using nonlinear contrast functions like in Equation 5.14.

$$J(y) \propto \left[\mathbb{E}\{G(y)\} - \mathbb{E}\{G(v)\}\right]^2 \tag{5.14}$$

where v is a standard Gaussian variable and $G(\cdot)$ is a chosen nonlinear function. Since $\mathbb{E}\{G(v)\}$ is constant in this problem, the optimization focuses on estimation y. In FastICA, y is the estimated component, so in this context $\mathbf{y} = \mathbf{w}^\mathbf{T}\mathbf{z}$. Taking this into account, the update rule (5.13) is derived from the negentropy approximation (5.14) under the unit-norm constraint.[3] Equation 5.15 shows the update step where the constraint is imposed through a Lagrange multiplier.[4]

$$\mathbf{w}^{(k+1)} = \mathbb{E}\left\{\mathbf{z}\, g\left(\mathbf{w}^{(k)T}\mathbf{z}\right)\right\} - \lambda \mathbf{w}^{(k)}, \qquad \lambda = \mathbb{E}\left\{g'\left(\mathbf{w}^{(k)T}\mathbf{z}\right)\right\} \tag{5.15}$$

Once fixed-point iteration is understood, FastICA can be summarized as three main steps:

1. **Preprocess the observations:** the EMG matrix is centered and whitened so that second-order dependencies are removed (already addressed in chapter 4).

2. **Update fixed-point iteration:** the algorithm applies a fixed-point update that searches for maximally non-Gaussian projections.

[3] This constraint ($||\mathbf{w}||^2 = 1$) fixes arbitrary scale and bounds feasible region for the maximization problem.

[4] Lagrange multiplier: $\mathcal{L}(w, \lambda) = g(x) - \lambda f(x)$ in this case is the constraint $f(x) = ||w||^2 - 1$

3. **Ensure orthogonality and convergence:** after each update, symmetric decorrelation is applied and the change in the separation vectors is evaluated.

Listing 5.1 shows the general implementation structure followed in this work. The line `FixedPointUpdate`(W, Z, g) represents the update in Equation 5.15, while `SymmetricDecorrelate(W)` ensures that the estimated components remain orthogonal.

```
Input: Observed EMG matrix X, number of components K,
       tolerance epsilon, maximum iterations Imax

Output: Estimated sources S_hat and separation matrix W

//Preprocessing
Xc <- X - mean(X)
Z  <- Whiten(Xc)
//Initialization
W <- RandomInitialization(K)
W <- SymmetricDecorrelate(W)

//Negentropy optimization
for i = 1 to Imax

    W_old <- W
    W <- FixedPointUpdate(W, Z, g)
    W <- SymmetricDecorrelate(W)
    delta <- max_j | |w_j * w_old_j^T| - 1 |

    if delta < epsilon
        break
    end

end

S_hat <- Xc * W^T

return S_hat, W
```

Listing 5.1: FastICA algorithm pseudocode

Overall, the main advantage of this implementation is that the optimization is reduced to repeated matrix updates. This makes FastICA suitable as a practical baseline method for the EMG separation experiments, where several noise levels and mixing conditions must be evaluated.

5.5 Weak-source and noise

In the context of this study, one of the main difficulties does not come only from the mixing itself, but from the fact that the target component may be significantly weaker than the interfering source. Under noisy conditions, source separation becomes more challenging, since the contribution of the weaker signal to the observed mixtures may be partially masked by both the dominant component and the additive noise. For this reason, it is crucial to analyze how weak-source conditions and noise affect the identifiability and practical recovery of the signals [32].

5.5.1 Instantaneous mixtures

Consider the instantaneous ($\tau = \mathbf{0}$ ms) noisy mixing model

$$\mathbf{x} = \mathbf{A}\mathbf{s} + \mathbf{n}, \qquad \mathbf{A} = \begin{bmatrix} a_{11} & a_{12} \\ a_{21} & a_{22} \end{bmatrix}, \tag{5.16}$$

where $\mathbf{n}$ denotes an additive noise vector. In the noiseless case, the presence of a weak source does not theoretically prevent exact recovery as long as the mixing matrix is invertible ($det(A) = a_{11}a_{22} - a_{12}a_{21} \neq 0$). Therefore, the main difficulty does not arise from the amplitude asymmetry alone, but from the way in which additive noise is transformed by the inverse mixing matrix.

Applying the ideal inverse transformation to (5.16) yields

$$\hat{\mathbf{s}} = \mathbf{A}^{-1}\mathbf{x} = \mathbf{A}^{-1}(\mathbf{A}\mathbf{s} + \mathbf{n}) = \mathbf{s} + \mathbf{A}^{-1}\mathbf{n}. \tag{5.17}$$

Therefore, even if the sources are theoretically separable, the recovered signal is affected by a noise term transformed by the inverse mixing matrix. This means that the practical difficulty of the recovery problem depends not only on the source amplitudes, but also on how $\mathbf{A}^{-1}$ amplifies the additive perturbations.

For a general 2×2 mixing matrix, the inverse can be written as

$$\mathbf{A}^{-1} = \frac{1}{a_{11}a_{22} - a_{12}a_{21}} \begin{bmatrix} a_{22} & -a_{12} \\ -a_{21} & a_{11} \end{bmatrix} \tag{5.18}$$

provided that $\det(\mathbf{A}) = a_{11}a_{22} - a_{12}a_{21} \neq 0$. If the objective is to recover the first source, the corresponding estimation error is given by the first component of $\mathbf{A}^{-1}\mathbf{n}$, namely

$$e_1 = \frac{1}{a_{11}a_{22} - a_{12}a_{21}} \left(a_{22}n_1 - a_{12}n_2\right). \tag{5.19}$$

Therefore, its variance can be written as

$$\mathrm{Var}(e_1) = \frac{a_{22}^2\mathrm{Var}(n_1) + a_{12}^2\mathrm{Var}(n_2) - 2a_{22}a_{12}\mathrm{Cov}(n_1, n_2)}{\left(a_{11}a_{22} - a_{12}a_{21}\right)^2}. \tag{5.20}$$

Assuming that n_1 and n_2 are zero-mean, uncorrelated and have equal variance σ^2, the variance of this error (and similarly e_2) becomes

$$\mathrm{Var}(e_1) = \frac{\sigma^2\left(a_{22}^2 + a_{12}^2\right)}{\left(a_{11}a_{22} - a_{12}a_{21}\right)^2} \qquad \mathrm{Var}(e_2) = \frac{\sigma^2\left(a_{21}^2 + a_{11}^2\right)}{\left(a_{11}a_{22} - a_{12}a_{21}\right)^2} \tag{5.21}$$

From equation (5.17), the recovered sources can be written as

$$\hat{s}_1 = s_1 + e_1 \qquad \hat{s}_2 = s_2 + e_2 \tag{5.22}$$

where e_1, e_2 are the error terms introduced by the transformed noise. This expression allows the previous result to be connected with two practical performance measures: the output SNR and the correlation between the true and recovered sources. Assuming that e_1 is uncorrelated with s_1, the output SNR for the first recovered source can be defined as

$$\text{SNR}_1 = \frac{\text{Var}(s_1)}{\text{Var}(e_1)} \tag{5.23}$$

Similarly, using (5.22) and the assumption that s_1 and e_1 are uncorrelated, the correlation between s_1 and $\hat{s}_1$ can be written as

$$\rho_{s_1,\hat{s}_1} = \frac{\text{Cov}(s_1, \hat{s}_1)}{\sqrt{\text{Var}(s_1)\text{Var}(\hat{s}_1)}} = \frac{1}{\sqrt{1 + \frac{\text{Var}(e_1)}{\text{Var}(s_1)}}} \tag{5.24}$$

The previous derivation provides general expressions for the output correlation and SNR by describing how additive noise propagates through the inverse mixing matrix A^{-1} and affects the recovered sources. It is worth noting that as $\mathbf{det(A)}$ approaches 0, both error variances grow rapidly. Given the equations 5.23 and 5.24, greater values of $\text{Var}(e_1)$ and $\text{Var}(e_2)$ worsen the SNR and correlation, which implies that noise has a greater effect on the separation when $\mathbf{det(A)} \to 0$. This can be seen in Figure 5.2, which shows the separation quality graph for different values of the determinant of the mixing matrix A in **symmetric attenuation scenario (model in 3.1.2)**.

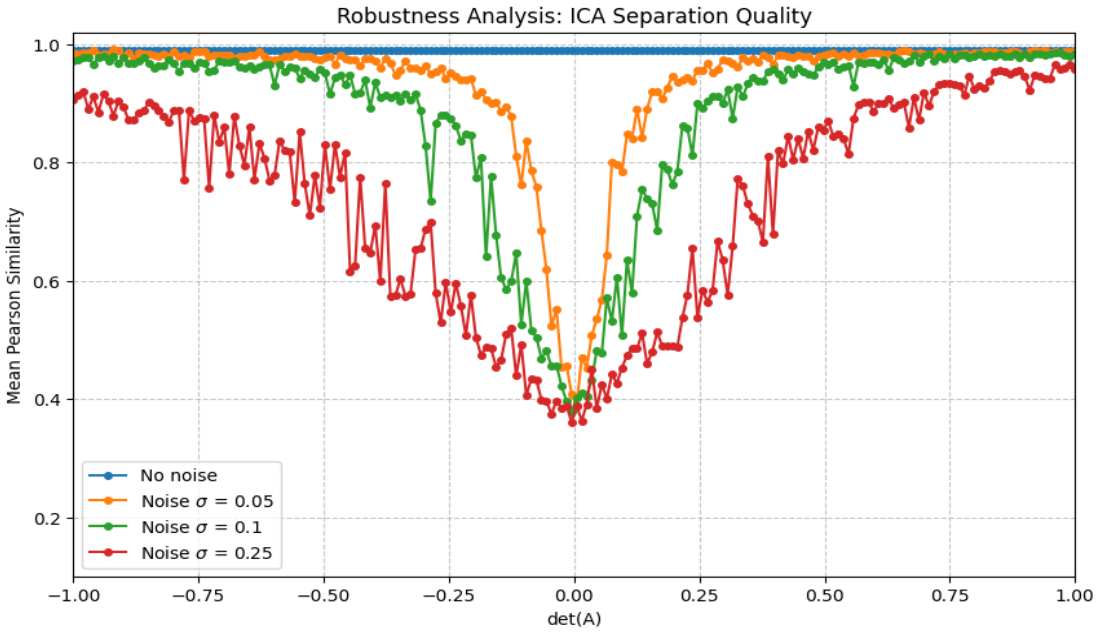

Figure 5.2: Robustness analysis: how the determinant values affect the mean correlation of the estimations $\hat{s}_1$ and $\hat{s}_2$ with the original sources s_1 and s_2 (**symmetrical attenuation case**).

Additionally, to relate these results to the specific problem addressed in this work, it is useful to consider these metrics under the model described in section 3.1.3, where $\mathbf{a_{11}} = \mathbf{a_{22}} = \mathbf{1} \gg \mathbf{a_{21}}$ and $\mathbf{a_{12}} = \beta \in [\mathbf{0}, \mathbf{1}]$. This substitution makes it easier to specifically explain how the parameter β influences the recovery of the weak target source. Consequently, the corresponding output SNR and source-estimate correlation can also be written as functions of β.

$$\rho_{s_1,\hat{s}_1} = \frac{1}{\sqrt{1 + \frac{\sigma^2(1+\beta^2)}{\mathrm{Var}(s1)}}} \qquad \mathrm{SNR}_1 = \frac{\mathrm{Var}(s1)}{\sigma^2(1+\beta^2)} \qquad \beta \in [0,1] \tag{5.25}$$

$$\rho_{s_2,\hat{s}_2} = \frac{1}{\sqrt{1 + \frac{\sigma^2}{\mathrm{Var}(s2)}}} \qquad \mathrm{SNR}_2 = \frac{\mathrm{Var}(s2)}{\sigma^2} \qquad \beta \in [0,1] \tag{5.26}$$

Given these expressions, it is easier to draw explicit conclusions about the influence of the parameter β on the separation process. Equation 5.25 demonstrates that the estimation of $s1$ (weak source) is worsened as β increases, since $\mathrm{SNR}_1 \propto \frac{1}{1+\beta^2}$, but not by much since in this case β is bounded to $[0,1]$. However, the dominant signal (in this case s_2) is theoretically not affected by the β parameter as it does not appear in the correlation and SNR expressions for s_2. Figures 5.3 and 5.4 graphically show how correlation and SNR of the estimated s_1 are affected by β in this case, but numerical values also depend on $\mathrm{Var}(s1)$.

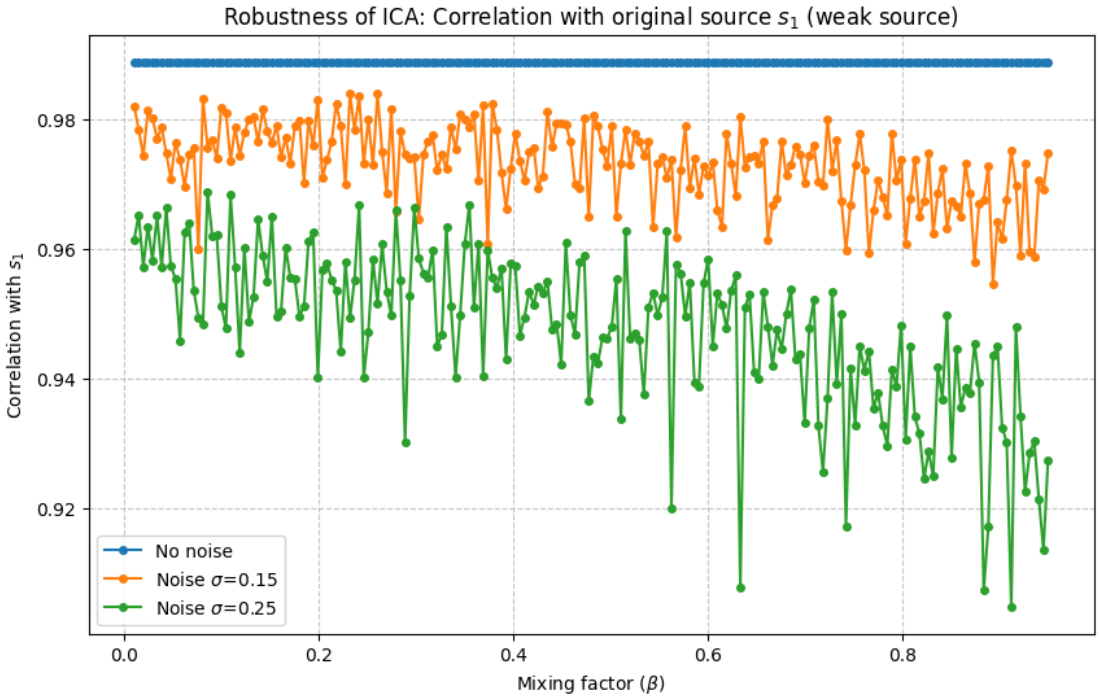

Figure 5.3: Robustness analysis: correlation of $\hat{s}_1$ with original source s_1 considering the weak source model (Section 3.1.3).

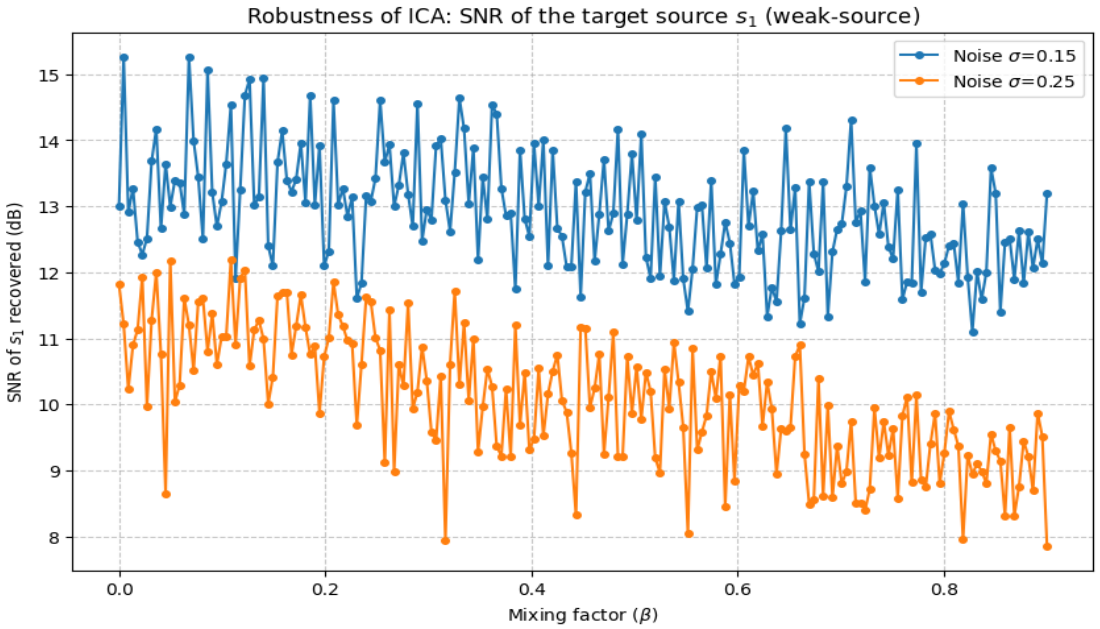

Figure 5.4: Robustness analysis: SNR of $\hat{s}_1$ considering the weak source model (Section 3.1.3).

Nevertheless, it is worth noting that in symmetric attenuation (model 3.1.2), this influence is greater as $\beta \in [0, 1)$ causes $det(a)$ to approach 0. Figures 5.5 and 5.6 show correlation and SNR for the estimated s_1 in this case.

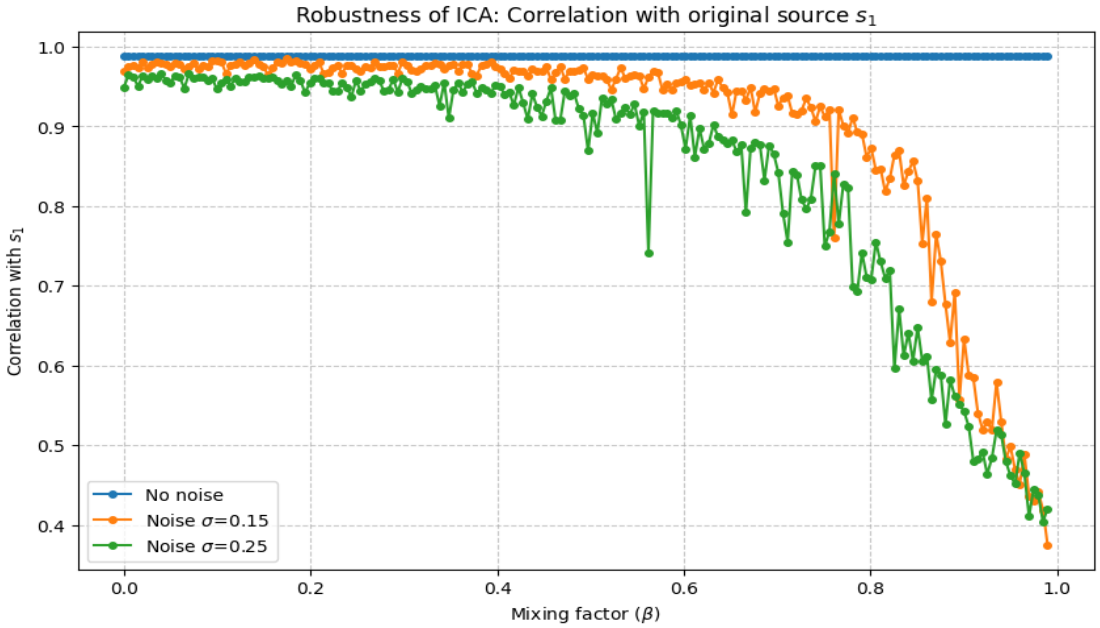

Figure 5.5: Robustness analysis: correlation of $\hat{s}_1$ with original source s_1 considering the symmetric attenuation model (Section 3.1.2)

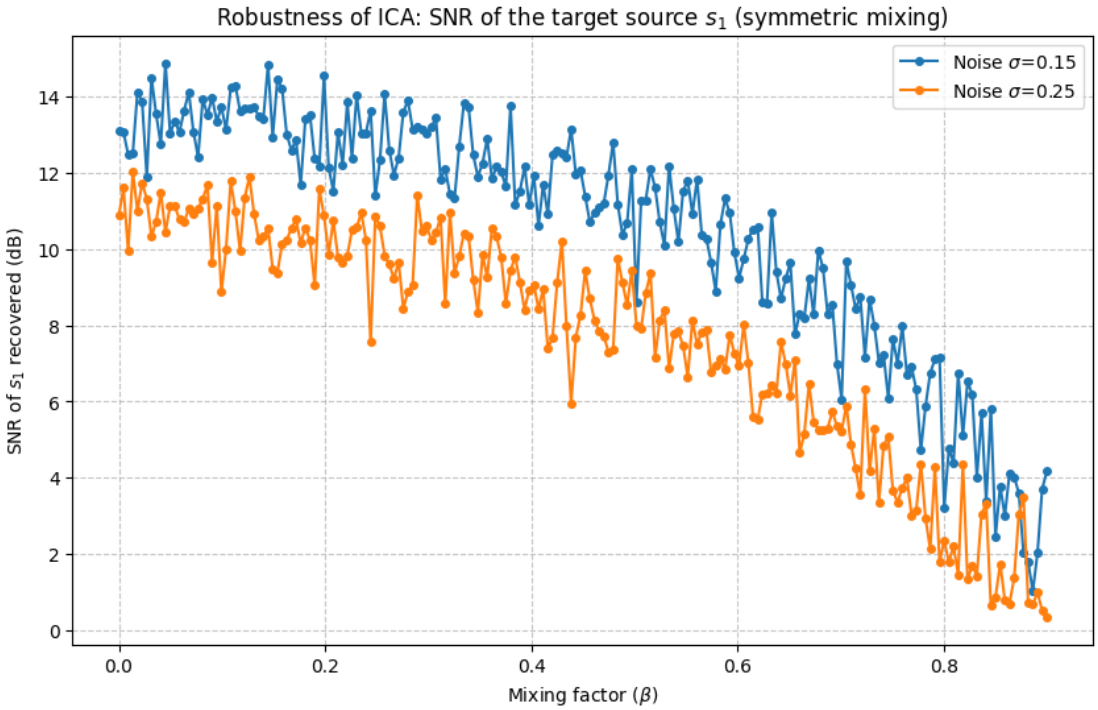

Figure 5.6: Robustness analysis: SNR of $\hat{s}_1$ considering the symmetric attenuation model (Section 3.1.2).

Overall, noise plays an important role in source separation, especially if the mixing matrix $\mathbf{A}$ is close to being singular. This effect is especially relevant in the symmetric attenuation model (Section 3.1.2), where $\beta \in [0, 1)$ is closer to a singular matrix. By contrast, in the weak source regime (Section 3.1.3) this issue is less important with $\beta \in [0, 1]$, since $det(A) = 0$ would only occur at $\beta = 100$. Therefore, in this model, the main limitation is the dominance of the stronger source over the weak target source, rather than the effect of noise alone.

5.5.2 Convolutive mixtures

The previous analysis assumes an instantaneous mixing model, which makes it possible to describe the separation process through a fixed constant mixing matrix. This makes it simple to derive closed-form expressions for the noise influence, the output SNR of each original signal and the source-estimate correlation. However, when delay is introduced, these assumptions no longer hold and the expressions derived in the previous section do not apply directly [33].

More specifically, if each source reaches the observed channels with a relative delay, denoted as τ, the model becomes convolutive. Let D_τ be the delay operator, defined as $D_\tau x(t) = x(t - \tau)$. Then the delayed mixing model can be expressed as

$$\mathbf{x}(t) = \mathbf{A}_\tau \mathbf{s}(t) + \mathbf{n}(t), \qquad \mathbf{A}_\tau = \begin{bmatrix} a_{11} & a_{12}D_\tau \\ a_{21}D_\tau & a_{22} \end{bmatrix} \tag{5.27}$$

For a conventional instantaneous FastICA model, the main problem is that the demixing matrix is assumed to be constant. Therefore, delayed contributions cannot be perfectly cancelled by an instantaneous inverse. In this case, the delayed source term acts as a residual interference component [34].

Let $r_{s_2}(\tau)$ express the normalized autocorrelation of the dominant source s_2 at lag τ,

$$r_{s_2}(\tau) = \frac{\mathbb{E}\{s_2(t)s_2(t-\tau)\}}{\mathrm{Var}(s_2)} \tag{5.28}$$

If an instantaneous model tries to approximate the delayed term $s_2(t-\tau)$ from the non-delayed signal $s_2(t)$, the best linear approximation is

$$s_2(t-\tau) \approx r_{s_2}(\tau)s_2(t) \tag{5.29}$$

The part that cannot be represented by the instantaneous model is therefore

$$e_\tau(t) = s_2(t-\tau) - r_{s_2}(\tau)s_2(t) \tag{5.30}$$

Assuming s_2 is zero-mean, its residual power becomes

$$P_{\mathrm{res}}(\tau) = \beta^2 \,\mathrm{Var}(e_\tau) = \beta^2 \,\mathrm{Var}(s_2)\left(1 - r_{s_2}^2(\tau)\right) \tag{5.31}$$

Consequently, the effective SNR of the estimated weak source can be approximated as

$$\mathrm{SNR}_{1,\tau} \approx \frac{\mathrm{Var}(s_1)}{\sigma^2 + \beta^2 \,\mathrm{Var}(s_2)\left(1 - r_{s_2}^2(\tau)\right)} \tag{5.32}$$

This expression shows that, when $\tau \approx 0$, then $r_{s_2}(\tau) \approx 1$ and the delayed model behaves similarly to the instantaneous case. Theoretically, if τ increases, $r_{s_2}(\tau)$ should decrease, the interference should increase and the SNR of the weak source estimation should be affected. However, this behavior mainly depends on the autocorrelation function, which can make the interference term oscillate in some regions, as shown in Table 5.1.

τ	$r_{s_2}(\tau)$	$r_{s_2}^2(\tau)$	$1 - r_{s_2}^2(\tau)$
1	0.522	0.273	0.727
2	-0.259	0.067	0.933
3	-0.493	0.243	0.757
4	-0.284	0.081	0.919
5	-0.106	0.011	0.989
6	-0.046	0.002	0.998
10	0.087	0.008	0.992

Table 5.1: Normalized autocorrelation values of s_2 and corresponding residual factor.

5.6 Scale reconstruction

As mentioned in Section 5.1, one limitation of ICA source separation is the scale indetermination of the recovered sources. Even if the estimated sources have the correct waveform, their amplitudes are often not the same. Therefore, denormalization (due to preprocessing stage) and an additional scaling step is required to obtain source estimates with amplitudes consistent with the observed mixtures.

In this work, for the scale reconstruction, negligible noise is assumed for simplification. This is done because the noise power cannot be reliably estimated from the available mixtures. For this reason, the resulting scale factors should be interpreted as approximate amplitude corrections. It is worth noting that this scaling step is not included in the experiments presented in this thesis. However, it is an important factor that should be considered in real world testing, where the amplitude of the recovered sources may be relevant for EMG detection.

This scale reconstruction can be estimated using either RMS or variance values, since both statistics are directly related for zero-mean signals. This relation is shown in Equation 5.33.

$$\mathrm{RMS}^2(x) = \frac{1}{N}\sum_{n=1}^{N} x[n]^2 = \mathrm{Var}(x) \qquad \text{if } \mathbb{E}[x] = 0 \tag{5.33}$$

For the asymmetric two-source mixture considered in this work, the observed channels are modeled as shown in Equations 5.34 and 5.35, which are discrete representations of the model studied in this thesis.

$$c_1[n] = s_1[n] + \beta s_2[n] \tag{5.34}$$

$$c_2[n] = 0.01 s_1[n] + s_2[n] \tag{5.35}$$

where β controls the interference of s_2 into the first channel and 0.01 represents a weak contribution of s_1 into the second channel. From 5.34, the squared RMS of the first channel can be written as

$$\mathrm{RMS}^2(c_1) = \mathrm{RMS}^2(s_1) + \beta^2 \mathrm{RMS}^2(s_2) + 2\beta\,\mathrm{Cov}(s_1, s_2) \tag{5.36}$$

Assuming that s_1 and s_2 are independent and approximately zero-mean, the **covariance term is approximately zero**. Since the recovered ICA sources are affected by an arbitrary scale factor, the true sources can be related to the estimated sources as

$$\mathrm{RMS}(s_i) = \alpha_i \mathrm{RMS}(\hat{s}_i) \qquad i = 1, 2 \tag{5.37}$$

where α_i is the scale reconstruction factor of source i. Substituting 5.37 into the RMS relations gives a system of two variables (α_1 and α_2).

$$\begin{cases} \mathrm{RMS}^2(c_1) \approx \alpha_1^2 \mathrm{RMS}^2(\hat{s}_1) + \beta^2 \alpha_2^2 \mathrm{RMS}^2(\hat{s}_2) \\ \mathrm{RMS}^2(c_2) \approx 0.01^2 \alpha_1^2 \mathrm{RMS}^2(\hat{s}_1) + \alpha_2^2 \mathrm{RMS}^2(\hat{s}_2) \end{cases} \tag{5.38}$$

Solving the system in 5.38 for the scale factor of the first source yields

$$\alpha_1(\beta) = \sqrt{\frac{\mathrm{RMS}^2(c_1) - \beta^2 \mathrm{RMS}^2(c_2)}{\mathrm{RMS}^2(\hat{s}_1)\,(1 - 0.01^2\beta^2)}} \tag{5.39}$$

Similarly, the scale factor of the second source can be obtained as shown in Equation 5.40

$$\alpha_2(\beta) = \sqrt{\frac{\mathrm{RMS}^2(c_2) - 0.01^2 \mathrm{RMS}^2(c_1)}{\mathrm{RMS}^2(\hat{s}_2)\,(1 - 0.01^2\beta^2)}} \approx \sqrt{\frac{\mathrm{RMS}^2(c_2)}{\mathrm{RMS}^2(\hat{s}_2)}} \tag{5.40}$$

The approximation in 5.40 is justified by the fact that 0.01^2 is very small, so the contribution of s_1 to the energy of c_2 is negligible. Equations 5.39 and 5.40 provide an approximate reconstruction of the source amplitudes from the observed channel energies, assuming that the mixing coefficients are known or controlled.

If a temporal delay is introduced in the cross-talk terms, like in Equations 5.41 and 5.42, then the RMS-based derivation remains approximately valid.

$$c_1[n] = s_1[n] + \beta s_2[n - \tau] \tag{5.41}$$

$$c_2[n] = 0.01 s_1[n - \tau] + s_2[n] \tag{5.42}$$

This is because a time shift does not significantly change the signal energy when boundary effects are negligible.

$$\mathrm{RMS}^2(x[n - \tau]) \approx \mathrm{RMS}^2(x[n]) \qquad \tau \ll N \tag{5.43}$$

For finite length EMG windows, a delay implemented with zero-padding may slightly alter the RMS value because samples at the boundaries are lost or replaced by zeros. However, when the delay is small compared to the window length, this effect is negligible. Therefore, the reconstruction in 5.39 and 5.40 remains approximately unchanged under the assumption that boundary effects are negligible.

An additional final note is that this scale factor estimation is not specific to ICA. The same rescaling procedure can be applied to the other separation algorithms considered in this thesis, since the recovered components also present arbitrary amplitude scales.

5.7 ICA results

Up to this point, this chapter has focused on explaining the theoretical considerations of ICA for all the proposed models. However, this final ICA section aims to test the performance of the algorithm for the case of the IIT study (model 3.7) on possible scenarios. The goal is not to recover the exact waveform of the target-flap related source (s_1), but to preserve its activations and behavior as accurately as possible. In these results, the main metric of interest is $corr_{rms}(\hat{s}_1, s1)$, which represents the correlation of the RMS envelopes of the estimated source $\hat{s}_1$ and s_1. For these experiments, $\beta = \mathbf{0.9}$ is assumed unless mentioned otherwise.

5.7.1 Ideal case

This case shows ICA performance when all of its main assumptions are satisfied. Figure 5.7 shows how the muscle signals s_1 and s_2 are recovered. The separation achieves perfect temporal and RMS envelope correlation, but, as mentioned in Section 5.1, the order and scale of the signals are lost. However, these two aspects can be easily addressed:

- **Order:** permutation does not result in a problem in this model. Since mixture $c_2 \approx s_2$, s_1 is simply the orthogonal direction.
- **Scale:** not critical as long as the recovered component remains correlated with the target source. Scale factor can be estimated as mentioned in 5.6.

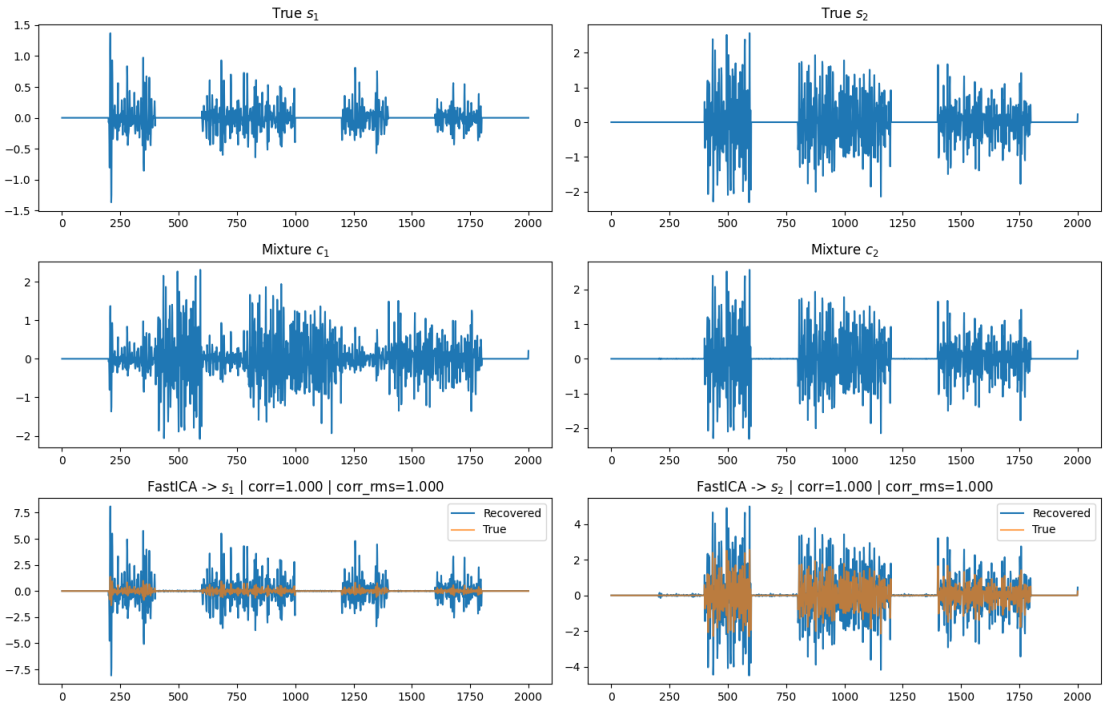

Figure 5.7: Ideal case. FastICA recovers both sources with perfect correlations, but suffers from the expected scale ambiguity. The estimation and the original source may have different amplitudes, but both signals behave the same.

5.7.2 Instantaneous mix with noise

This case maintains all simulation variables from previous section, but adds additive white gaussian noise with variance σ^2. Since the signals are normalized, $\sigma = 0.1$ and $\sigma = 0.15$ can be considered as relative noise levels. This is consistent with EMG methodology reports suggesting that differences in detection conditions can introduce around 10% to 15% variability in repeated measurements [35]. For this reason, the experiments were run with $\sigma = 0.1$ for simplification.

Figure 5.8 shows that the estimation s_1 has a worse temporal correlation with its original source, but maintains a remarkable RMS envelope correlation. This can be explained as small waveform errors directly impact temporal correlation while activation patterns are maintained. By contrast, s_2 is less affected by noise due to two main reasons:

- **Dominance in the mixing model:** as established in Equation 5.26, $\rho_{s_2,\hat{s}_2}$ and SNR_2 do not depend on the β parameter.
- $\text{Var}(\mathbf{s_2}) >> \text{Var}(\mathbf{s_1}), \text{Var}(\mathbf{n})$**:** in this case the noise variance is negligible compared to s_2, but not for s_1.

It is also worth noting that, even though the values of β and σ are fixed, $corr(\hat{s}_1, s_1)$ and $corr_{rms}(\hat{s}_1, s_1)$ still depend on $\text{Var}(s_1)$.

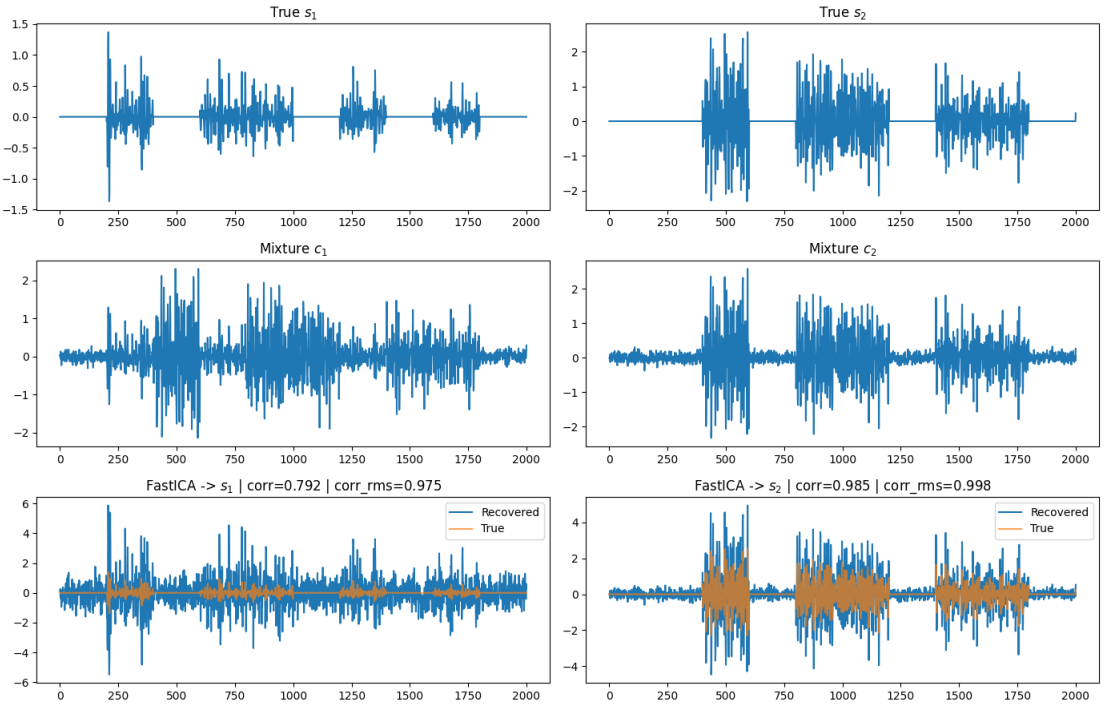

Figure 5.8: Separation under noisy instantaneous mixing. Parameters were set to $\sigma = 0.1$, $\beta = 0.9$ and $\tau = 0\,\text{ms}$. FastICA struggles to maintain temporal correlation with s_1, but recovers activation patterns.

5.7.3 Convolutive mixture with noise

This final scenario adds to the previous instantaneous noisy mixture by including delay between EMG sources, making it a convolutional mixture problem. As mentioned in Section 5.5.2, FastICA's quality of separation is degraded by the presence of a delay τ, which makes the recovery of the weak source s_1 dependent on the dominant signal's autocorrelation $\mathbf{r_{s_2}}(\tau)$. For this experiment, $\tau = 5$ ms is set to accurately relate to a real world scenario [21].

Compared to previous cases, Figure 5.9 shows that the estimation $\hat{s}_1$ for s_1 has a noticeably lower temporal correlation and significantly worse correlation with the original RMS envelope. This points to the delayed interference term (Equation 5.32) drastically impacting the structure of the signal. However, it can be noticed that the estimation for s_2 remains optimal due to the factors mentioned throughout the chapter.

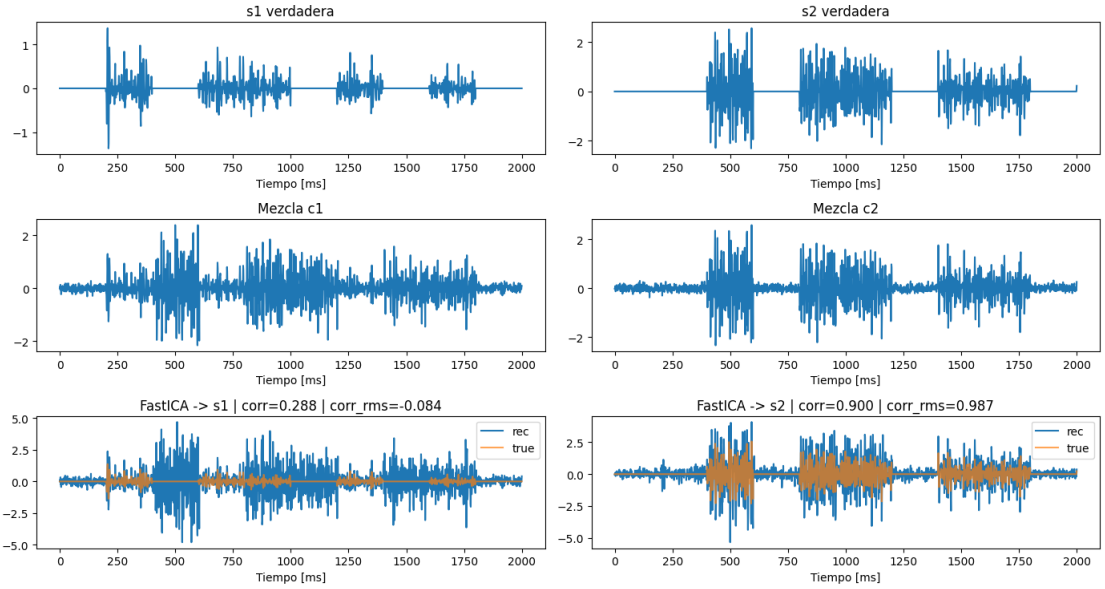

Figure 5.9: Separation under noisy convolutive mixing. Parameters were set to $\sigma = 0.1$, $\beta = 0.9$ and $\tau = 5\,\text{ms}$. FastICA now fails to maintain both temporal correlation and activation patterns for s_1 due to the significant delayed contribution interference from s_2.

Since the delayed contribution interference is also dependent on β^2, decreasing the influence of the dominant source significantly improves the separation. Figure 5.10 shows the results of the exact same experiment, but with $\beta = 0.3$. The separation of the target source s_1 sees a significant improvement in both temporal and RMS envelope correlations after reducing the value of the β parameter.

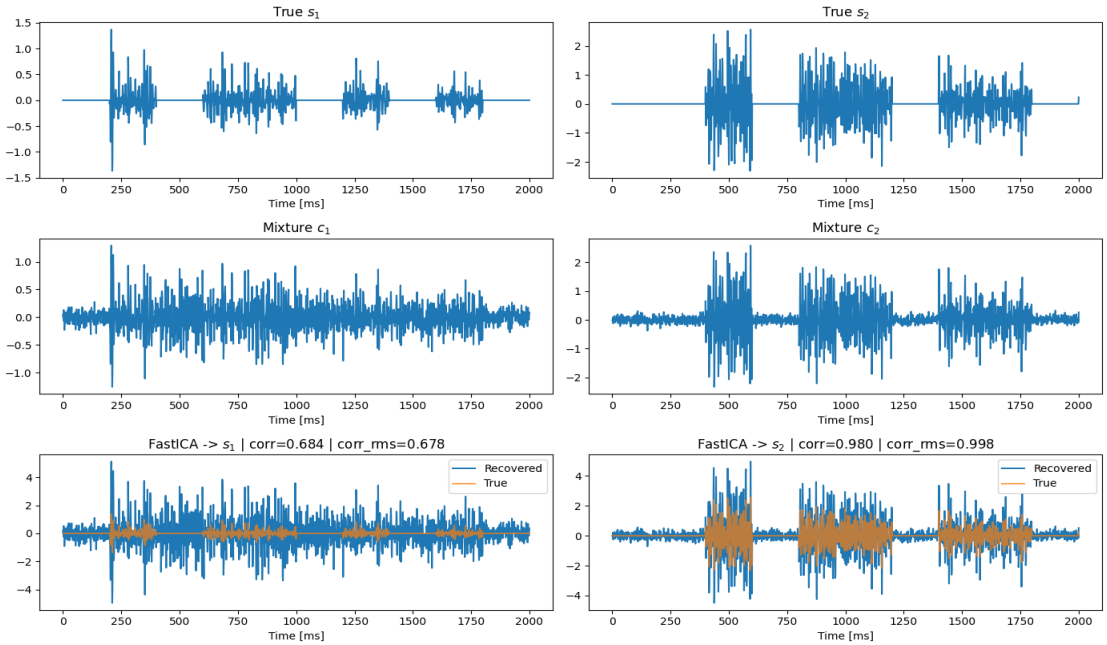

Figure 5.10: Separation under noisy convolutive mixing. Parameters were set to $\sigma = 0.1$, $\beta = 0.3$ and $\tau = 5\,\text{ms}$. FastICA now experiences a smaller delayed contribution interference due to the reduction of the β parameter.

One final aspect to consider is that the effect of the delay τ does not necessarily follow a linear relationship with separation quality. This is because the interference introduced by the delayed contribution (Equation 5.32) depends on the autocorrelation of the interference source at that specific delay $\mathbf{R}_{s2}(\tau)$. Therefore, the experiments focused on representative delay conditions rather than sweeping isolated delay values.

5.7.4 ICA Experiments Conclusion

ICA results in a considerably effective algorithm for the problem involving the IIT study. However, the algorithm depends mainly on the variances of the EMG signals, which cannot be easily controlled even in an experimental environment. Additionally, temporal delays between channels combined with noise compromise the assumptions of the algorithm, leading to a separation with erroneous activation patterns.

More specifically, ICA is likely to recover s_1 in ideal or semi-ideal cases because of the structure of the two-source problem formulation. The algorithm first finds the direction that best optimizes the non-Gaussianity, which is usually aligned with the statistically dominant source s_2. Once this direction is identified, the second component is estimated as the remaining orthogonal direction after whitening, which theoretically corresponds to s_1. However, when noise and delay become more significant, $s1$ is no longer necessarily aligned with the dominant component direction.

In the next chapters, other algorithms will be discussed in order to assess if they can achieve a better performance where ICA fails.

Chapter 6

Second-Order Blind Identification

Second-Order Blind Identification (SOBI) is a Blind Source Separation technique that separates observed mixtures by exploiting differences in the temporal structure of the sources. Unlike ICA, which relies mainly on non-Gaussianity, SOBI is limited to second-order statistics like time-lagged covariance matrices [36].

This chapter presents the basic foundations, assumptions and implementation of the SOBI algorithm, followed by its evaluation in the proposed weak-source separation problem.

6.1 Assumptions

Like the ICA algorithm, SOBI relies on a series of assumptions that should be at least partially satisfied for the separation to be effective. Some of these assumptions are common to both methods, such as the presence of a linear instantaneous mixture (or small delays), a full-rank mixing matrix A and a number of observations greater than or equal to the number of sources, as discussed in Section 5.2. Therefore, this section focuses on the assumptions that are specific to SOBI and explain their relevance in the context of the proposed problem.

- **Sources have temporal structures**

  $$\mathbf{R_s}(\tau) \neq \mathbf{0}$$

  SOBI requires that samples close in time should have some relationship with each other. For EMG, this is reasonable since muscle activations have temporal continuity and their RMS envelope changes progressively over time.

- **Sources have different temporal structures**

  $$\mathbf{R_{s1}}(\tau) \not\approx \mathbf{R_{s2}}(\tau)$$

  This assumption is essential because SOBI separates sources through differences in their temporal patterns. If two sources evolve similarly over time, reliable separation becomes difficult, which may occur for nearby or functionally related EMG sources.

- **Sources have no time-lagged cross-correlation**

  $$\mathbf{E}\left[\mathbf{s_i}(\mathbf{t})\mathbf{s_j}(\mathbf{t}-\tau)\right] = \mathbf{0}, \quad \forall \quad \mathbf{i} \neq \mathbf{j}$$

  This means that each source may be correlated with itself over time, but not with lagged versions of other sources. In EMG, this assumption can be challenged when several muscles are activated simultaneously.

6.2 Working principle

Second-Order Blind Identification starts from the same linear mixture model introduced previously and shares initial preprocessing steps with ICA. The observed mixtures are first centered to remove their mean and then whitened so that the channels become uncorrelated and have unit variance. After whitening, the separation problem is reduced to finding an orthogonal transformation that removes the remaining mixing effect in $\mathbf{z}(t)$. Instead of searching for the rotation that maximizes non-Gaussianity, as in ICA, SOBI estimates this transformation using delayed covariance matrices. For a given delay τ, Equation 6.1 defines the covariance matrix of the whitened observations $\mathbf{z}(t)$.

$$\mathbf{R}_z(\tau) = E\left[\mathbf{z}(t)\mathbf{z}^T(t-\tau)\right] \tag{6.1}$$

Given the assumptions presented in the previous section (6.1), the delayed covariance matrix of the sources should be diagonal, since each source may be correlated with itself over time but not with delayed versions of the other sources. This is shown in Equation 6.2.

$$\mathbf{R}_s(\tau) = \begin{bmatrix} R_{s_1}(\tau) & \approx 0 \\ \approx 0 & R_{s_2}(\tau) \end{bmatrix} \tag{6.2}$$

This implies that each source only contributes to its own autocorrelation term. Since the whitened observations are still a rotated version of the original sources, SOBI searches for a rotation matrix $\mathbf{B}$ that makes the delayed covariance matrices of the whitened data as diagonal as possible.

$$\mathbf{B}\mathbf{R}_z(\tau)\mathbf{B}^T \approx \mathbf{D} = \begin{bmatrix} d_1(\tau) & 0 \\ 0 & d_2(\tau) \end{bmatrix} \tag{6.3}$$

where d_1, d_2 are the autocorrelation values of the source signals at a given lag. Nevertheless, this condition has to be applied to several delays. SOBI considers delays $\tau_1, \tau_2, \ldots, \tau_K$ as each delay contains significant temporal information about the sources. Therefore, the goal is to find a unique rotation matrix $\mathbf{B}$ that approximately diagonalizes all delayed covariance matrices at considered delays.

$$\mathbf{B}\mathbf{R}_z(\tau_k)\mathbf{B}^T \approx \mathbf{D}_k \qquad \forall k = 1, 2, \ldots, K \tag{6.4}$$

where $\mathbf{D}_k$ is an approximately diagonal matrix for the delay τ_k. This process is called **joint diagonalization**, since this unique transformation is applied jointly to all delayed covariance matrices. Joint diagonalization can be implemented in different ways, but it essentially evaluates a series of rotations and selects the one that minimizes the energy outside the main diagonal of these matrices. This idea is expressed in Equation 6.5.

$$\mathbf{B}^\star = \arg\min_{\mathbf{B}} \sum_{k=1}^{K} \operatorname{off}\left(\mathbf{B}\mathbf{R}_z(\tau_k)\mathbf{B}^T\right), \qquad \operatorname{off}(\mathbf{M}) = \sum_{i \neq j} M_{ij}^2 \tag{6.5}$$

Overall, SOBI has a geometric interpretation considerably similar to the one presented for ICA in Figure 5.1, since both methods reduce the separation problem to a single rotation of the whitened observations. However, the principle used to select this rotation is completely different. While ICA searches the rotation that maximizes non-Gaussianity, SOBI searches for the rotation that jointly diagonalizes the time lagged covariance matrices.

6.3 Implementation

Unlike FastICA, which is available through well-established public libraries such as `scikit-learn`, SOBI does **not** have an equally standardized implementation that could be directly applied to the signals considered in this thesis. Consequently, a custom SOBI implementation was developed, allowing greater control over the selection of time delays and the approximate joint diagonalization procedure.

More specifically, a **Jacobi/Givens rotation strategy** was used for the joint diagonalization [37], [38]. This procedure essentially aims to find the matrix $\mathbf{B}$ by progressively combining 2D rotation matrices. For each pair (p, q), the Givens rotation $G_{p,q}(\theta)$ is defined as a matrix where the only non-trivial part is the 2x2 acting on rows and columns p and q. This rotation is applied to every delayed covariance matrix $\mathbf{R}_z(\tau_k)$ at the same time the $\mathbf{B}$ matrix is updated, like shown in Equation 6.6.

$$\mathbf{R}_z(\tau_k) \leftarrow \mathbf{G}_{pq}(\theta)\mathbf{R}_z(\tau_k)\mathbf{G}_{pq}^T(\theta), \qquad \mathbf{B} \leftarrow \mathbf{G}_{pq}(\theta)\mathbf{B} \tag{6.6}$$

For each (p, q) pair, the elements of $\mathbf{R}_z(\tau_k)$ are used to compute the next rotation angle as defined in Equations 6.7 and 6.8.

$$\begin{bmatrix} a_{pp} & a_{pq} \\ a_{pq} & a_{qq} \end{bmatrix}, \qquad g_{11} = \sum_{k=1}^{K} \left(a_{pp}^{(k)} - a_{qq}^{(k)} \right), \qquad g_{12} = \sum_{k=1}^{K} 2a_{pq}^{(k)} \tag{6.7}$$

$$\theta = \frac{1}{2} \operatorname{atan2}\left(g_{12}, g_{11}\right) \tag{6.8}$$

Finally, the algorithm repeats this process until either all the (p, q) pairs are included or consecutive iterations do not significantly minimize off-diagonal energy. After $\mathbf{m}$ iterations ($\leq N$ dimensions), the final $\mathbf{B}$ matrix is summarized as expressed in Equation 6.9.

$$\mathbf{B} = \mathbf{G}_{p_m q_m}(\theta_m) \cdots \mathbf{G}_{p_2 q_2}(\theta_2)\mathbf{G}_{p_1 q_1}(\theta_1) \tag{6.9}$$

In the experiments of this thesis, only two sources are considered so the computation is simplified to a single Givens rotation $G_{12}(\theta)$. However, the function was implemented for a generic NxN dimension input. **See code in Appendix II.3.1 for reference**.

With a joint diagonalization strategy defined, the SOBI implementation can be divided into four main sections.

- **Preprocessing:** center and whiten the data (already mentioned in Chapter 4). However, it is crucial to keep the whitening matrix **V** to later build the separation matrix **W**.
- **Delayed covariance estimation:** compute an array of lagged covariance matrices for a list T of delays. This step is explicitly included in the SOBI function.
- **Joint diagonalization:** applies the Jacobi/Givens strategy detailed in this section to find the matrix **B**.
- **Separation matrix:** combine matrix **B** with whitening transform V to obtain final separation matrix W.

Listing 6.1 illustrates the general SOBI pseudocode followed in this thesis. **For full code implementation reference, see Appendix II.3.2**

```
Input: Observed EMG matrix X, number of components K,
       set of delays T, tolerance epsilon, maximum iterations Imax

Output: Estimated sources S_hat and separation matrix W

//Preprocessing
Xc <- X - mean(X)
Z, V <- Whiten(Xc, K)
//Delayed covariance estimation
R_list <- LaggedCovarianceMatrices(Z, T)

//Joint diagonalization
B <- IdentityMatrix(K)
for sweep = 1 to Imax
    B_old <- B
    B <- JacobiJointDiagonalizationStep(B, R_list)
    delta <- OffDiagonalEnergy(R_list)
    if delta < epsilon
        break
    end
end
//Source estimation
W <- B * V
S_hat <- Xc * W^T

return S_hat, W
```

Listing 6.1: SOBI algorithm pseudocode.

6.4 Experiments

Once Second-Order Blind Identification is explained and implemented, it is crucial to test its performance with EMG signals. Since ICA already works relatively well in some experimental scenarios, this section aims to compare and ultimately assess if SOBI is better suited to separate EMG signals. Additionally, different scenarios are tested in order to understand when the two algorithms may or may not behave similarly. Finally, a conclusion about SOBI's role in EMG signal separation is included at the end of this section.

6.4.1 TMR Database

Figure 6.1 illustrates the results of the implemented SOBI algorithm in the TMR patients dataset. The parameters were set to $\beta = 0.3$, $\sigma = 0.1$ and $\tau = 5\,\text{ms}$. In this experiment, SOBI and ICA seem to perform similarly, achieving slightly different temporal and RMS envelope correlations. Further testing reveals that increasing the β parameter in this setting has an even stronger effect for SOBI.

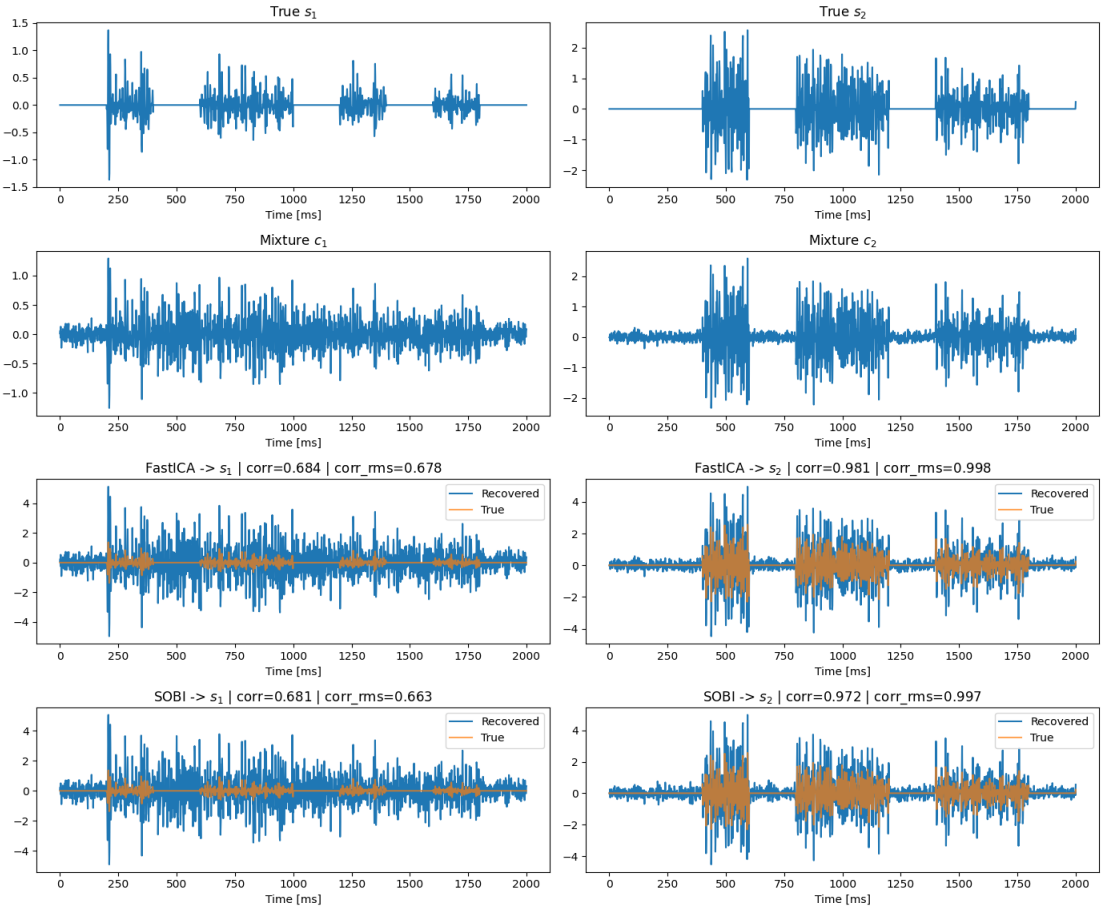

Figure 6.1: Comparison of the signal separation performed by FastICA and the designed SOBI method in the **TMR patients dataset**. Both algorithms achieve similar results as non-gaussianity and temporal structure appear to provide similar information about the original sources.

To evaluate whether SOBI can be actually favorable for the signals in this dataset, the autocorrelation functions of the original sources were computed. Figure 6.2 shows the normalized autocorrelation of both signals. The results point to the fact that both sources present temporal structure at small lags, but their autocorrelation functions become close to zero and oscillate around as the lag increases. In fact, during the first few lags, both curves follow a very similar pattern. All of this suggests that the temporal information available for SOBI is limited, since the sources in this dataset do not present significantly distinguishable autocorrelation structures.

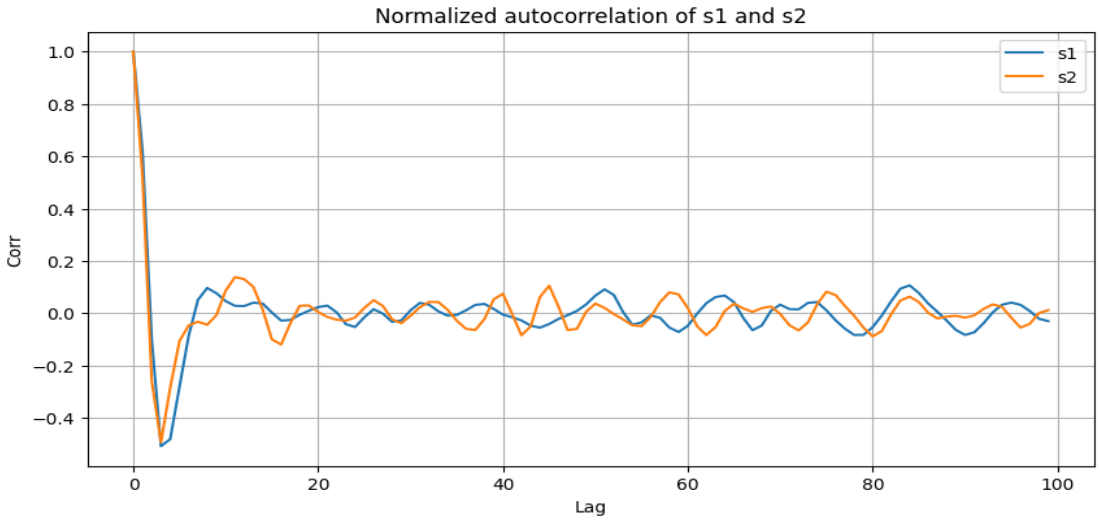

Figure 6.2: Normalized autocorrelation function for both s_1 and s_2 in the **TMR patients dataset**. Both sources have similar autocorrelation functions, especially for smaller lags.

6.4.2 Artificial dataset

Due to the limited differences observed in the autocorrelation functions of the previous signals, the synthetic dataset introduced in Subsection 3.3.2 was also considered. As explained previously, this dataset was designed to simulate EMG signals from different muscles under controlled conditions [25]. This makes it possible to evaluate SOBI in a scenario where the sources present different temporal autocorrelation structures. Figure 6.3 illustrates the normalized autocorrelation of the selected two sources in this new dataset, which display significantly different behavior overall.

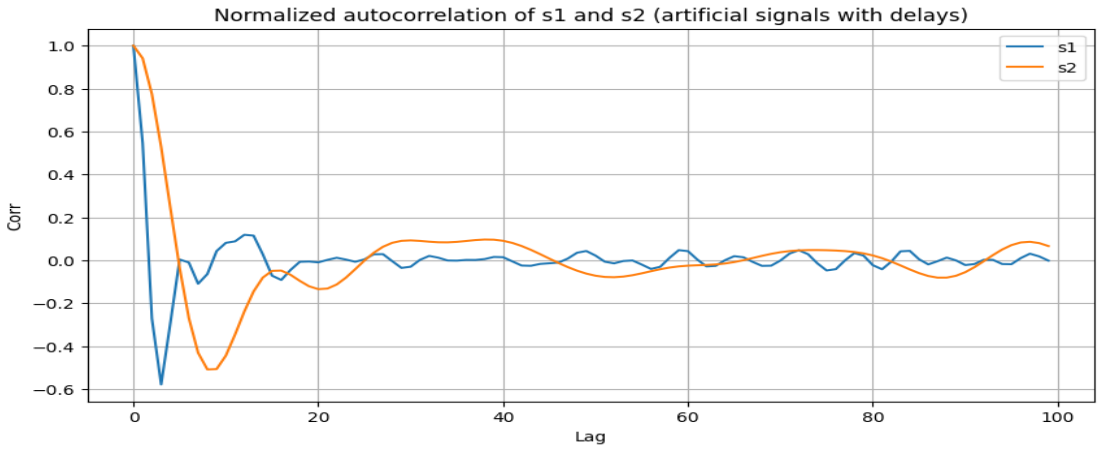

Figure 6.3: Normalized autocorrelation function for both s_1 and s_2 in **the synthetic dataset**. These new sources now present more different autocorrelation functions.

However, in practice this does not mean that ICA is outperformed by SOBI in this dataset. Figure 6.4 graphically shows that an almost identical separation in the experiment performed with the new synthetic data. Though both algorithms work well under worse conditions ($\sigma = 0.1$, $\beta = 0.8$ and $\tau = 8\,\text{ms}$), SOBI does not present a significant improvement over ICA.

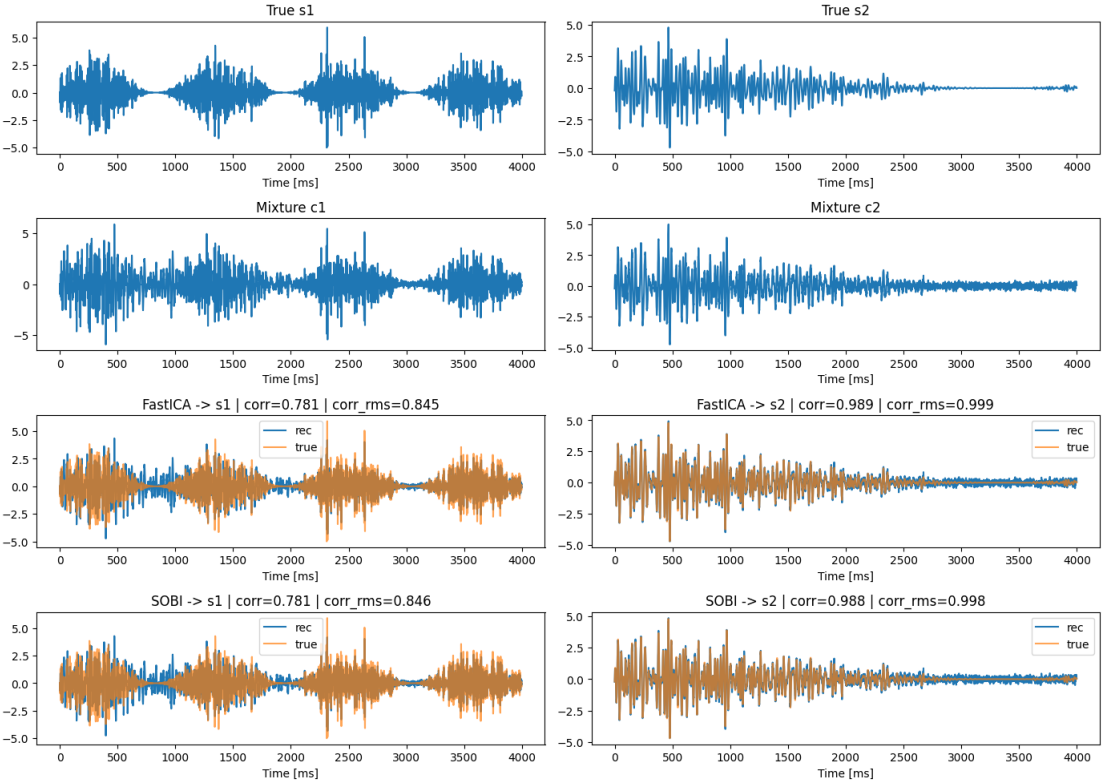

Figure 6.4: Comparison of ICA and SOBI in the new synthetic data. Parameters were set to $\sigma = 0.1$, $\beta = 0.8$ and $\tau = 8\,\text{ms}$. Results seem to indicate that the new temporal structure of the signals provides similar information as non-Gaussianity.

These results suggest that alternating or non-simultaneous EMG activations may increase the differences in sparsity and amplitude distribution between sources. As a result, the non-Gaussianity exploited by ICA can provide more information than the second-order temporal structure exploited by SOBI.

This raises the question: under which conditions would SOBI be preferred over ICA? That would happen when the temporal structure of the sources is significantly more important than their non-Gaussianity. For this reason, Figure 6.5 illustrates the algorithm's performance in an artificial scenario in which both EMG sources are simultaneously active and share similar envelope, but present different activation frequencies.

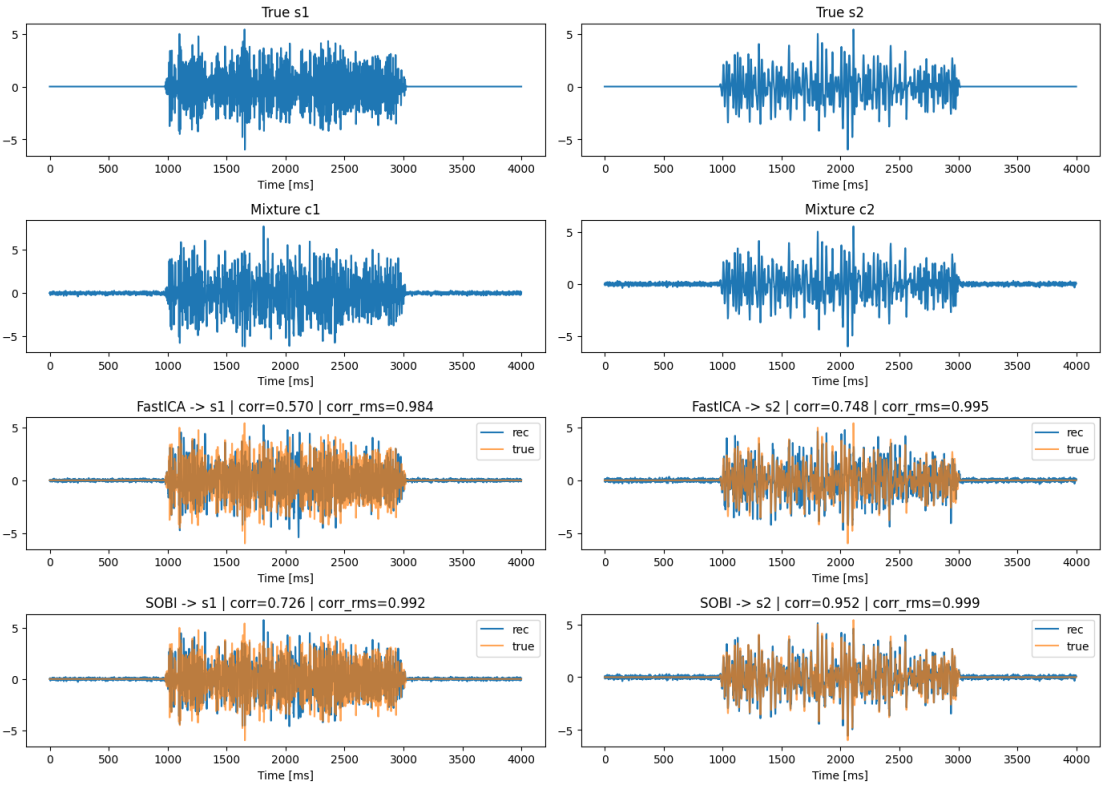

Figure 6.5: Separation under SOBI favorable artificial scenario. Simultaneous EMG sources present similar envelopes, but have different temporal structures. Parameters were set to $\sigma = 0.1$, $\beta = 0.8$ and $\tau = 8\,\text{ms}$. In this scenario, SOBI achieves a significant improvement in temporal correlation over ICA, but obtains similar RMS envelope correlations.

In this case, SOBI shows a clear improvement over ICA in terms of waveform correlation, which indicates better recovery of the temporal structure of the sources. However, even under this favorable scenario for SOBI, both separation algorithms achieve similar RMS envelope correlations. This suggests that, even though SOBI recovers with more detail the temporal waveform, both methods capture the overall activation pattern with similar accuracy.

6.4.3 SOBI experiments conclusion

Overall, although SOBI is a useful blind source separation method, the results obtained suggest that, for the EMG signals considered in this work, non-Gaussianity provides more relevant information than second-order temporal structure. In particular, the autocorrelation functions were often not different enough to give SOBI a clear advantage over ICA.

Since the main objective of this study is to recover the activation pattern of the target source and ICA demonstrated better performance for this, the next step is to improve the ICA algorithm. Therefore, the following chapter focuses on a modified version of ICA in which additional optimization constraints are introduced to guide the separation towards the desired source.

Chapter 7
Constrained ICA

As discussed in previous chapters, Independent Component Analysis is a standard algorithm for Blind Source Separation. The term blind refers to the fact that the algorithm has no prior knowledge of the mixing matrix **A** or the original sources. This means that this method attempts to recover the original sources by only using the statistical properties of the observed mixtures.

Therefore, the purpose of this chapter is to revisit ICA and study whether adding physiological information or additional knowledge about the separation problem can improve source separation in those cases where standard ICA fails.

7.1 Principle

In Section 5.3, ICA was described as a sequence of geometrical transformations. As explained in that section, the main difficulty appears after whitening, when the data Z has already been decorrelated and normalized, but still in need of one last final rotation. For this reason, ICA is commonly formulated as an optimization problem, where the objective function is an estimator of non-Gaussianity, such as kurtosis or negentropy (FastICA).

$$\theta^{\star} = \arg\max_{\theta} J\left(\mathbf{y}(\theta)\right) \tag{7.1}$$

However, since non-Gaussianity is computed using higher order statistics, ICA generally becomes a **non-convex optimization problem**. As a result, the algorithm may converge to different optima due to the initialization, preprocessing and noise level interference [39], [40]. In the weak-source problem considered for this thesis, this is especially important, since the component that best satisfies the ICA objective function may correspond to the dominant source s_2, not the target source s_1.

For this reason, when s_1 and s_2 are not easily separable through the standard ICA rotation, it may be useful to guide the optimization towards a specific local optimum. This can be achieved by introducing constraints that restrict the feasible region and guide the solution to converge towards a component that is more physiologically meaningful for the target source s_1. Equation 7.2 shows the mathematical representation of this idea, where each function g_i defines a constraint that limits the feasible region.

$$\begin{aligned} \underset{\theta}{\text{maximize}} \quad & J\left(\mathbf{y}(\theta)\right) \\ \text{subject to} \quad & g_1(\theta) \leq 0 \\ & g_2(\theta) \leq 0 \\ & \vdots \\ & g_n(\theta) \leq 0 \end{aligned} \tag{7.2}$$

To further clarify this concept, Figure 7.1 provides a visual interpretation of the presented ICA constrained formulation. In the unconstrained case, ICA selects the global maximum of this objective, which in the weak-source model may correspond to the dominant source s_2. By adding problem related constraints, the feasible region (blue shaded area in graph) can be restricted to a local optimum that is more consistent with the target source s_1.

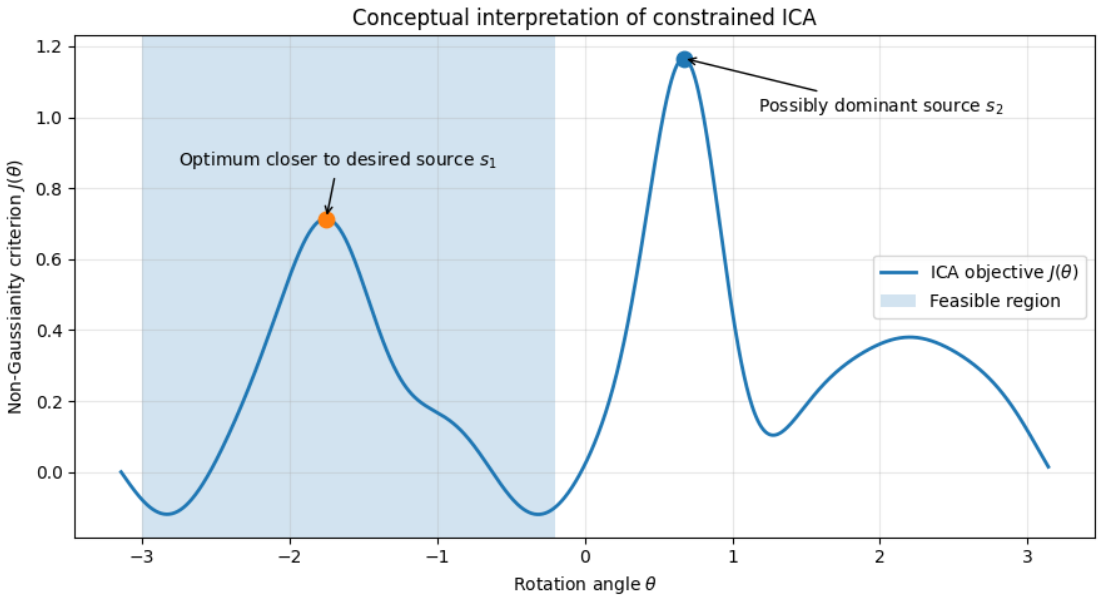

Figure 7.1: Conceptual illustration of constrained ICA in weak-source scenario. The curve represents a generic non-Gaussianity objective, not real experimental negentropy values.

Conceptually, this version of ICA is only expected to improve standard ICA in scenarios where interferences such as noise or delay prevent the orthogonal component from aligning correctly with s_1. In these cases, the constraints guide the optimization algorithm towards an optimum that is more aligned with the target source s_1, even if this slightly reduces the quality of the recovered dominant source s_2. Since the main objective of this thesis is to recover s_1 (target flap-related source), this trade-off is acceptable.

7.2 Constraints

The key idea introduced in the previous section is only useful if the added constraints are specifically related to the target source s_1. In other words, the constraints must provide information that helps identify s_1 from the dominant source s_2. This information can either describe expected properties of the signal itself, such as temporal pattern or envelope or knowledge about the separation problem.

This section aims to present ideas and possibilities for these constraints as well as relevant considerations for their application in the weak-source EMG separation problem.

7.2.1 Constraint Examples

Spatial constraints

In high-density EMG studies, such as the TMR dataset used in this thesis [24], information about electrode placement can be valuable because it provides spatial context about the recorded channels. This information may allow the algorithm to consider that signals recorded by nearby electrodes may contain similar sources due to volume conduction or anatomical proximity [41]. Equation 7.3 denotes a simplified spatial constraint example, where the estimated projection $\mathbf{a}_i$ is considered to remain close to a reference topography $\mathbf{a_{c,i}}$. The parameter ϵ controls the allowed deviation.

$$g_i(\mathbf{A}) = \|\mathbf{a}_i - \mathbf{a}_{c,i}\|^2 \leq \epsilon \tag{7.3}$$

However, in the weak-source scenario considered in this work, these constraints may not be helpful since the target source s_1 is not necessarily aligned with a dominant spatial projection. Observing the weak-source model in Section 3.1.3, s_1 is weakly represented across the electrodes, which makes defining a reliable reference topography $\mathbf{a}_{c,i}$ considerably difficult. As a result, the spatial constraints could guide the algorithm towards dominant source s_2 rather than improving the recovery of s_1.

Temporal constraints

Temporal constraints introduce prior information about the expected time behavior of the source signals. Instead of guiding the separation through spatial projections, these constraints guide the algorithm based on how the desired component is expected to behave over time [42], [43]. This can be useful in EMG when some information about the activation pattern of the target source is available, such as reference signals, calibration contractions or expected RMS envelopes. Equation 7.4 denotes a simplified temporal constraint example where $\hat{s}_i$ is the estimated source, r_i the temporal reference with the desired component.

$$g_i(\mathbf{s}) = \|\hat{s}_i - r_i\|_2^2 \leq \epsilon \tag{7.4}$$

However, for EMG this kind of constraints may become too restrictive in some cases, since the waveform can change due to phase shifts and delays.

RMS envelope constraints

In EMG context of this thesis, RMS envelope constraints can be considered as a less restrictive version of temporal reference constraints. Instead of requiring the estimated source to align sample by sample, they compare their RMS envelopes. This is more appropriate for EMG because it focuses on the activation pattern of s_1 and is less sensitive to shifts and delays. Equation 7.5 shows this idea mathematically, where the RMS envelope of the estimated source is constrained to remain close to the RMS envelope of the reference signal.

$$g_i(\mathbf{s}) = \|\text{RMS}(\hat{s}_i) - \text{RMS}(r_i)\|_2^2 \leq \epsilon \tag{7.5}$$

Though this type of constraint may be the best fit for this thesis, its implementation is not trivial. Since the RMS envelope is a nonlinear transformation of the signal, incorporating it directly into the FastICA optimization would considerably complicate the update rule. This would likely require a redesign of the algorithm rather than modification of the existing fixed-point iteration.

Considerations

One final consideration is that the constraints **must be expressed as functions of the optimization variable** (rotation angle θ or the separation vector $\mathbf{w}$). Even if they are initially defined in terms of source properties, spatial projections or RMS envelopes, they must ultimately be linked to the variable being optimized so that they can modify or restrict the ICA solution. This point will be especially relevant in Section 7.3.

7.2.2 Constraint strength

Given a specific separation problem, there may be occasions where some constraints are required to be met, while others may be met partially. Therefore, it is important to distinguish between two types:

Hard constraints

These constraints impose conditions that must be strictly satisfied. Mathematically, constraints are usually represented as functions of the decision variable that must be equal to zero or less than or equal to zero.

$$\max_{\theta} J(\theta) \quad \text{s.t.} \quad g_i(\theta) \leq 0$$

In real world scenarios, these constraints may become problematic sometimes because an inaccurate or overly restrictive constraint can potentially make the optimization infeasible. In other words, there may be no solution that satisfies all imposed conditions while still optimizing the ICA objective.

Soft constraints

These constraints can be partially met in case an objective optimum requires it. This means they allow some deviation and can be mathematically represented as a penalty term that is added to the objective function.

$$\max_{\theta} \left[J(\theta) - \lambda g_i(\theta) \right]$$

where λ controls the weight of the constraint. Larger values of λ force the solution to satisfy the constraint more strongly and when $\lambda \to \infty$ it can be understood as a hard constraint.

7.3 Implementation

Since this approach is tailored to specific separation problems and depends on the type of prior information available, there is no standardized library function for constrained ICA in the same way there is for conventional FastICA. For this reason, the main objective of this section is to describe which constraints can be considered viable for this work and how they can be added into the fixed-point iteration.

Specifically, this implementation focuses on **soft reference constraints**, where standard fixed point update is not replaced. Instead, it is guided using constraint information related to the target source and the dominant source.

To impose the soft constraints and modify the fixed point update, the reference signal must first be transformed into a direction in the whitened space [44]. This allows the temporal information contained in the reference to be expressed in terms of the optimization variable $\mathbf{w}$ (can also be expressed in terms of θ). Equation 7.6 shows this transformation, where the reference direction is computed from the correlation between the whitened data $\mathbf{z}$ and reference signal r.

$$\mathbf{q}(\tau) = \mathbb{E}\left[\mathbf{z}(t) r(t-\tau)\right] \tag{7.6}$$

Since the magnitude of this vector depends on the scale of the reference signal and the strength of its correlation, it has to be normalized before being used in the update rule. This guarantees that $\mathbf{q}$ only represents a direction in the whitened space.

$$\mathbf{q} = \frac{\mathbf{q}(\tau^\star)}{\|\mathbf{q}(\tau^\star)\|} \tag{7.7}$$

This idea is implemented in the `BuildReferenceDirection` function which can be found in **Appendix II.4.1** .

After transforming the reference into a suitable direction, the fixed point update is extended with two extra steps. The positive correction term is derived from a soft constraint that **rewards** alignment between $\mathbf{w}$ and $\mathbf{q}_{target}$. This can be measured using the scalar product $\mathbf{w}^T\mathbf{q}_{target}$, which leaves the corresponding objective term as shown in Equation 7.8.

$$\lambda_{pos} \left(\mathbf{w}^T \mathbf{q}_{target}\right)^2 \tag{7.8}$$

After this, taking the gradient of the term with respect to $\mathbf{w}$ gives the correction applied to the fixed point update.

$$\Delta \mathbf{w}_{target} = 2\lambda_{pos} \left(\mathbf{w}^T \mathbf{q}_{target}\right) \mathbf{q}_{target} \tag{7.9}$$

where λ_{pos} controls the weight of the correction towards the target reference. By contrast, the negative correction term is derived in a similar way, but by **penalizing** the dominant direction.

$$\lambda_{neg} \left(\mathbf{w}^T \mathbf{q}_{bad}\right)^2 \tag{7.10}$$

where λ_{neg} controls how strongly the solution avoids the undesired direction. Overall, the complete update can be seen as shown in Equation 7.11.

$$\mathbf{w} \leftarrow \text{FixedPointUpdate}(\mathbf{w}) + \Delta \mathbf{w}_{target} - \Delta \mathbf{w}_{bad} \tag{7.11}$$

Theoretically, the main advantage of this implementation is that the weights of each reference can be adjusted based on the confidence. If a reference is considered reliable, its corresponding weight can be increased so that the algorithm follows that information more strongly. By contrast, if a reference is only an approximation of the desired activation pattern, a lower weight can be used, which makes the method closer to the standard FastICA.

Taking all the mentioned considerations into account, the constrained ICA algorithm can be structured in a similar way to the traditional FastICA implementation described in Section 5.4. The main difference is the introduction of an additional step to include the reference directions before the fixed point iteration begins.

- **Preprocessing:** same idea as in FastICA (for more preprocessing detail refer to Chapter 4).
- **Build reference direction:** before starting fixed point iteration, references must be transformed into directions in the whitened space.
- **Fixed point update:** this update adds the two weighted reference terms to the original FastICA fixed point update.
- **Ensure convergence:** at the end of each iteration, it is necessary to normalize the $\mathbf{w}$ term to guarantee the convergence of the algorithm.

Listing 7.1 illustrates the constrained ICA pseudocode of the implementation designed for this thesis.

```
Input: Observed EMG matrix X, target reference r_target,
       interference reference r_bad, constraint weights lambda_pos,
       lambda_neg, tolerance epsilon, maximum iterations Imax

Output: Estimated target source y_hat and separation vector w

//Preprocessing
Xc <- X - mean(X)
Z  <- Whiten(Xc)

//Reference directions
q_target <- ReferenceDirection(Z, r_target)
q_bad    <- ReferenceDirection(Z, r_bad)
//Initialization
w <- Initialize(q_target)
w <- Normalize(w)
//Constrained optimization
for i = 1 to Imax

    w_old <- w
    w <- FastICAUpdate(w, Z, g)
    w <- w + Δw_target
    w <- w - Δw_bad
    delta <- | |w * w_old^T| - 1 |
    if delta < epsilon
        break
    end

end

y_hat <- Xc * w

return y_hat, w
```

Listing 7.1: Reference-constrained FastICA

However, this implementation does not guarantee an improvement over the traditional ICA, especially if the reference does not provide valuable information about the non-Gaussianity of s_1. In real world scenarios, the best reference that would be available for the weak source would at most be a binary mask of the target muscle activation.

7.4 Baseline comparison: Linear Regression

Before evaluating the proposed constrained ICA approach, it is useful to consider a simpler baseline to compare constrained ICA with other algorithms that use references or prior information. In the specific case where the second observed channel can be interpreted as an approximate reference of the dominant source (model in Equation 5.16), the recovery of the weak source can be expressed as an interference cancellation problem. This theoretically enables the use of the classic linear regression algorithms to estimate the contribution of the reference channel c_2 in the contaminated c_1 [45].

Recalling the weak source model explained in Section 3.1.3 ($\tau = 0$), channel c_1 is defined as s_1 with a contamination from s_2 and additive noise.

$$c_1(t) = s_1(t) + \beta s_2(t) + n_1(t), \tag{7.12}$$

Assuming that c_2 provides an approximate observation of the interfering component s_2, a linear estimate of the contamination in c_1 can be obtained by projecting c_1 onto c_2. The regression coefficient is therefore computed as shown in Equation 7.13.

$$\hat{\beta} = \frac{\mathbf{c}_2^T \mathbf{c}_1}{\mathbf{c}_2^T \mathbf{c}_2}. \tag{7.13}$$

The estimated weak source is then obtained by subtracting this contribution from the first observed channel:

$$\hat{s}_1^{\text{reg}}(t) = c_1(t) - \hat{\beta} c_2(t) \tag{7.14}$$

This approach is computationally simple and does not require an iterative optimization algorithm. However, it relies on the assumption that c_2 is an accurate reference of the dominant source. In the model considered in this thesis, s_2 may be dominant in c_2, but it also contains noise and small contribution from the target source s_1.

$$c_2(t) = 0.01 s_1(t - \tau) + s_2(t) + n_2(t), \tag{7.15}$$

Therefore, standard linear regression is not expected to provide an ideal recovery of s_1, but it represents an important baseline for evaluating whether the added complexity of constrained ICA produces a meaningful improvement. One final note is that, unlike the previously mentioned separation algorithms, linear regression can better estimate the original scale of s_1, but its accuracy depends on the contamination in c_2.

Alternatively, if delay is accurately estimated, a modified version of linear regression can be rewritten.

$$\hat{\beta} = \frac{\mathbf{c}_2^T (t - \tau) \mathbf{c}_1}{\mathbf{c}_2^T (t - \tau) \mathbf{c}_2 (t - \tau)}. \tag{7.16}$$

$$\hat{s}_1^{\text{reg}}(t) = c_1(t) - \hat{\beta} c_2(t - \tau) \tag{7.17}$$

7.5 Constrained ICA Experiments

For this final constrained ICA section, the goal is to present a series of experiments to assess whether this modified algorithm can improve the separation in the weak-source scenario. To simulate a more realistic scenario, the true source signals are not directly used as references. Instead, binary masks representing the activation periods of s_1 and s_2 are used.

7.5.1 Convolutive mixture with noise

Considering the last experimental case presented in the ICA chapter ($\sigma = 0.1$, $\beta = 0.3$ and $\tau = 5\,\text{ms}$) the appropriate values of λ_{pos} and λ_{neg} must be determined. For this purpose, a calibration stage is introduced, in which the objective is to maximize Corr_{RMS}. Table 7.1 shows the resulting values of Corr_{RMS} for each combination of λ_{pos} and λ_{neg}, which show a minimal improvement over the standard ICA implementation ($\lambda_{pos} = 0$ and $\lambda_{neg} = 0$).

$\lambda_{\text{pos}} \backslash \lambda_{\text{neg}}$	0.00	0.05	**0.10**	0.20	0.50	1.00	2.00	5.00	10.00
0.00	0.6838	0.6833	0.6804	0.6767	0.6726	0.6708	0.6698	0.6692	0.6689
0.05	0.6833	0.6804	0.6782	0.6755	0.6723	0.6707	0.6698	0.6692	0.6689
0.10	0.6774	0.6825	**0.6846**	0.6747	0.6721	0.6707	0.6698	0.6691	0.6689
0.20	0.6511	0.6792	0.6747	0.6735	0.6717	0.6705	0.6697	0.6691	0.6689
0.50	0.6632	0.6638	0.6643	0.6649	0.6709	0.6702	0.6696	0.6691	0.6689
1.00	0.6662	0.6663	0.6664	0.6666	0.6671	0.6698	0.6695	0.6691	0.6689
2.00	0.6675	0.6675	0.6675	0.6676	0.6678	0.6679	0.6692	0.6690	0.6689
5.00	0.6682	0.6682	0.6682	0.6682	0.6683	0.6683	0.6683	0.6690	0.6689
10.00	0.6685	0.6685	0.6685	0.6685	0.6685	0.6685	0.6685	0.6685	0.6689

Table 7.1: RMS envelope correlation for different values of λ_{pos} and λ_{neg}. Parameters set to $\beta = 0.3, \sigma = 0.1, \tau = 5\,\text{ms}$.

Once the weights have been selected, Figure 7.2 illustrates the RMS envelopes recovered by FastICA, constrained ICA and standard linear regression. The three methods achieve very similar results, suggesting that the main difficulty in this case is the convolutive weak source scenario itself rather than the lack of prior information. Though the methods manage to preserve the most prominent peaks, the delayed contributions from s_2 seem to introduce artificial peaks when compared to the original RMS envelope of the target source s_1.

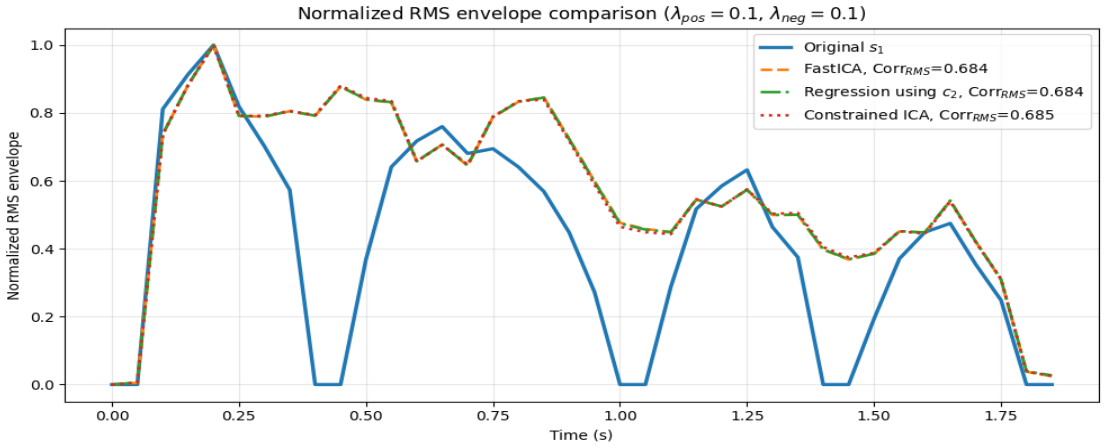

Figure 7.2: Comparison of the RMS envelopes recovered by constrained ICA, regression and standard FastICA algorithms. Parameters were set to $\sigma = 0.1$, $\beta = 0.3$ and $\tau = 5\,\text{ms}$. Prior information about the signal does not significantly improve recovery if the delayed contribution interference is not specifically addressed.

However, if the exact delay is known, a modified version of linear regression can be applied. As shown in Figure 7.3, this approach leads to a substantial improvement over the non-delayed regression method. Nevertheless, this result is only possible because the delay is known (in this case 5 ms). In a real scenario, where only an approximate range may be available (2 ms to 10 ms for example) and the delay may take non-integer values, the separation quality would likely decrease considerably.

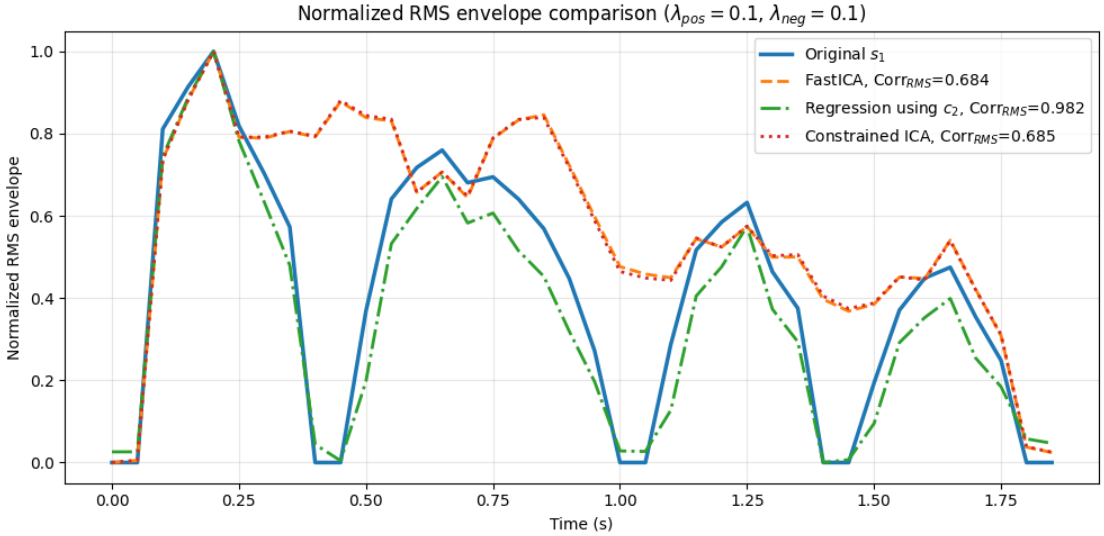

Figure 7.3: Comparison of the RMS envelopes recovered by constrained ICA, **modified regression** and standard FastICA algorithms. Parameters were set to $\sigma = 0.1$, $\beta = 0.3$ and $\tau = 5\,\text{ms}$. The delayed regression achieves an almost perfect reconstruction as it removes the delayed interference from s_2 (only if delay can be estimated with precision beforehand).

7.5.2 Best use scenario

When testing multiple scenarios to assess under which conditions constrained ICA can improve standard ICA, the most noticeable improvement is observed in the instantaneous mixture case with a high noise level ($\sigma = 0.5$). Table 7.2 shows the values of Corr_{RMS} obtained for different combinations of λ_{pos} and λ_{neg}. The best result is achieved when $\lambda_{\text{pos}} = \lambda_{\text{neg}} = 0.05$, resulting in an improvement of approximately 4% with respect to standard ICA.

This may indicate that the reference signals provide valuable information when the noise level is high and there is no significant delayed contribution from s_2.

$\lambda_{pos} \backslash \lambda_{neg}$	0.00	**0.05**	0.10	0.20	0.50	1.00	2.00	5.00
0.00	0.6638	0.7019	0.7026	0.7025	0.7020	0.7018	0.7016	0.7016
0.05	0.6440	**0.7026**	0.7026	0.7024	0.7020	0.7018	0.7016	0.7016
0.10	0.6921	0.6971	0.7025	0.7023	0.7020	0.7018	0.7016	0.7016
0.20	0.6987	0.6995	0.6999	0.7021	0.7019	0.7017	0.7016	0.7016
0.50	0.7007	0.7008	0.7008	0.7009	0.7018	0.7017	0.7016	0.7015
1.00	0.7011	0.7011	0.7012	0.7012	0.7013	0.7017	0.7016	0.7015
2.00	0.7013	0.7013	0.7013	0.7013	0.7014	0.7014	0.7015	0.7015
5.00	0.7014	0.7014	0.7014	0.7014	0.7014	0.7014	0.7015	0.2473

Table 7.2: RMS correlation values for different combinations of λ_{pos} and λ_{neg}. Parameters set to $\beta = 0.5, \sigma = 0.5, \tau = 0\,\text{ms}$.

However, this slight improvement does not solve the main limitations of FastICA in the recovery of the RMS envelope. Figure 7.4 illustrates the RMS envelope estimates retrieved by the three algorithms. Although constrained ICA follows the original envelope trends more accurately in some regions, noise artifacts still introduce some artificial peaks in the estimated signal.

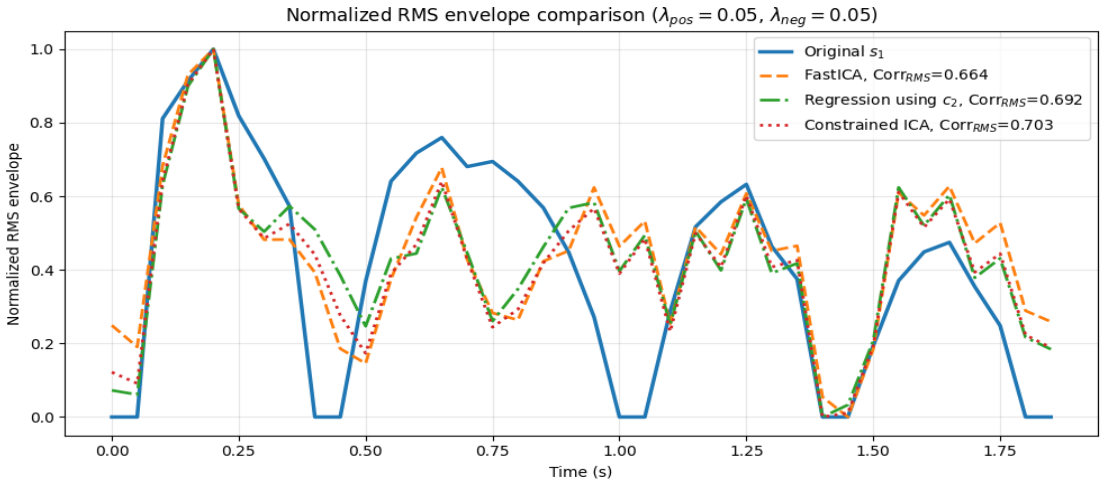

Figure 7.4: Comparison of the RMS envelopes recovered by constrained ICA, regression and standard FastICA algorithms. Parameters were set to $\sigma = 0.5$, $\beta = 0.3$ and $\tau = 0\,\text{ms}$. Results indicate that prior information may help in strong noise scenarios, but there is a limitation due to the weak source scenario.

7.5.3 Constrained ICA Experiments Conclusion

Overall, in the cases where standard FastICA does not perform optimally, adding prior information about the structure and behavior of the signals can only provide a slight improvement. However, the references used in these constrained ICA experiments are binary activation masks, since in real-world scenarios the true RMS envelope of the target signal would not be available (it is precisely the signal that must be recovered).

Additionally, using c_2 as an approximate reference of s_2 does not provide a significant improvement when s_1 remains clearly weak, both in the mixing matrix and in terms of variance. This suggests that, even though reference information can help guide the separation process, it does not fully overcome the major limitation imposed by the weak-source scenario.

A possible scenario where this algorithm could provide a more significant improvement over baseline ICA is a higher dimensional setting with several more channels and more sources. In the two source scenario case considered in this thesis, once one component is identified (often s_2 due to dominance), the remaining component is strongly dependent on orthogonality. However, when multiple sources are present, there are multiple possible orthogonal directions and ICA may have more difficulty selecting components. In that case, reference constraints could help the algorithm towards the desired source. Nevertheless, this scenario is outside the scope of this thesis.

Chapter 8
Conclusion and future work

This final chapter presents the main conclusions extracted from the work developed throughout this thesis. First, a global comparison of the implemented separation algorithms is included, assessing their performance, limitations and relevance for the weak source EMG separation problem addressed in this study. This comparison includes blind, temporal and semi-blind approaches, with special attention to their behavior under noise, signal imbalance and mixing conditions.

This chapter also aims to discuss important considerations for the online implementation of these algorithms. Since the original motivation of this work is related to improving EMG prosthetic control, these considerations are essential to assess whether the proposed approaches could be adapted to real-time applications. Finally, the main limitations of the present work are addressed and future research directions are proposed. In this way, the chapter closes the thesis by summarizing its contributions while indicating possible paths for further development in EMG source separation.

8.1 Global algorithm comparison

The experiments presented throughout this thesis have shown that the evaluated separation algorithms can perform well in ideal or semi-ideal weak source scenarios, especially when the mixing process is instantaneous and the noise level is low. However, when more realistic effects are introduced, such as additive noise and delayed source contributions, standard blind source separation methods struggle to recover the weak target source with precision.

This limitation is mainly caused by the nature of the weak source mixing problem. Since the target component s_1 has a much smaller representation in the mixing matrix compared to the dominant source s_2, small non-idealities may produce a significant degradation in its recovery. Although semi-blind approaches, such as regression and constrained ICA, can potentially compensate for some of these effects by introducing additional information into the separation process, their performance is still limited by the amount of target information actually present in the observed channels.

The results also suggest that the algorithms are more capable of compensating for additive noise than for delayed contributions. While noise mainly reduces the signal quality, temporal delays modify the effective mixing model and make the instantaneous separation dependent on the dominant source. As a result, delayed interference represents one of the most important challenges for the weak-source separation problem considered in this work.

Overall, the dominant source is generally easier to retrieve than the weak target source. This is expected, since the dominant component has higher variance,

is less affected by contamination from the weak source and better satisfies the assumptions used by the separation algorithms. Consequently, the recovery of s_2 tends to be more stable, while the recovery of s_1 is much more sensitive to noise, delay and mixing imbalance.

As a summary, Table 8.1 details the main assumptions, strengths and limitations of each algorithm studied in this thesis.

Method	**Main assumption**	**Strengths**	**Limitations**
FastICA	Statistical independence and non-Gaussianity	Effective in ideal instantaneous mixtures and computationally efficient	Sensitive to noise, delay, source imbalance and statistical dependence
SOBI	Different temporal correlation structures	Useful when sources have different autocorrelation patterns	Limited when EMG sources have similar temporal behavior and depends strongly on selected lags
Regression	c_2 approximates the dominant interference s_2	Simple, interpretable and suitable for online implementation	Imperfect reference of s_2 significantly impacts the separation quality
Constrained ICA	Prior information can guide the separation	Less dependent on the reference. Useful in high-dimensionality cases	Requires a representative reference or constraint

Table 8.1: Global comparison of the evaluated separation methods.

8.2 Considerations

8.2.1 Ground truth

For the experiments presented in this thesis, the ground truth sources were available as the mixing process was controlled in simulation. However, in real world scenarios, the original sources are not directly obtainable, since recovering them is precisely the objective of the separation process. For this reason, the validation of the separated components becomes a challenge.

A possible solution would be to compare the estimated components with the intended or self-reported activation of the patient. For example, if the patient is asked to perform a specific movement, the separated source should show an

activation pattern consistent with that task. An additional possibility would be to apply different separation algorithms and compare the consistency of their outputs.

8.2.2 Online implementation

Live implementation requires causal algorithms. Although all the methods considered in this thesis satisfy this requirement, their practical implementation is not equally straightforward.

Linear regression is the simplest method to implement in real time, since the only parameter that needs to be updated is the coefficient $\hat{\beta}$, either for each window or sample by sample. Once this coefficient is estimated, the target source is obtained by subtracting the estimated interference from the observed channel.

For the remaining algorithms, two main strategies can be considered. The first is to estimate the separation parameters during a calibration stage using representative mixtures and then apply the resulting separation matrix to each incoming EMG window. This makes the online stage more computationally efficient, which reduces processing time, but less adaptable.

The second strategy is to recompute or update the parameters for each window. This makes the system more adaptive to changes in the EMG recordings, but it also increases processing time and may reduce stability if the window is too short to estimate the required statistics reliably.

Table 8.2 shows some considerations for each algorithm when using this second approach, where the separation parameters are updated for each incoming EMG window.

Algorithm	**Updated parameters**	**Main considerations**
Linear regression	$\hat{\beta}$	Efficient, but depends on c_2 representing the interference well.
FastICA	Separation matrix $\mathbf{W}$	Requires stable independence estimates.
SOBI	Lagged covariance matrices and $\mathbf{W}$	Needs enough samples to estimate reliable lagged covariance matrices. Longer processing times.
Constrained ICA	$\mathbf{W}$ and reference constraint	Depends strongly on representative constraints.

Table 8.2: Considerations for window online parameter updating.

8.3 Future work

Although the results obtained in this thesis show that source separation methods can provide useful insight into weak-source EMG mixtures, the proposed algorithms still rely on several assumptions. The experiments were mainly designed to evaluate the behavior of different algorithms under controlled conditions, where the sources and mixing process were carefully defined. Future work should move towards more realistic signal models, experimental validation with real subjects and evaluation procedures that do not require access to the true underlying sources.

Given all these considerations, future work could explore the following directions:

- **Convolutive separation methods**

  In the initial hypothesis of this work, it was assumed that small delays could be approximated by instantaneous models. However, the results showed that including delayed contributions in the separation process could potentially improve the separation of these EMG sources. This would considerably increase the complexity of the problem, since separation filters would need to be estimated instead of a single instantaneous matrix. Additionally, the permutation problem would become much harder as the source order may change across frequency bands. These considerations make the final reconstruction significantly more difficult.

- **Testing with real subjects**

  The proposed methods should be validated with real subjects under controlled movement tasks. In this case, the separated components could be compared with the intended movement, patient feedback or expected activation patterns.

- **Indirect validation without ground truth**

  Since the original sources are not directly obtainable in real world scenarios, future work could compare multiple separation algorithms and analyze whether they recover consistent components in terms of activation timing and RMS envelope.

- **Scale reconstruction**

  The separation algorithms, excluding regression, suffer from scale indetermination. Section 5.6 addressed this issue from a theoretical level, but future work should focus on developing a reliable way to estimate the scale factors in real-world tests.

8.4 Final Reflection

Overall, this thesis has provided a structured analysis of source separation methods for weak EMG components in mixed recordings in different settings. The results show that the recovery of the target signal depends strongly on the mixing conditions, the variance of the sources, the presence of noise and delayed contributions of the signals.

While no single method can be considered ideal for every case, the comparison between regression, ICA, SOBI and constrained ICA demonstrates the advantages and limitations of each approach. For the IIT project scenario, linear regression may be the most practical option if the reference channel is accurate enough and the delay can be estimated. Otherwise, constrained ICA can potentially provide a more flexible and personalized approach, especially when additional sources or less ideal mixing conditions are present.

Although further validation with real subjects is still necessary, the methodology developed in this thesis represents a useful first step towards more reliable EMG processing strategies for prosthetic applications. In particular, the results suggest that including prior information or physiologically meaningful constraints may help improve separation in non-trivial cases. Additionally, convolutive models could also be explored to reduce interference from delayed contributions.

This is especially relevant in the weak source scenario, where the target component has significantly lower variance than the dominant source. As a result, small amounts of noise or residual interference can have a much larger impact on its recovery. Consequently, this work opens the door to future work in semi-blind, adaptive and convolutive EMG separation methods, with the goal of improving the reliability of myoelectric control systems.

Appendix I
GitHub Repository

The code and supplementary material developed during this Bachelor's Thesis are available in the following GitHub repository:

https://github.com/acobianiregui/TFG

The repository contains the implementation used for the experimental work, including signal preprocessing, mixture generation, source separation algorithms and evaluation metrics. The main purpose of the repository is to support reproducibility and to provide access to the scripts used to obtain the results presented in this thesis.

Since the original work was developed in Spanish, some comments, variable names or notebook sections may remain in Spanish. In addition, the notebooks are mainly used as experimental workspaces and may contain exploratory tests (especially for *"prueba ICA.ipynb"*). For this reason, the most relevant and reusable parts of the implementation are organized in Python modules under the source code directory.

The repository also includes basic GitHub Actions workflows for continuous integration. These workflows are included to perform simple quality control checks with each contribution. In particular, they check that the Python files can be compiled without syntax errors and that undefined variables are detected before changes are added to the repository. This helps maintain the reusable code modules in a more reliable state, while the notebooks remain mainly as exploratory experimental material.

The repository includes:

- Python implementations of the main source separation methods used in the thesis, including FastICA, SOBI and constrained ICA.
- Auxiliary functions for preprocessing, signal generation, evaluation metrics and visualization.
- Jupyter notebooks used for experimental testing and comparison of methods.
- The LaTeX source files of the thesis.
- Figures containing results of the experiments. **Figures that I do not own can be found at their respective sources**.
- Basic continuous integration workflows for syntax checking and detection of undefined variables in the Python source files.

The repository should be understood as a complementary resource to the thesis rather than as a standalone software package.

Appendix II
Relevant Code Fragments

Even though the majority of the files used for this thesis are included in the GitHub repository, it may be of interest to dedicate an appendix to relevant code fragments. This is done with the intention to facilitate the comprehension of the implementations throughout this thesis.

II.1 Experimental procedure

II.1.1 Synthetic signal generation

```
def generate_artificial_signals(fs=1000, duration=10, seed=None, eps=1e-12):
    """
    Generate two artificial EMG source signals with different frequency
    bands and envelopes

    Returns
    t : ndarray
        Time vector.
    S_true : ndarray
        Source matrix with shape (N, 2).
    """

    rng = np.random.default_rng(seed)

    t = np.arange(0, duration, 1 / fs)
    N = len(t)

    #s1: fast component
    raw_s1 = rng.normal(0, 1, N)
    b1, a1 = signal.butter(2, [90, 180], btype="bandpass", fs=fs)
    s1 = signal.filtfilt(b1, a1, raw_s1)
    s1 *= 0.5 * (1 + np.sin(2 * np.pi * 0.9 * t))

    #s2: slow component
    raw_s2 = rng.normal(0, 1, N)
    b2, a2 = signal.butter(2, [20, 50], btype="bandpass", fs=fs)
    s2 = signal.filtfilt(b2, a2, raw_s2)
    s2 *= 0.6 * (1 + np.cos(2 * np.pi * 0.15 * t))

    #RMS normalization
    s1 = s1 / (np.sqrt(np.mean(s1**2)) + eps)
    s2 = s2 / (np.sqrt(np.mean(s2**2)) + eps)

    S_true = np.column_stack([s1, s2])

    return t, S_true, s1, s2
```

Listing II.1: Artificial signal generator function. These signals are mainly used to test SOBI hypothesis in EMG.

II.1.2 Signal conditioning

```
def condition_signals(u1,u2,pattern=[0, 3, 2,1, 3, 3, 1, 2, 3, 0,2,
    3,1],dur_block1=0.5,dur_block2=0.5,fs=1000):
    N = min(len(u1), len(u2))
    u1 = u1[:N]

    u2 = u2[:N]
    N = len(u1)
    t = np.arange(N) / fs

    m1 = np.zeros(N)
    m2 = np.zeros(N)
    m3 = np.zeros(N)

    block = int(dur_block1*fs)
    block2 = int(dur_block2*fs)
    for i, state in enumerate(pattern):
        a = i * block
        a2= i * block2
        b = min((i + 1) * block, N)
        b2= min((i + 1) * block2, N)
        if state == 1:
            m1[a:b] = 1.0
            m3[a:b] = 1.0
        elif state == 2:
            m2[a2:b2] = 1.0
        elif state == 3:
            m1[a:b] = 1.0
            m3[a:b] = 1.0
            m2[a2:b2] = 1.0


    #Apply binary mask
    s1 = m1 * u1
    s2 = m2 * u2
    return s1,s2
```

Listing II.2: Condition signals function. Adapts original signals from TMR database into more appropriate activations for the thesis study. **DISCLAIMER:** original function in Spanish is "construir senales" which is used in the notebooks.

II.1.3 Build case

```
def build_case(
    u1, u2_raw, fs=1000, beta=1.0, a11=1.0, a21=0.01,
    tau_ms=0.0, noise_std=0.0, pattern=None, block_ms=200,
    target_scale=1.0, contam_scale=1.0, ref_flip_prob=0.0,
    ref_fn_prob=0.0, ref_fp_prob=0.0, random_state=0
):
    """
    THIS FUNCTION COMBINES ALL METHODOLOGY STEPS.
    Mainly used for constrained ICA testing, but can be used for any algorithm.
    Builds observed channels by mixing original sources
        c1 = a11*s1 + beta*s2(t-tau) + n1
        c2 = a21*s1 + 1.0*s2 + n2

    Returns:
        dictionary with signals, mixtures, masks and references
    """
    rng = np.random.default_rng(random_state)

    u1 = np.asarray(u1).ravel().astype(float)
    u2_raw = np.asarray(u2_raw).ravel().astype(float)
    N = min(len(u1), len(u2_raw))
    u1 = eliminar_continua(u1[:N])
    u2_raw = eliminar_continua(u2_raw[:N])

    if pattern is None:
        pattern = [0, 1, 2,1, 3, 2, 1, 2, 3, 0,2, 3,1]

    block = int(block_ms * fs / 1000)
    m1 = np.zeros(N)
    m2 = np.zeros(N)

    for i, estado in enumerate(pattern):
        a = i * block
        b = min((i + 1) * block, N)
        if a >= N:
            break
        if estado == 1:
            m1[a:b] = 1.0
        elif estado == 2:
            m2[a:b] = 1.0
        elif estado == 3:
            m1[a:b] = 1.0
            m2[a:b] = 1.0

    s1 = target_scale * m1 * u1
    s2 = contam_scale * m2 * u2_raw

    tau = int(fs * tau_ms / 1000)
    s2_del = delay_signal(s2, tau)

    n1 = noise_std * rng.standard_normal(N)
    n2 = noise_std * rng.standard_normal(N)

    c1 = a11 * s1 + beta * s2_del + n1
    c2 = a21 * s1 + 1.0 * s2 + n2

    X = np.column_stack([c1, c2])
    S_true = np.column_stack([s1, s2_del])

    #Ideal binary references
    ref_good = (m1 > 0).astype(float)
    ref_bad = (m2 > 0).astype(float)

    #Imperfections
    ref_imp = ref_good.copy()
    idx = np.arange(N)

```

```
    #false negatives
    pos = idx[ref_imp == 1]
    if len(pos) > 0 and ref_fn_prob > 0:
        k = int(ref_fn_prob * len(pos))
        if k > 0:
            off = rng.choice(pos, size=k, replace=False)
            ref_imp[off] = 0.0

    #false positives
    neg = idx[ref_imp == 0]
    if len(neg) > 0 and ref_fp_prob > 0:
        k = int(ref_fp_prob * len(neg))
        if k > 0:
            on = rng.choice(neg, size=k, replace=False)
            ref_imp[on] = 1.0

    #arbitrary flips
    if ref_flip_prob > 0:
        k = int(ref_flip_prob * N)
        if k > 0:
            flip = rng.choice(idx, size=k, replace=False)
            ref_imp[flip] = 1.0 - ref_imp[flip]

    return {
        "u1": u1, "u2_raw": u2_raw, "m1": m1, "m2": m2,
        "s1": s1, "s2": s2, "s2_del": s2_del,
        "X": X, "S_true": S_true,
        "c1": c1, "c2": c2,
        "ref_good": ref_good,
        "ref_bad": ref_bad,
        "ref_good_imperfect": ref_imp,
        "tau": tau
    }
```

Listing II.3: Build case function. It unifies all experimental procedure/generation functions. It is mainly used for constrained ICA testing, but it is also suitable for other tests.

II.2 Preprocessing

II.2.1 Whitening function

```
def whiten(X, eps=1e-12):
    """
    X: shape (N, m)
    returns:
      Xw: whitened data (same as Z in the thesis theory!!!!!!)
      whitening_mat
      dewhitening_mat
      mean_
    """
    X = np.asarray(X, dtype=float)
    mean_ = np.mean(X, axis=0, keepdims=True)
    Xc = X - mean_

    C = np.cov(Xc, rowvar=False)
    eigvals, eigvecs = np.linalg.eigh(C)

    idx = np.argsort(eigvals)[::-1]
    eigvals = eigvals[idx]
    eigvecs = eigvecs[:, idx]

    D_inv_sqrt = np.diag(1.0 / np.sqrt(eigvals + eps))
    D_sqrt = np.diag(np.sqrt(eigvals + eps))
```

```
23
24      whitening_mat = eigvecs @ D_inv_sqrt @ eigvecs.T
25      dewhitening_mat = eigvecs @ D_sqrt @ eigvecs.T
26
27      Xw = Xc @ whitening_mat.T
28      return Xw, whitening_mat, dewhitening_mat, mean_
```

Listing II.4: Whitening function. Aims to achieve decorrelated data and unit variance.

II.3 SOBI implementation

II.3.1 Jacobi Joint Diagonalization

```
1  def _joint_diag_jacobi(mats, eps=1e-7, max_sweeps=100):
2      n = mats[0].shape[0]
3      B = np.eye(n)
4
5      for _ in range(max_sweeps):
6          improved = False
7          #One sweep over pairs (p,q)
8          for p in range(n - 1):
9              for q in range(p + 1, n):
10                 #Build 2x2 problem
11                 g11 = 0.0
12                 g12 = 0.0
13
14                 for A in mats:
15                     app = A[p, p]
16                     aqq = A[q, q]
17                     apq = A[p, q]
18                     #Objective quantities
19                     g11 += (app - aqq)
20                     g12 += 2.0 * apq
21
22                 #If already diagonal, skip
23                 if abs(g12) <= eps:
24                     continue
25
26                 #Calculate rotation angle
27                 theta = 0.5 * np.arctan2(g12, g11)
28                 c = np.cos(theta)
29                 s = np.sin(theta)
30
31                 if abs(s) <= eps:
32                     continue
33
34                 improved = True
35
36                 #Apply rotation to B
37                 Bp = B[p, :].copy()
38                 Bq = B[q, :].copy()
39                 B[p, :] = c * Bp + s * Bq
40                 B[q, :] = -s * Bp + c * Bq
41
42                 #Update of rows/cols p,q
43                 for k in range(len(mats)):
44                     A = mats[k]
45
46                     #Rotate rows p,q
47                     Ap = A[p, :].copy()
48                     Aq = A[q, :].copy()
49                     A[p, :] = c * Ap + s * Aq
50                     A[q, :] = -s * Ap + c * Aq
```

```
51
52                      #Rotate cols p,q
53                      Ap = A[:, p].copy()
54                      Aq = A[:, q].copy()
55                      A[:, p] = c * Ap + s * Aq
56                      A[:, q] = -s * Ap + c * Aq
57
58                      mats[k] = A
59
60          if not improved:
61              break
62
63      return B
```

Listing II.5: Jacobi/Givens approximate joint diagonalization.

II.3.2 SOBI code

```
1  def sobi(X, num_delays=50, delays=None, n_sources=None, eps=1e-7, max_sweeps=100):
2      """
3      Inputs
4      X: array (n_samples, n_channels)
5      delays: list of delays (in samples), referenced as T in the pseudocode
6      n_sources: how many sources to estimate (None => n_channels)
7      Returns
8      S: (n_samples, n_sources) estimated sources
9      W: (n_sources, n_channels) separation matrix
10     """
11     #Initial check
12     X = np.asarray(X, dtype=float)
13     if X.ndim != 2:
14         raise ValueError("X must be 2D: (n_samples, n_channels)")
15     n_samples, n_channels = X.shape
16     if n_sources is None:
17         n_sources = n_channels
18     n_sources = int(n_sources)
19
20     #1 center (if not done already)
21     Xc = X - X.mean(axis=0, keepdims=True)
22
23     #2 Whitening (if not whitened already)
24     R0 = (Xc.T @ Xc) / n_samples
25     d, E = np.linalg.eigh(R0)
26     idx = np.argsort(d)[::-1]
27     d = d[idx]
28     E = E[:, idx]
29     E = E[:, :n_sources]
30     d = np.maximum(d[:n_sources], 1e-12)
31     Wh = np.diag(1.0 / np.sqrt(d)) @ E.T
32     Xw = Xc @ Wh.T
33
34     #3 lagged covariance matrices
35     if delays is None:
36         delays = list(range(1, int(num_delays) + 1))
37     mats = []
38     for tau in delays:
39         if tau <= 0 or tau >= n_samples:
40             continue
41         R = (Xw[tau:, :].T @ Xw[:-tau, :]) / (n_samples - tau)
42         R = 0.5 * (R + R.T)  #symmetric
43         mats.append(R)
44     if len(mats) == 0:
45         raise ValueError("No valid set of delays T was provided")
46
47     #4 joint diagonalization (jacobi rotations,see function)
48     mats_copy = [A.copy() for A in mats]
49     B = _joint_diag_jacobi(mats_copy, eps=eps, max_sweeps=max_sweeps)
```

```
    B = _sym_decorrelation(B)

    #5 separation
    W = B @ Wh
    S = Xc @ W.T

    return S, W
```

Listing II.6: General sobi implementation, based on the Jacobi/Givens approximate joint diagonalization.

II.4 Constrained ICA Implementation

II.4.1 Build Reference Direction

```
def build_reference_direction(Xw, ref, max_lag=0, smooth=True, smooth_win=25,
    eps=1e-12):
    ref = np.asarray(ref).ravel().astype(float)
    ref = ref - np.mean(ref)

    if smooth:
        ref = smooth_reference(ref, win_samples=smooth_win)
        ref = ref - np.mean(ref)

    best_q = None
    best_lag = 0
    best_score = -np.inf

    for lag in range(-max_lag, max_lag + 1):
        ref_lag = shift_no_circular(ref, lag)
        ref_lag = ref_lag - np.mean(ref_lag)

        q = (Xw * ref_lag[:, None]).mean(axis=0)
        score = np.linalg.norm(q)

        if score > best_score:
            best_score = score
            best_q = q.copy()
            best_lag = lag

    if best_q is None:
        return None, None, 0.0

    nrm = np.linalg.norm(best_q)
    if nrm < eps:
        return None, None, 0.0

    best_q = best_q / nrm
    return best_q, best_lag, best_score
```

Listing II.7: Function to transform a reference into a suitable direction for the fixed point update.

II.4.2 Constrained ICA Dual Reference

```
def constrained_fastica_dualref_twounits(
    X,
    ref_s1=None,
    ref_s2=None,
    lambda_pos=0.1,
    lambda_neg=0.1,
    max_lag=0,
    fun="logcosh",
    alpha=1.0,
    whiten_data=True,
    max_iter=1000,
    tol=1e-7,
    random_state=0,
    smooth_ref=True,
    smooth_win=25,
    eps=1e-12,
):
    rng = np.random.default_rng(random_state)

    X = np.asarray(X, dtype=float)
    N, M = X.shape

    #Whitening included if needed
    if whiten_data:
        Xw, whitening_mat, dewhitening_mat, mean_ = whiten(X, eps=eps)
    else:
        mean_ = np.mean(X, axis=0, keepdims=True)
        Xw = X - mean_
        whitening_mat = np.eye(M)
        dewhitening_mat = np.eye(M)

    #Build reference directions, see build_reference_direction() for details
    q_s1, lag_s1, score_s1 = (None, None, 0.0)
    q_s2, lag_s2, score_s2 = (None, None, 0.0)

    if ref_s1 is not None:
        q_s1, lag_s1, score_s1 = build_reference_direction(
            Xw,
            ref_s1,
            max_lag=max_lag,
            smooth=smooth_ref,
            smooth_win=smooth_win,
            eps=eps,
        )

    if ref_s2 is not None:
        q_s2, lag_s2, score_s2 = build_reference_direction(
            Xw,
            ref_s2,
            max_lag=max_lag,
            smooth=smooth_ref,
            smooth_win=smooth_win,
            eps=eps,
        )

    #Initialize W with two rows
    W = rng.standard_normal((2, Xw.shape[1]))

    if q_s1 is not None:
        W[0] = q_s1 + 0.05 * rng.standard_normal(Xw.shape[1])
    if q_s2 is not None:
        W[1] = q_s2 + 0.05 * rng.standard_normal(Xw.shape[1])

    #Symmetric decorrelation
    W = _sym_decorrelation(W)

    converged = False
```

```
68
69      for n_iter in range(max_iter):
70          W_old = W.copy()
71
72          #Standard FastICA fixed point update
73          U = Xw @ W.T
74          G, Gp = g_fun(U, fun=fun, alpha=alpha)
75
76          W_new = (G.T @ Xw) / N - np.diag(Gp.mean(axis=0)) @ W
77
78          #constraints for component 1. Target s1, avoid s2
79          if q_s1 is not None and lambda_pos > 0:
80              W_new[0] += 2 * lambda_pos * np.dot(W[0], q_s1) * q_s1
81
82          if q_s2 is not None and lambda_neg > 0:
83              W_new[0] -= 2 * lambda_neg * np.dot(W[0], q_s2) * q_s2
84
85          #constraints for component 2. Target s2, avoid s1
86          if q_s2 is not None and lambda_pos > 0:
87              W_new[1] += 2 * lambda_pos * np.dot(W[1], q_s2) * q_s2
88
89          if q_s1 is not None and lambda_neg > 0:
90              W_new[1] -= 2 * lambda_neg * np.dot(W[1], q_s1) * q_s1
91
92          #Decorrelate
93          W_new = _sym_decorrelation(W_new)
94
95          #check convergence
96          lim = np.max(np.abs(np.abs(np.diag(W_new @ W_old.T)) - 1.0))
97
98          W = W_new
99
100         if lim < tol:
101             converged = True #Solution found
102             break
103
104     #Once converged, restore data
105     W_full = W @ whitening_mat.T
106
107     Xc = X - mean_
108     S_hat = Xc @ W_full.T
109     #Useful information if needed
110     info = {
111         "q_s1": q_s1,
112         "q_s2": q_s2,
113         "lag_s1": lag_s1,
114         "lag_s2": lag_s2,
115         "score_s1": score_s1,
116         "score_s2": score_s2,
117         "n_iter": n_iter + 1,
118         "converged": converged,
119         "W_whitened": W,
120     }
121
122     return S_hat, W_full, info
```

Listing II.8: Constrained ICA algorithm implemented in this thesis. Two references are used. The target reference is the one associated to s1 and target bad is associated to s2

Appendix III

Appendix: Sustainable Development Goals

The analysis and separation of electromyographic (EMG) signals developed throughout this Bachelor's Thesis not only aims to contribute to advances in the field of biomedical signal processing, but also naturally aligns with several Sustainable Development Goals, also known as SDGs. The application of techniques such as preprocessing, artifact removal and separation and classification methods contributes to the development of technological solutions that improve health, promote innovation and support equal access to biomedical tools.

Therefore, the main SDGs addressed by this Bachelor's Thesis and their role in the project are presented below:

- Goal 3: Good Health and Well-being

Improving the quality of the acquired signals enables more accurate clinical assessments, supports the early detection of muscular dysfunctions and optimizes rehabilitation processes. The development of more robust and reliable algorithms has a direct impact on the quality of healthcare by supporting decision-making among healthcare professionals.

- Goal 9: Industry, Innovation and Infrastructure

The project promotes technological innovation by applying engineering tools, such as digital signal processing and machine learning, to a biomedical context. The study and comparison of separation algorithms reinforce the development of new tools that can be integrated into medical devices, prostheses or monitoring systems. Therefore, this work contributes to building scientific and technological infrastructures to improve health.

- Goal 10: Reduced Inequalities

By advancing techniques that make it possible to obtain accurate muscular information without relying on high-cost equipment, this project supports the development of more accessible solutions. It favors the extension of EMG technologies to clinical and research environments with fewer available resources. The standardization and validation of separation methods allow these tools to be reproduced more reliably, facilitating their use in a wider variety of centers. In this way, the project promotes more equitable access to prosthetic technologies, contributing to the reduction of inequalities in the healthcare field.

Bibliography

[1] S. H. Tuffaha, C. Glass, G. Rosson, J. Shores, A. Belzberg, and A. Wong, "Vascularized, Denervated Muscle Targets: A Novel Approach to Treat and Prevent Symptomatic Neuromas", *Plastic and Reconstructive Surgery Global Open*, vol. 8, no. 4, e2779, Apr. 2020, ISSN: 2169-7574. DOI: 10.1097/GOX.0000000000002779. [Online]. Available: https://pmc.ncbi.nlm.nih.gov/articles/PMC7209893/.

[2] G. Clifford, *Biomedical Signal and Image Processing | Health Sciences and Technology*, en, 2008. [Online]. Available: https://ocw.mit.edu/courses/hst-582j-biomedical-signal-and-image-processing-spring-2007/.

[3] R. Giannetti, J. D. Muñoz Frías, and E. Alonso Rivas, *Ortesis mioeléctricas con electrodos implantables: Optimizando la reconstrucción biónica tras lesiones graves de nervio periférico | Instituto de Investigación Tecnológica (IIT)*. [Online]. Available: https://www.iit.comillas.edu/proyectos/mostrar_proyecto.php.es?nombre_abreviado=MYORTESIS.

[4] J. E. Cheesborough, L. H. Smith, T. A. Kuiken, and G. A. Dumanian, "Targeted Muscle Reinnervation and Advanced Prosthetic Arms", *Seminars in Plastic Surgery*, vol. 29, no. 1, pp. 62–72, Feb. 2015, ISSN: 1535-2188. DOI: 10.1055/s-0035-1544166. [Online]. Available: https://pmc.ncbi.nlm.nih.gov/articles/PMC4317279/.

[5] E. Pettersen, P. Sassu, F. A. Pedrini, *et al.*, "Regenerative Peripheral Nerve Interface: Surgical Protocol for a Randomized Controlled Trial in Postamputation Pain", en, [Online]. Available: https://www.jove.com/t/66378/regenerative-peripheral-nerve-interface-surgical-protocol-for.

[6] J. González-Prieto, L. Cristóbal, M. Arenillas, *et al.*, "Regenerative Peripheral Nerve Interfaces (RPNIs) in Animal Models and Their Applications: A Systematic Review", eng, *International Journal of Molecular Sciences*, vol. 25, no. 2, p. 1141, Jan. 2024, ISSN: 1422-0067. DOI: 10.3390/ijms25021141.

[7] S. V, S. Ej, C. Na, G. Am, and T. Sh, "Use of Vascularized, Denervated Muscle Targets for Prevention and Treatment of Upper-Extremity Neuromas", en, *PubMed*, 2022. [Online]. Available: https://pubmed.ncbi.nlm.nih.gov/36704382/.

[8] C. M. Frost, D. C. Ursu, S. M. Flattery, *et al.*, "Regenerative peripheral nerve interfaces for real-time, proportional control of a Neuroprosthetic hand", *Journal of NeuroEngineering and Rehabilitation*, vol. 15, p. 108, Nov. 2018, ISSN: 1743-0003. DOI: 10.1186/s12984-018-0452-1. [Online]. Available: https://pmc.ncbi.nlm.nih.gov/articles/PMC6245539/.

[9] M. Klug and K. Gramann, "Identifying key factors for improving ICA-based decomposition of EEG data in mobile and stationary experiments", en, *European Journal of Neuroscience*, vol. 54, no. 12, pp. 8406–8420, 2021, _eprint: https://onlinelibrary.wiley.com/doi/pdf/10.1111/ejn.14992, ISSN: 1460-9568. DOI: 10.1111/ejn.14992. [Online]. Available: https://onlinelibrary.wiley.com/doi/abs/10.1111/ejn.14992.

[10] R. K. Kanna and R. Vasuki, "Advanced Study of ICA in EEG and Signal Acquisition using Mydaq and Lab view Application", en, vol. 8, no. 7, 2019.

[11] T.-P. Jung, C. Humphries, T.-w. Lee, *et al.*, "Extended ICA Removes Artifacts from Electroencephalographic Recordings", *Neural Inf. Process. Syst.*, vol. 10, Feb. 1998.

[12] W. Sato and T. Kochiyama, "Crosstalk in Facial EMG and Its Reduction Using ICA", en, *Sensors*, vol. 23, no. 5, p. 2720, Mar. 2023, ISSN: 1424-8220. DOI: 10.3390/s23052720. [Online]. Available: https://www.mdpi.com/1424-8220/23/5/2720.

[13] Y. Kim, S. Stapornchaisit, M. Miyakoshi, N. Yoshimura, and Y. Koike, "Frontiers | The Effect of ICA and Non-negative Matrix Factorization Analysis for EMG Signals Recorded From Multi-Channel EMG Sensors", en, DOI: 10.3389/fnins.2020.600804. [Online]. Available: https://www.frontiersin.org/journals/neuroscience/articles/10.3389/fnins.2020.600804/full.

[14] G. R. Naik, S. Arjunan, and D. Kumar, "Applications of ICA and fractal dimension in sEMG signal processing for subtle movement analysis: A review", En, *Australasian Physical & Engineering Sciences in Medicine*, vol. 34, no. 2, pp. 179–193, Mar. 2011, ISSN: 1879-5447. DOI: 10.1007/s13246-011-0066-4. [Online]. Available: https://link.springer.com/article/10.1007/s13246-011-0066-4.

[15] M. Chen and P. Zhou, "2CFastICA: A Novel Method for High Density Surface EMG Decomposition Based on Kernel Constrained FastICA and Correlation Constrained FastICA", *IEEE Transactions on Neural Systems and Rehabilitation Engineering*, vol. 32, pp. 2177–2186, 2024, ISSN: 1558-0210. DOI: 10.1109/TNSRE.2024.3398822. [Online]. Available: https://ieeexplore.ieee.org/document/10526297/.

[16] C. Tang, Y. Li, X. Fan, *et al.*, "Improving nerve and muscle function: An exploration of targeted nerve function replacement following differential delay periods in a rat model", *Journal of NeuroEngineering and Rehabilitation*, vol. 22, no. 1, p. 145, Jul. 2025, ISSN: 1743-0003. DOI: 10.1186/s12984-025-01666-0. [Online]. Available: https://doi.org/10.1186/s12984-025-01666-0.

[17] G. Kalogiannis, N. Karampelas, and G. Hassapis, "A Reworked SOBI Algorithm Based on SCHUR Decomposition for EEG Data Processing", in *2017 IEEE 30th International Symposium on Computer-Based Medical Systems (CBMS)*, ISSN: 2372-9198, Jun. 2017, pp. 268–271. DOI: 10.1109/CBMS.20

17.88. [Online]. Available: https://ieeexplore.ieee.org/abstract/document/8104200.

[18] K. Gokcesu, M. Ergeneci, E. Ertan, and H. Gokcesu, "An Adaptive Algorithm for Online Interference Cancellation in EMG Sensors", *IEEE Sensors Journal*, vol. 19, no. 1, pp. 214–223, Jan. 2019, ISSN: 1558-1748. DOI: 10.1109/JSEN.2018.2874724. [Online]. Available: https://ieeexplore.ieee.org/abstract/document/8485693.

[19] X. Jiang, G.-B. Bian, and Z. Tian, "Removal of Artifacts from EEG Signals: A Review", en, *Sensors*, vol. 19, no. 5, p. 987, Feb. 2019, ISSN: 1424-8220. DOI: 10.3390/s19050987. [Online]. Available: https://www.mdpi.com/1424-8220/19/5/987.

[20] P. P. Vu, A. K. Vaskov, Z. T. Irwin, *et al.*, "A regenerative peripheral nerve interface allows real-time control of an artificial hand in upper limb amputees", *Science translational medicine*, vol. 12, no. 533, eaay2857, Mar. 2020, ISSN: 1946-6234. DOI: 10.1126/scitranslmed.aay2857. [Online]. Available: https://pmc.ncbi.nlm.nih.gov/articles/PMC8082695/.

[21] S. Muceli and R. Merletti, "Tutorial. Frequency analysis of the surface EMG signal: Best practices", *Journal of Electromyography and Kinesiology*, vol. 79, p. 102 937, Dec. 2024, ISSN: 1050-6411. DOI: 10.1016/j.jelekin.2024.102937. [Online]. Available: https://www.sciencedirect.com/science/article/pii/S1050641124000816.

[22] B. M, H. Pw, V. D. J, *et al.*, "Consensus for experimental design in electromyography (CEDE) project: Electrode selection matrix", en, *PubMed*, [Online]. Available: https://pubmed.ncbi.nlm.nih.gov/31352156/.

[23] M. L, D. V. G, and L. Mm, "Analysis and Biophysics of Surface EMG for Physiotherapists and Kinesiologists: Toward a Common Language With Rehabilitation Engineers", en, *PubMed*, 2020. [Online]. Available: https://pubmed.ncbi.nlm.nih.gov/33178118/.

[24] S. R. A. Todd Kuiken and S. R. A. Levi Hargrove, *Electromyography (EMG) data from individuals with transradial amputation and targeted muscle reinnervation (TMR) surgery*, en, Jun. 2023. DOI: 10.3886/E184165V1. [Online]. Available: https://www.openicpsr.org/openicpsr/project/184165/version/V1/view.

[25] A. Hamilton-Wright and D. Stashuk, "Physiologically based simulation of clinical EMG signals", *IEEE Transactions on Biomedical Engineering*, vol. 52, no. 2, pp. 171–183, Feb. 2005, ISSN: 1558-2531. DOI: 10.1109/TBME.2004.840501. [Online]. Available: https://ieeexplore.ieee.org/abstract/document/1386554.

[26] O. S. Powar, K. Chemmangat, and S. Figarado, "A novel pre-processing procedure for enhanced feature extraction and characterization of electromyogram signals", *Biomedical Signal Processing and Control*, vol. 42, pp. 277–286, Apr. 2018, ISSN: 1746-8094. DOI: 10.1016/j.bspc.2018.02.006. [On-

line]. Available: https://www.sciencedirect.com/science/article/pii/S1746809418300375.

[27] *designNotchPeakIIR - Design and implement high-order Butterworth notch or peak IIR filter - MATLAB*, en. [Online]. Available: https://www.mathworks.com/help/dsp/ref/designnotchpeakiir.html.

[28] D. Hoaglin, "Volume 16: How to Detect and Handle Outliers", 2013. [Online]. Available: https://www.semanticscholar.org/paper/Volume-16%3A-How-to-Detect-and-Handle-Outliers-Hoaglin/d524a172b49e25f888376d662ee364aa77d99e8a#paper-topics.

[29] M. Boyer, L. Bouyer, J.-S. Roy, and A. Campeau-Lecours, "Reducing Noise, Artifacts and Interference in Single-Channel EMG Signals: A Review", en, *Sensors*, vol. 23, no. 6, p. 2927, Mar. 2023, ISSN: 1424-8220. DOI: 10.3390/s23062927. [Online]. Available: https://www.mdpi.com/1424-8220/23/6/2927.

[30] X. Shi, *Blind Signal Processing*, en. Berlin, Heidelberg: Springer, 2011, ISBN: 978-3-642-11346-8 978-3-642-11347-5. DOI: 10.1007/978-3-642-11347-5. [Online]. Available: http://link.springer.com/10.1007/978-3-642-11347-5.

[31] scikit-learn, *Scikit-learn/sklearn/decomposition/_fastica.py at fe2edb3cdbd75ae4e662fda67dcb19277258792b · scikit-learn/scikit-learn*, en. [Online]. Available: https://github.com/scikit-learn/scikit-learn/blob/fe2edb3cdbd75ae4e662fda67dcb19277258792b/sklearn/decomposition/_fastica.py.

[32] G. R. Naik and W. Wang, Eds., *Blind Source Separation: Advances in Theory, Algorithms and Applications* (Signals and Communication Technology), en. Berlin, Heidelberg: Springer Berlin Heidelberg, 2014, ISBN: 978-3-642-55015-7 978-3-642-55016-4. DOI: 10.1007/978-3-642-55016-4. [Online]. Available: https://link.springer.com/10.1007/978-3-642-55016-4.

[33] A. Brendel, T. Haubner, and W. Kellermann, "A Unifying View on Blind Source Separation of Convolutive Mixtures Based on Independent Component Analysis", *IEEE Transactions on Signal Processing*, vol. 71, pp. 816–830, 2023, ISSN: 1941-0476. DOI: 10.1109/TSP.2023.3255552. [Online]. Available: https://ieeexplore.ieee.org/abstract/document/10066846.

[34] L. Parra and C. Spence, "Convolutive blind separation of non-stationary sources", en, *IEEE Transactions on Speech and Audio Processing*, vol. 8, no. 3, pp. 320–327, May 2000, ISSN: 10636676. DOI: 10.1109/89.841214. [Online]. Available: http://ieeexplore.ieee.org/document/841214/.

[35] P. Konrad, "The abc of emg", *A practical introduction to kinesiological electromyography*, vol. 1, no. 2005, pp. 30–5, 2005. [Online]. Available: https://doctorchoice.cl/wp-content/uploads/2018/04/ABC-of-EMG-min.pdf.

[36] Y. Pan, M. Matilainen, S. Taskinen, and K. Nordhausen, "A review of second-order blind identification methods", en, *WIREs Computational Statistics*, vol. 14, no. 4, e1550, 2022, _eprint: https://wires.onlinelibrary.wiley.com/doi/pdf/10.1002/wics.1550, ISSN: 1939-0068. DOI: 10.1002/wics.1550. [Online]. Available: https://onlinelibrary.wiley.com/doi/abs/10.1002/wics.1550.

[37] C. Févotte and F. J. Theis, "Pivot Selection Strategies in Jacobi Joint Block-Diagonalization", en. DOI: 10.1007/978-3-540-74494-8_23. [Online]. Available: https://link.springer.com/chapter/10.1007/978-3-540-74494-8_23.

[38] A.-J. van der Veen, "Joint diagonalization via subspace fitting techniques", in *2001 IEEE International Conference on Acoustics, Speech, and Signal Processing. Proceedings (Cat. No.01CH37221)*, ISSN: 1520-6149, vol. 5, May 2001, 2773–2776 vol.5. DOI: 10.1109/ICASSP.2001.940221. [Online]. Available: https://ieeexplore.ieee.org/abstract/document/940221.

[39] D. Trehan, "Non-Convex Optimization: A Review", in *2020 4th International Conference on Intelligent Computing and Control Systems (ICICCS)*, May 2020, pp. 418–423. DOI: 10.1109/ICICCS48265.2020.9120874. [Online]. Available: https://ieeexplore.ieee.org/abstract/document/9120874.

[40] M. Danilova, P. Dvurechensky, A. Gasnikov, *et al.*, "Recent Theoretical Advances in Non-Convex Optimization", en, in Apr. 2022. DOI: 10.1007/978-3-031-00832-0_3. [Online]. Available: https://link.springer.com/chapter/10.1007/978-3-031-00832-0_3.

[41] C. Hesse and C. James, "The FastICA algorithm with spatial constraints", *IEEE Signal Processing Letters*, vol. 12, no. 11, pp. 792–795, Nov. 2005, ISSN: 1558-2361. DOI: 10.1109/LSP.2005.856867. [Online]. Available: https://ieeexplore.ieee.org/abstract/document/1518903.

[42] H. Yang, T. Vu, E. A. Dhrubo, V. D. Calhoun, and T. Adali, "A Flexible Constrained ICA Approach for Multisubject fMRI Analysis", en, *International Journal of Biomedical Imaging*, vol. 2025, no. 1, p. 2 064 944, 2025, _eprint: https://onlinelibrary.wiley.com/doi/pdf/10.1155/ijbi/2064944, ISSN: 1687-4196. DOI: 10.1155/ijbi/2064944. [Online]. Available: https://onlinelibrary.wiley.com/doi/abs/10.1155/ijbi/2064944.

[43] W. Lu and J. C. Rajapakse, "ICA with Reference", *Neurocomputing*, Brain Inspired Cognitive Systems, vol. 69, no. 16, pp. 2244–2257, Oct. 2006, ISSN: 0925-2312. DOI: 10.1016/j.neucom.2005.06.021. [Online]. Available: https://www.sciencedirect.com/science/article/pii/S0925231205003176.

[44] Z. Wang, "Fixed-point algorithms for constrained ICA and their applications in fMRI data analysis", *Magnetic Resonance Imaging*, vol. 29, no. 9, pp. 1288–1303, Nov. 2011, ISSN: 0730-725X. DOI: 10.1016/j.mri.2011.07.017. [Online]. Available: https://www.sciencedirect.com/science/article/pii/S0730725X11002475.

[45] F. J. Samaniego and M. R. Watnik, "The Separation Principle in Linear Regression", *Journal of Statistics Education*, vol. 5, no. 3, Nov. 1997, _eprint: https://doi.org/10.1080/10691898.1997.11910599, ISSN: null. DOI: 10.1080/10691898.1997.11910599. [Online]. Available: https://doi.org/10.1080/10691898.1997.11910599.